HETERO-MULTIVALENT BINDING OF *Pseudomonas aeruginosa* LECTIN, LECA, AND *Vibrio Cholerae* LECTIN, CHOLERA TOXIN SUBUNIT B

A Dissertation

by

NOLAN CECIL WORSTELL

Submitted to the Office of Graduate and Professional Studies of
Texas A&M University
in partial fulfillment of the requirements for the degree of

DOCTOR OF PHILOSOPHY

Chair of Committee,	Hung-Jen Wu
Committee Members,	Jeffery D. Cirillo
	M.M. Faruque Hasan
	Katy C. Kao
Head of Department,	Muhammad N. Karim

May 2018

Major Subject: Chemical Engineering

ABSTRACT

Adhesion of carbohydrate binding proteins called lectins to cell membrane components mediates pathogen interactions with host cells. In working with cell membrane mimicking lipid bilayers, we observed that weak affinity receptors could be activated by high affinity receptors leading to significantly higher binding of the pentameric lectin cholera toxin subunit B, CTB. Weak receptor activation was probably mediated via the Reduction of Dimensionality (RD) mechanism. In RD, once a protein has attached to a strong receptor, subsequent binding events are confined to a two-dimensional cell membrane surface enabling weak affinity receptors to be secondary receptors due to the enhanced effective concentration. Based on our CTB experiments, we expected that the inherent RD mechanism could induce heteromultivalent binding in most multivalent systems.

To confirm RD as a fundamental mechanism, we studied a second multivalent binding lectin. This lectin, LecA, is a tetrameric lectin that mediates *Pseudomonas aeruginosa* adhesion to host cells and biofilm formation. Our data showed enhanced LecA binding to mixture bilayers composed of both Gb3 and moderate or weak affinity receptors. Furthermore, moderate affinity receptors enhanced weak affinity receptors. Interestingly, our data showed that multivalent binding affinity and binding capacity were not necessarily correlated with their monovalent counterparts. A colloidal aggregation assay of LecA interacting with Gb3 and LacCer demonstrated that LecA's binding affinity was Gb3 > Gb3+LacCer > LacCer. The colloidal binding affinity agreed with prior data binding affinities confirming that multivalent binding affinity and binding capacity cannot be assumed from monovalent data. Therefore, our data suggest the RD mechanism is a fundamental multivalent binding mechanism. To efficiently

discover hetero-multivalency in various multivalent systems, we developed a turbidity-based emulsion agglutination (TEA) assay amenable to high-throughput screening of lectin binding. This assay utilizes the coagulation of emulsions to determine heteromultivalent binding. The results of the TEA assay matched our prior LecA data and were corroborated by dynamic light scattering. In summary, we have demonstrated the RD mechanism, verified that the RD mechanism can play a role in multiple multivalent systems, and developed an assay to efficiently screen large molecular libraries for heteromultivalent binding resulting from the RD mechanism.

DEDICATION

"Our imagination is stretched to the utmost, not, as in fiction, to imagine things which are not really there, but just to comprehend those things which are there." [sic]

-Richard Feynman[1]

ACKNOWLEDGEMENTS

I thank my committee chair, Dr. Hung-Jen Wu, and my committee members, Dr. Cirillo, Dr. Hasan, and Dr. Kao, for their guidance and support throughout the course of this research.

Thanks also to my mother, father, great uncle, and great aunt for their encouragement and endurance of innumerable attempts to explain my research.

Lastly, thanks to my wife for following me in my Ph.D. pursuit, her patience, her considerate listening of unending presentations, and her love.

CONTRIBUTORS AND FUNDING SOURCES

This work was supported by a dissertation committee consisting of Professor Hung-Jen Wu and Professors M.M. Farque Hasan, and Katy C. Kao of the Department of Chemical Engineering and Professor Jeffery D. Cirillo of the Department of Microbial Pathogenesis and Immunology.

Chapter II experiments were: conceived and designed by myself, Pratik Krishnan, and Hung-Jen Wu of the Department of Chemical Engineering; performed by myself, Pratik Krishnan, and Joshua D. Weatherston of the Department of Chemical Engineering; and analyzed by myself, Pratik Krishnan, Joshua D. Weatherston, and Hung-Jen Wu of the Department of Chemical Engineering. The contributed reagents/materials/analysis tools for Chapter II were from myself, Pratik Krishan, Joshua D. Weatherston, and Hung-Jen Wu of the Department of Chemical Engineering. Chapter II was written by myself, Pratik Krishnan, Joshua D. Weatherston and Hung-Jen Wu of the Department of Chemical Engineering.

Chapter III experiments were: conceived and designed by myself, Pratik Krishnan, Akshi Singla and Hung-Jen Wu of the Department of Chemical Engineering; performed by Pratik Krishnan, and Akshi Singla of the Department of Chemical Engineering; and analyzed by Pratik Krishnan, Akshi Singla and Hung-Jen Wu of the Department of Chemical Engineering. The contributed reagents/materials/analysis tools for Chapter II were from myself, Pratik Krishan, Akshi Singla, Chin-An Lee, Joshua D. Weatherston, and Hung-Jen Wu of the Department of Chemical Engineering. Chapter III was written by myself, Pratik Krishnan, Akshi Singla and Hung-Jen Wu of the Department of Chemical Engineering.

Chapter IV experiments were: conceived and designed by myself and Hung-Jen Wu of the Department of Chemical Engineering; performed by myself and Akshi Singla of the Department of Chemical Engineering; and analyzed by myself, Akshi Singla and Hung-Jen Wu of the Department of Chemical Engineering and Panatda Saenkham and Professor Jeffery D. Cirillo of the Department of Microbial Pathogenesis and Immunology. The contributed reagents/materials/analysis tools for Chapter IV were from myself, Akshi Singla, and Hung-Jen Wu of the Department of Chemical Engineering. Chapter IV was written by myself, Akshi Singla and Hung-Jen Wu of the Department of Chemical Engineering and Panatda Saenkham of the Department of Microbial Pathogenesis and Immunology.

Chapter V experiments were: conceived and designed by myself and Hung-Jen Wu of the Department of Chemical Engineering; performed by myself; and analyzed by myself and Hung-Jen Wu of the Department of Chemical Engineering. The contributed reagents/materials/analysis tools for Chapter V were from myself and Hung-Jen Wu of the Department of Chemical Engineering. Chapter V was written by myself and Hung-Jen Wu of the Department of Chemical Engineering.

This work was supervised by a dissertation committee consisting of Professor Hung-Jen Wu and Professors M.M. Farque Hasan, and Katy C. Kao of the Department of Chemical Engineering and Professor Jeffery D. Cirillo of the Department of Microbial Pathogenesis and Immunology. Graduate study was supported by a fellowship from Texas A&M and funds from the National Institutes of Health under award number R03AI113585.

TABLE OF CONTENTS

Page

LIST OF FIGURES

Page

Page

Page

Page

Page

LIST OF TABLES

Page

CHAPTER I

INTRODUCTION AND LITERATURE REVIEW

In biological systems, chemical species are generally dilute, often no more than 50 μM.[2] However, biological systems are clearly still capable of accomplishing necessary chemical reactions on biologically relevant timescales. One way biology addresses the issue of dilute chemical species is by localizing the reacting species.[3-6] This can be done by compartmentalizing the species onto the same surface or the same region.[3-6] One example of this is membrane partitioning of intestinal epithelial cells into apical and basolateral membrane sections separated by tight junctions.[7] Another example is the general orientation of cell glycolipids toward the extracellular milieu.[7,8] The result of this compartmentalization is that the chemical species interact much sooner than if they were freely diffusing enabling reactions to occur on relevant time scales.[5]

However, not all chemical species that interact start localized to the same cell, much less to the same region. Two common examples of this are host-pathogen interactions and cell-cell communication.[9-13] An example of one host-pathogen interaction is influenza (specifically strain A/Oklahoma/323/03) binding to sugar groups containing a terminal α2-6-linked sialic acid such as are found in the human body.[14] An example of cell-cell communication is proinflammatory secretagogues activating P-selectin for leukocyte recruitment. After activation, P-selectin binds to P-selectin glycoprotein ligand-1 on leukocytes to contribute to leukocyte recruitment in inflammation.[14] Therefore, this type of cross-cell interaction requires a way to recognize the region where the partner chemical species is located. This typically is achieved using multivalent proteins that recognize cell membrane receptors. [13]

What is Multivalency?

Multivalent proteins are proteins that contain multiple binding sites, such as the pentavalent (five binding site) Cholera Toxin subunit B (CTB) from *Vibrio cholerae* and tetravalent PA-IL (LecA) from *Pseudomonas aeruginosa*.[15,16] Now, these multivalent proteins typically bind differently than the classical concept of protein binding.[13] Unlike the traditional lock and key model, these multivalent proteins, often, do not specifically recognize a single receptor.[13] Rather these multivalent proteins bind a wide range of receptors, albeit with varying degrees of binding affinity.[13,17,18] However, one should not conclude that the total binding of these multivalent proteins is weak. The cumulative binding of multiple weak binding events is strong.[13] This becomes problematic due to the vast array of potential receptors present on the typical cell membrane.[13] Therefore, to understand multivalent protein binding, it is necessary to know the binding affinity of the multivalent protein to many different receptors. This introduces part of the complexity of understanding multivalent protein binding.

There is also the issue of multivalent proteins sharing primary receptors, but binding differently to the same type of cell.[19-21] Two multivalent proteins are considered to have a shared primary receptor when both proteins have the same receptor as their highest binding affinity receptor.[17] One such pair is Shiga Toxin from *Escherichia coli* and LecA. Both have globotriaosylceramide (Gb3) as their highest affinity receptor.[20,21] Another example of this is *Amaranthus caudatus* lectin, *Agaricus bisporus* lectin, *Colchicum autumnale* lectin, *Maackia amurensis* lectin I, and *Phytolacca Americana* lectin all bind to the structure β-galactose-N-acetyl galactosamine (Galβ-GalNAc).[19] In all of these cases, if we only consider monovalent binding, one would assume that each of these proteins would exhibit binding to cells in proportion to their observed binding affinities. However that is not the case, the *in vitro* and *in*

vivo binding of these multivalent proteins to various cell lines demonstrates that each multivalent protein binds differently to a given cell line.[22] Therefore, it is important to not only consider the binding affinity of the multivalent protein to a given receptor by itself, but also to study the receptor-protein interaction in its proper context.[17] This summarizes the effects of hetero-multivalency.

Multivalency in Cell Membranes

Some of the most typical cell membrane receptors for multivalent proteins are glycolipids and glycoproteins.[13] These are lipids and proteins, respectively, which have sugar groups attached to them.[13] Lectins are proteins that recognize the sugar groups on cell membrane receptors, typically via multivalent interactions.[13] Originally, lectins were primarily used for blood typing.[13] Since the 1960s, lectins have been shown to play a role in multiple areas and are widely used in biochemistry and biology.[14] One application is using lectins as stains for detecting and quantifying the presence of glycolipids on cell membranes.[23,24] Lectins, i.e. galectins, are also being used as cancer markers.[14] Increasingly, research has focused on targeting lectins for drug delivery or viewing lectins as virulence factors that can be treated.[25-28] Thus, it is becoming increasingly important to understand how multivalent proteins, especially lectins, bind and interact with the cell membrane.

Despite the importance of understanding lectin binding and the wide spread use of lectins, we still have several fundamental questions to answer about how lectins interact with cell membranes. As mentioned earlier, the question has been raised of why lectins that have the same shared primary receptor bind differently to the same cell line.[17] Similarly, it has been observed that lectins used for staining for a given glycolipid do not always correlate with antibody binding for that same glycolipid, but no explanation has been given as to why this is.[29] Furthermore, the

governing mechanism behind lectin binding is uncertain.[18] This hinders our ability to understand more application oriented question such as how lectins can bind to cells when their strongest affinity receptor is of low abundance.[30] An example of this is CTB can bind to cell lines that have < 0.003 mol% GM1.[31] In summary, there is much we do not know about lectin binding.

Despite a lack of direct answers to how lectins interact with cell membranes, the literature has observed that lectins can bind to receptors in mixtures that they do not bind to as individual receptors. Klassen et al. have done work demonstrating that CTB can bind to mixtures of glycolipids using pico-discs and micelles as part of Catch and Release Electrospray Ionization Mass Spectroscopy (CaR-ESI-MS).[32,33] However, the mechanism of how the lectins bind to receptor mixtures is still unclear.[33] Therefore, while it is insightful to demonstrate that CTB can bind to receptors in a mixture that it would not individually; it is hard to understand the fundamental interactions at work in this system. Other groups have used binary mixtures of glycolipids in combinatorial arrays of 1:1 ratios and studied lectins binding to these mixtures.[34] In this set up, it was also shown that lectins bound differently to the mixtures as opposed to the individual glycolipids.[34-37] However, none of the authors provided potential mechanisms or studied unequal mixtures limiting direct comparisons to real cell membranes.[32-37] Therefore, the evidence of lectins binding differently to mixtures of receptors than they would to the receptors individually has been demonstrated in *in vitro* as well as the aforementioned *in vivo* systems. However, the limited scope of the measurements and lack of a model hinders the translation of these results into meaningful answers to questions of lectin binding.

Mechanistic Features of Multivalency

In systems similar to lectins, researchers have begun looking more at the potential mechanisms behind multivalent binding to cell membranes. Looking at bivalent antibody staining for glycolipids, Mazor et al. noted that there was improved binding affinity if the antibody was localized to the membrane surface.[38] This phenomenon was explained using a model given by Sengers et al. that demonstrated the difference between two-dimensional and three-dimensional reaction rates.[39] Sengers et al. showed that two-dimensional reaction rates can be up to 10^4 times greater than those in three-dimensional.[39] Therefore, it is possible some of the differences between observed binding between lectins and their receptors individually as opposed to the receptors being present as a mixture can be explained by the difference between two-dimensional and three-dimensional reaction rates. However, these studies focused on bivalent antibodies. Therefore, this research highlights differences between free versus localized reactions as important mechanistic features of multivalent binding, but it is unclear if this is translatable to lectin binding.

Research into lectin inhibition has also provided some potential mechanistic insights into how multivalent lectins interact with multiple receptors. Using glycodendrimers (chemical species with multiple antenna displaying the same sugar group, or glycan), Imberty et al. have demonstrated that using multiple copies of a high binding affinity glycan linked together results in the resulting glycodendrimer having a higher binding affinity to LecA than the sugar group by itself.[27,40-42] This is not unique to LecA, but has been demonstrated by other researchers for lectins such as the homotetrameric Concanavalin A from *Canavalia ensiformis* (Jack bean) and the aforementioned CTB.[43,44] [45,46] Similarly, it has been observed that glycodendrimersomes (particles that are coated with multiple copies of a glycan tethered to the surface) can bind to

lectins with higher affinity than the same glycan in solution.[47-50] As part of the design of these glycodendrimers and glycodendrimersomes, it has also been shown that the spacing between the glycans directly affects their binding affinity.[27,50]This demonstrates that glycan density alters multivalent lectin binding and identifies the second mechanistic feature of multivalent binding.

Research Aims

The presented research has built off this prior research by focusing on three things. First, we demonstrated why lectins that have the same shared primary receptor bind differently to the same cell line. Second, we provided and validated a mechanism to explain multivalent lectin binding in two lectin systems. Third, we built off the fundamental understanding gained to develop a facile TEA assay to efficiently screen for lectin binding capacity to lipid surfaces using only common laboratory equipment. Underpinning this endeavor was a novel nanocube sensor developed by Dr. Hung-Jen Wu.[51] The nanocube sensor is comprised of a label-free silver nanocube sensor coated with a silica shell that acts as a surface to form a fluidic supported lipid bilayer.[17,51] In addition, the nanocube sensor is a freely diffusing colloidal probe, which allows it to be compatible with UV/Vis well plate readers for high-throughput quantification.[17] This nanocube sensor directly addresses many of the problems faced by research groups in the literature.

Limitations of Current Tools

Unlike the nanocube sensor, prior tools fixed the glycan spacing creating an environment that is dissimilar to the cell membrane. As previously noted, appropriate spacing of glycans is important to achieve improved binding affinity. This has created problems for many of the high throughput analysis methods, such as glycoarrays, used to study lectins. These problems result from either the glycolipids or the lectin being printed onto a surface thereby fixing the spacing of

the glycans or potentially inhibiting normal lectin function or rearrangement.[35,52-54] The nanocube sensor addresses this problem by way of the supported lipid bilayer.[17,51] This bilayer is fluidic allowing constituent glycolipids to achieve the appropriate spacing and still effectively model the cell membrane.[17,51] Prior research has also used fluidic lipid bilayers to study lectins, i.e. supported lipid bilayers in the Biacore system or micelles as part of mass spectroscopy studies.[55-59] However, these methods are labor intensive, time consuming, and/or required specialized equipment.[55-59] These limitations have likely prevented the widespread use of the prior techniques to study lectins. Furthermore, these concerns are especially relevant to studying lectin binding to heterogeneous glycolipid bilayers (bilayers containing mixtures of glycolipids) because of the necessity to study not only each receptor individually, but also mixed with other receptors in varying receptor densities and lectin concentrations. Therefore, there are a wide variety of experimental conditions to be tested. This is not a problem for the colloidal nanocube sensor because is compatible with a 384 well plate format.[17,18] Furthermore, the nanocube system also avoids the potential problems resulting from the labelling of either lectins or glycolipids that are common with many similar techniques such as fluorescence spectroscopy.[60,61] This label-free quantification is possible because the nanocube sensor relies on changes in the local dielectric constant caused by the protein displacing buffer near the sensor rather than a tag to identify protein binding. This detection by changes in local dielectric constant is a phenomenon called localized surface plasmon resonance (LSPR).[17,18] Thus, the nanocube sensor is a novel technology that facilitated the in depth binding analysis required for the successful completion of our research by coupling an easy-to-use, label-free supported lipid bilayer sensor to a high-throughput format.

Overview of Following Chapters

In the following chapters, we will go into further detail about our specific research. Chapter II will focus on developing the basics of homogeneous binding and begin to explore heterogeneous binding of CTB to various glycolipids. Chapter III will expand upon CTB binding to heterogeneous mixtures and propose a two-step binding mechanism to describe how CTB binds to cell membrane glycolipids. We established a new technique to streamline the identification of glycolipids that only bind in mixtures and not by themselves. After establishing the basics of multivalent lectin binding and proposing a mechanism, we will apply these techniques to analyze LecA. In Chapter IV, we will establish LecA binding to homogeneous (individual glycolipid) and heterogeneous (mixed glycolipid) bilayers and demonstrate how the mechanism proposed in the study of CTB accurately predicts the data observed with LecA binding to glycolipids. Chapter V will introduce a TEA assay to assess lectin binding capacity. This assay will be compatible with high-throughput formation of the emulsion so that it can be used as a quick, semi-quantitative screen for changes in lectin binding. The results of the TEA assay will be confirmed using DLS to ensure that changes in turbidity are linked to actual droplet aggregation rates. A major benefit of this assay is that it eliminates the batch functionalization step required for nanocube binding studies in favor of potential continuous emulsion formation. In summary,wewill demonstrate the fundamentals of multivalent lectin binding in both CTB and LecA, propose and demonstrate the usefulness of a two-step binding mechanism in explaining multivalent lectin binding, and develop a TEA assay amenable to high-throughput emulsion formation and screening.

CHAPTER II

BINDING COOPERATIVITY MATTERS: A GM1-LIKE GANGLIOSIDE-CHOLERA TOXIN SUBUNIT B BINDING STUDY USING A NANOCUBE-BASED LIPID BILAYER ARRAY*

Chapter Summary

Protein-glycan recognition is often mediated by multivalent binding. These multivalent bindings can be further complicated by cooperative interactions between glycans and individual glycan binding subunits. Here we have demonstrated a nanocube-based lipid bilayer array capable of quantitatively elucidating binding dissociation constants, maximum binding capacity, and binding cooperativity in a high-throughput format. Taking cholera toxin subunit B (CTB) as a model cooperativity system, we studied both GM1 and GM1-like gangliosides binding to CTB. We confirmed the previously observed CTB-GM1 positive cooperativity. Surprisingly, we demonstrated fucosyl-GM1 has approximately 7 times higher CTB binding capacity than GM1. In order to explain this phenomenon, we hypothesized that the reduced binding cooperativity of fucosyl-GM1 caused the increased binding capacity. This was unintuitive, as GM1 exhibited higher binding avidity (16 times lower dissociation constant). We confirmed the hypothesis using a theoretical stepwise binding model of CTB. Moreover, by taking a mixture of fucosyl-GM1 and GM2, we observed the mild binding avidity fucosyl-GM1 activated GM2 receptors enhancing the binding capacity of the lipid bilayer surface. This was unexpected as GM2 receptors have negligible binding avidity in pure GM2 bilayers. These discoveries demonstrate

*Reprinted with permission from "Binding cooperativity matters: A GM1-like ganglioside-cholera toxin B subunit binding study using a nanocube-based lipid bilayer array" by Worstell, Nolan C., Krishnan, Pratik, Weatherston, Joshua D., Wu, H. J., 2016, *PLoS ONE*, 11,

the importance of binding cooperativity in multivalent binding mechanisms. Thus, quantitative analysis of multivalent protein-glycan interactions in heterogeneous glycan systems is of critical importance. Our user-friendly, robust, and high-throughput nanocube-based lipid bilayer array offers an attractive method for dissecting these complex mechanisms.

Introduction

Glycan binding proteins (GBPs) often recognize glycans present on cell surfaces via multivalent binding mechanisms. Many GBPs contain multiple glycan binding subunits that bind multiple glycans attached to lipids or membrane proteins on cell surfaces. These glycans can freely diffuse and rotate on a two-dimensional fluidic cell membrane, enabling self-organization for multivalent interactions with GBPs. Such multivalent interactions are mediated by cooperative effort between glycan-bound subunits that influence binding avidity and/or specificity.[14] A good example of this cooperative binding is the interaction of cholera toxin subunit B (CTB) with gangliosides. CTB is a homopentamer that strongly associates with GM1 gangliosides. Positive cooperativity between bound GM1 molecules can raise CTB-GM1 binding avidity by several orders of magnitude [43,62]. The CTB-GM1 stepwise binding mechanism has been studied by isothermal titration calorimetry (ITC) and mass spectrometry (MS).[63,64] In one study, Klassen and coworkers observed that the binding affinity (association constant) of the unbound subunit doubles in value when a bound GM1 is adjacent to the unbound pocket, demonstrating the positive cooperativity of GM1-CTB binding.[64] Furthermore, this concept of binding cooperativity has been widely utilized to design high affinity inhibitors for various multivalent GBPs, including biotoxins and lectins.[26]

Due to its high GM1 binding avidity, CTB has been widely used to monitor the quantity and localization of GM1 in cell staining.[65,66] However, Yanagisawa et al. observed CTB could

bind to cell surfaces in the absence of GM1 gangliosides.[22] They hypothesized that CTB binding to mouse embryonic neuroepithelial cells could be caused by the other GM1-like gangliosides, including fucosyl-GM1. However, the mechanism is not clear and requires additional cross-reactivity data to elucidate. In order to quantify the cross-reactivity between CTB and mixed gangliosides, a high-throughput, easy-to-use, and robust analytical tool is of critical importance.

A typical tool for glycan recognition is the glycan microarray where various synthetic or natural glycans are immobilized on a solid surface.[67,68] In this technique, bound analytes are detected by labeling, such as fluorescent and immunostaining assays, or by label-free detection technologies that require special instrumentation.[67] A limitation of current glycan microarray technologies is the immobilization of glycan receptors onto the substrate. This creates a problem because immobilized glycans cannot achieve optimal multivalent binding. It is impossible to control the spacing and orientation of glycans to match precisely the configuration of binding pockets in the target GBPs. Hence, the presentation of glycans on microarray surfaces, including linker effects and glycan density, influences GBP binding.[68] This intrinsic drawback limits the ability of glycan microarrays to quantify the complex multivalent interactions. To overcome this drawback, an alternative approach is to insert glycans (e.g. glycolipids or neoglycolipids) into fluidic bilayers instead of immobilizing them onto a substrate.[63,69-72] In a fluidic bilayer system, glycans can freely move and encounter target GBPs to enable multivalent interactions. Although the fluidic bilayer array format has been demonstrated by different research groups [55,56,70,71,73], none of these techniques has become wide spread throughout the biological sciences. This is probably due to a lack of accessibility and flexibility.

To address the lack of accessibility and flexibility of prior systems, we introduced a unique nanocube sensor for direct measurements of CTB binding onto lipid bilayer surfaces.[74]

(**Figure 1a**) This $Ag@SiO_2$ core-shell nanocube sensor enables label-free detection of protein binding to lipid bilayer surfaces by taking advantage of the fluidic bilayer system. To create the fluidic bilayer, a thin water layer mediates the supported lipid bilayer's interaction with the sensor's silica surface. This thin layer provides a flexible buffer that enables the bilayers to mimic an idealized cell membrane and possess similar two-dimensional fluidity. Protein binding to lipid bilayers is monitored by observing the extinction spectra shift of the localized surface plasmon resonance (LSPR) using a standard UV\Vis spectrophotometer. Our previous study has demonstrated the application of this nanocube sensor.[74] The advantages of this platform are (1) high accessibility (only requiring a standard spectrophotometer), (2) ease of use (a simple "mix-and-then-detect" protocol), (3) high flexibility (allowing end users to build their own assays in-house without special equipment), and (4) label-free detection. In contrast to conventional techniques that require labeling, this label-free sensor can directly quantify absolute surface densities of bound proteins without calibration prior to binding measurements. These outstanding features enable the quantitative analysis of GBP binding mechanisms.

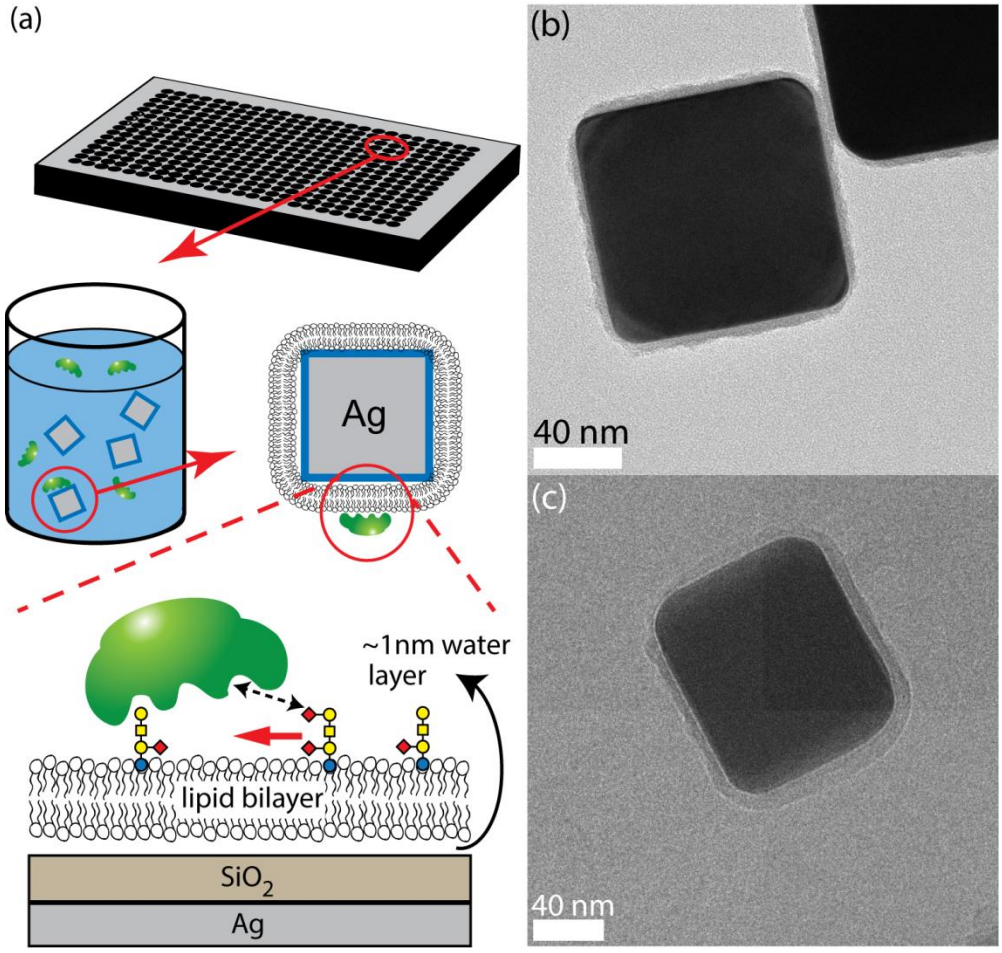

Figure 1: Overview schematic of the nanocube-based sensor with confirmation by TEM (a) A schematic of the nanocube-based lipid bilayer array. Silica coated silver nanocubes ($Ag@SiO_2$ nanocubes) are covered by a supported fluidic lipid bilayer that incorporates gangliosides. Equilibrium binding was detected in a 384 well plate by monitoring the extinction spectra in a microplate spectrophotometer. (b) A TEM image of the silica shell coated onto the Ag nanocubes. (c) A cryo-TEM image of the supported lipid bilayer coated onto the $Ag@SiO_2$ nanocubes. Reprinted with permission from Worstell *et al.*[75]

In this study, we improved the prior nanocube-based sensing platform to enable high-throughput detection. We successfully achieved large-scaled synthesis of high quality nanocube sensors (one synthesis batch allowing up to 20,000 measurements), and adapted the sensors to a high-throughput microplate reader (384 well plate). This novel nanocube-based lipid bilayer

array allowed us to simultaneously perform many CTB binding measurements under different experimental conditions, facilitating the dissection of complex binding mechanisms. In this article, we measured the cross-reactivity of CTB with various gangliosides, including GM1, GM2, and fucosyl-GM1. We observed approximately 7 times higher CTB binding capacity on the fucosyl-GM1 surface than the GM1 surface. This was unexpected, as GM1 is known to exhibit higher binding avidity (i.e. lower dissociation constant). Moreover, we observed the very weak binding receptor, GM2, was activated by fucosyl-GM1. This activation increased the number of CTB molecules binding to the fucosyl-GM1-GM2 lipid bilayer. To the best of our knowledge, these phenomena have never been reported. To explore the observed phenomena theoretically, we analyzed the stepwise binding model reported by Klassen and his coworkers [64]. From probing Klassen's model, we found binding cooperativity plays an essential role in CTB binding. This analysis may answer the question posed by Yanagisawa et al., "why is the amount of bound CTB not correlated with the GM1 expression level in neural cells?" [22]. Our discovery demonstrates the essential nature of cooperativity in multivalent GBP binding. Furthermore, our sensor provides a facile method to analyze GBP cooperativity as its fluidic bilayer provides unconstrained binding for CTB and its high-throughput methodology enables the study of cross-reactivity. By leveraging our nanocube-based lipid bilayer array, we can assist biologists in dissecting the complex binding mechanisms of multivalent GBPs.

Materials and Methods

Materials

Monosialoganglioside, GM1, (2Galβ1-3GalNAcβ1-4(Neu5Acα2-3)Galβ1-4Glc-Ceramide) was acquired from three different vendors, including Matreya LLC (State College, PA), Avanti Polar Lipids (Alabaster, AL), and Sigma-Aldrich. Fucosylated monosialoganglioside GM1 (Fucα1-2Galβ1-3GalNAcβ1-4(Neu5Acα2-3)Galβ1-4Glc-Ceramide, fucosyl-GM1), was purchased from Matreya LLC. 1, 2-dioleoyl-sn-glycero-3-phosphocholine (DOPC), 1, 2-dioleoyl-sn-glycero-3-phospho-L-serine - sodium salt (DOPS) and 1,2-dioleoyl-sn-glycero-3-phosphoethanolamine-N-(biotinyl) (biotin-PE) were obtained from Avanti Polar Lipids (Alabaster, AL). Cholera Toxin subunit B (CTB) from *Vibrio cholerae*, GM2 (3GalNAcβ1-4(Neu5Acα2-3)Galβ1-4Glc-Ceramide), streptavidin from *Streptomyces avidinii* (StP), copper (II) chloride dihydrate, polyvinylpyrrolidone (PVP) (MW ~55,000), tetraethyl orthosilicate (TEOS), and silicone oil (useable range -50^{o}C to +200^{o}C) were purchased from Sigma-Aldrich. Silver nitrate (Premion, 99.9995%) was purchased from Alfa-Aesar. 1,5-Pentanediol 98% (PD) was purchased from Acros Organics through Fisher Scientific. The calibration experiments were performed in 1X phosphate buffered saline (PBS) solution diluted from a 10X PBS stock from CulGenX. CTB binding was performed in 1X Tris-buffered saline (TBS) solution (20mM Tris 0.9% NaCl pH~7.4) diluted from a 10X TBS stock from Sigma-Aldrich.

Methods

Silver nanocube synthesis procedure

The nanocube synthesis procedure was taken from Tao et al.[76] The procedure was based on the polyol method and described in brief as follows. First, 0.2 g of PVP was dissolved into 10

mL of PD. Next, 0.2 g of $AgNO_3$ was dissolved into 10 mL of PD with 30 μL of a 0.082 g/mL $CuCl_2$ in PD solution. Then, 20 mL of PD was heated in a 190 °C silicone oil bath. After the PD was heated sufficiently, 500 μL of the $AgNO_3$ solution and 500 μL of the PVP solution were added sequentially every minute. This was continued until all 10 mL of both the $AgNO_3$ and PVP solutions were added. When finished, the nanocubes were washed with 200 proof ethanol using a centrifuge.

Modified nanocube silica coating procedure

Our silica coating procedure was adapted from Wu et al. with a few alterations and presented with alterations as follows.[74] To improve silica shell quality in the scaled-up synthesis batch, the silica coating reaction was conducted in 2-propanol, instead of ethanol. 20 mL of stock silver nanocubes stored in ethanol was first transferred into 2-propanol. Then, the silver nanocube solution was suspended into 55 mL of 2-propanol and mixed with 22.1 mL of water, 6.80 mL of TEOS, and 3.4 mL of 0.84 w/v% ammonium hydroxide solution. Next, the solution was stirred at room temperature for 80 minutes. After the reaction finished, 50 mL of ethanol were added to quench the reaction. The resultant particles were washed with Milli-Q® water a few times, and stored in Milli-Q® water for future use. (**Figure 1b**)

Calibration of the silica coated silver nanocubes

The thickness of the silica coated onto the silver nanocube was imaged directly using a transmission electron microscope (FEI Technai G2 F20 FE-TEM). The size and uniformity of the silver nanocubes prior to silica coating was determined by direct imaging with a scanning electron microscope (FEI Quanta 600 FE-SEM). The sensitivity of the silica coated silver nanocubes was determined by the method given by Wu et al. using a figure of merit (FOM) that

was calculated by dividing refractive index sensitivity by the line width of the resonance spectrum.[74]

The relationship between the quadrupole LSPR peak shift and the surface mass density of protein bound was measured by binding streptavidin to biotin-PE on the bilayer surface. [74] (**Figure 22**) Our previous work established a protocol to change bound streptavidin by titrating streptavidin concentration.[74] Briefly, bilayer (89 mol% DOPC/10 mol% DOPS/1 mol% biotin-PE) coated Ag@SiO_2 nanocubes were titrated with streptavidin in a 384 well plate (Greiner Bio-one). The average streptavidin surface density on the nanocubes was evaluated by approximating each lipid as a single DOPC lipid to obtain the surface area coverage in the supported bilayers.[74]

Supported bilayer preparation

Small unilamellar vesicles (SUVs) were prepared as follows. The desired composition of lipids in chloroform was mixed and then dried using a rotary evaporator (Heidolph Hei-VAP Value®). Then, the dried lipids were rehydrated with Milli-Q® water and extruded through 100 nm polycarbonate filters (Whatman®) using a Mini-extruder (Avanti Polar Lipids) to achieve an extruded lipid concentration of 3 mg/mL. Supported lipid bilayers were formed by a modified vesicle-fusion technique. In this technique, Ag@SiO_2 nanocubes were sequentially added into a SUV solution with a high SUV concentration in the initial coating solution. Briefly, 10 µL of nanocube solution and 30 µL of 2X TBS buffer were added to 20 µL of concentrated SUV solution (3 mg/mL) followed by 10 seconds of sonication in a bath sonicator (Branson). Then, 10 µL of the nanocube solution and 10 µL of 2X TBS buffer were added followed by 10 seconds of sonication. This process was repeated until all of the nanocube solution had been added. After coating the supported bilayer, additional TBS buffer was added to the solution to reach the desired concentration of salt (1X TBS), SUV's, and nanocubes in the final solution.

Protein binding measurement

Bilayer coated nanocubes were incubated with the desired protein concentration in a 384 well plate for 1.5 hours. Blank solutions were prepared for each CTB concentration by mixing buffer, SUVs, and CTB corresponding to that composition. Next, the 384 well plate was placed in a vacuum chamber at 40 cm Hg of vacuum for 15 minutes to remove air bubbles before collecting extinction spectra with a UV/Vis microplate spectrophotometer equipped with a CCD (FLUOstar Omega®, BMG-Labtech). The location of the quadrupole LSPR peak was detected by fitting a seventh order polynomial to the spectrum. The fitted spectrum resulted from averaging 200 flashes per well at a 1 nm spectral resolution; the scanning rate for each well was less than 1 second. All experiments were performed at room temperature.

The total amount of the CTB was calculated from the amount of CTB added. The amount of bound CTB was calculated from the observed LSPR shifts. The individual replicate LSPR shift was obtained by finding the wavelength corresponding to the maximum absorbance given by the seventh order polynomial peak fitting. Then the LSPR shifts of eight replicate wells were averaged to give the observed LSPR shift used to calculate the amount of bound CTB based on the streptavidin-biotin binding calibration. The difference between the total amount of CTB and the amount of bound CTB gave the amount of unbound CTB.

Cryo-TEM measurements

Supported lipid bilayer morphology and quality was assessed by cryo-TEM (FEI Technai G2 F20 FE-TEM with a Gatan Tridiem® GIF-CCD using a Gatan 626 cryo-specimen holder) (**Figure 1c**). Measurements were conducted on silica-coated silver nanoparticles supporting 88 mol%-90 mol% DOPC/10 mol%DOPS/0-2 mol% ganglioside lipid bilayers. The lipid bilayers were coated 1 hour before vitrification and stored in a 1X TBS buffer. The samples were vitrified

on Quantifoil® grids, with holey carbon films (shape R2/2); the sample, suspended in 1X TBS aqueous solution, was rapidly frozen via submersion in liquid ethane and cooled to liquid nitrogen temperature using an FEI Vitrobot®.

Simulation of localized surface plasmon resonance (LSPR)

To simulate the electric field environment near a single silica-coated silver nanocube, the observed particle geometry (from TEM) was used to construct a Finite Element Method (FEM) model in the COMSOL Multiphysics RF Module®. We simulated a quarter cube of side length 112 nm, radius of curvature 12 nm, and silica shell thickness of 4 nm on the sides smoothly transitioning to 3.1 nm on the corners, oriented such that symmetry was imposed in the planes perpendicular to the x and y axes. A plane wave, propagating in the +x direction and polarized along the z-axis, was introduced and then Maxwell's equations were solved for the resulting scattered electric field. The extinction coefficient, which is equal to the extinction spectrum when scaled by path length and particle concentration, was calculated from the scattered field. The simulation was repeated, varying dielectric properties of the model environment, until the refractive index sensitivity calibration experiment was repeated *in silico*.

Statistical analysis and regression

Each data point of each binding curve is represented as the mean ± standard deviation (S.D.) where n=8. Then, the Hill-Waud model was fit to the binding curves. To fit the Hill-Waud model to our data, we used the Levenberg Marquardt iterative algorithm (*fitnlm* function in Matlab 2013b®). The choice of the Levenberg Marquardt function was based on fitting a relatively simple function, desiring fast solution times, and having very precise instrument measurements of the wavelength. The *fitnlm* function returned the calculated value, standard error, and R^2 value presented for each variable in **Table 1**.

Results

Scaled-up Synthesis of Ag@SiO_2 Nanocubes for High-Throughput Detection

Analysis of multivalent ganglioside-CTB interactions required many measurements under different experimental conditions with replication. Therefore, large-scale synthesis of high quality sensors was critical to perform the analysis. The current silver nanocube synthesis is large-scale (allowing up to 20,000 measurements per batch); however, the silica coating process remained at a smaller scale (<5mL batch reactor). The prior protocol required extensive sonication throughout the reaction. However, it was difficult to provide sufficient mixing power in a large batch reactor by sonication. To scale up Ag@SiO_2 synthesis, we modified the prior Stöber silica coating procedures.[74] Instead of ethanol, 2-propanol was used in the silica coating reaction to increase the hydrolysis reaction rate of TEOS.[77] This was necessary as ammonium hydroxide forms an ammonium silver complex that prevents the formation of the SiO_2 shell.[78] Hence, the hydrolysis reaction rate was increased to be competitive with the formation of the ammonium silver complex and improve SiO_2 shell uniformity. In addition to preventing SiO_2 shell formation, the ammonium silver complex occurs preferentially at the exposed [111] crystal plane resulting in etching. The localization of the ammonium silver complex formation is due to the strong adsorption of PVP on [100] facets that prevents/slows the reaction between the silver and ammonium ions.[79] Problematically, etching by the ammonium silver complex results in rounded nanocube corners, reducing electro-magnetic field enhancement and lowering sensor sensitivity. Thus, the increased hydrolysis rate minimized these drawbacks and improved the quality of silica coating in the scaled-up synthesis. (**Figure 21**)

The quality of Ag@SiO_2 nanocubes was determined by TEM. (**Figure 1b and Figure 21**) The refractive index sensitivity of the Ag@SiO_2 sensor was measured by suspending the

sensor in various glycerol-water solutions. (**Figure 2)** In order to confirm the variation of the $Ag@SiO_2$ nanocubes, we modeled the LSPR of the $Ag@SiO_2$ nanocubes based on their geometry observed in TEM images (averaged length 112 nm and corner curvature 12 nm). In **Figure 2,** the experimental sensitivity has been compared with the LSPR simulation. The refractive index sensitivity of the single simulated cube (254±9 nm/RI, mean ± S.E., n=5) was observed to be very similar to the ensemble average of the experimental response (242±4 nm/RI, mean ± S.E., n=20). This simulation result suggested that our nanocube synthesis yielded high quality nanoparticles with low polydispersity.

After characterization of $Ag@SiO_2$, the cubes were covered with a supported lipid bilayer and characterized again. Supported lipid bilayer morphology and quality was imaged by cryo-TEM. (**Figure 1c**) The $Ag@SiO_2$ nanocube was uniformly covered by a continuous supported lipid bilayer with approximately 4nm thickness, which is similar to the known thickness of a lipid bilayer [80].

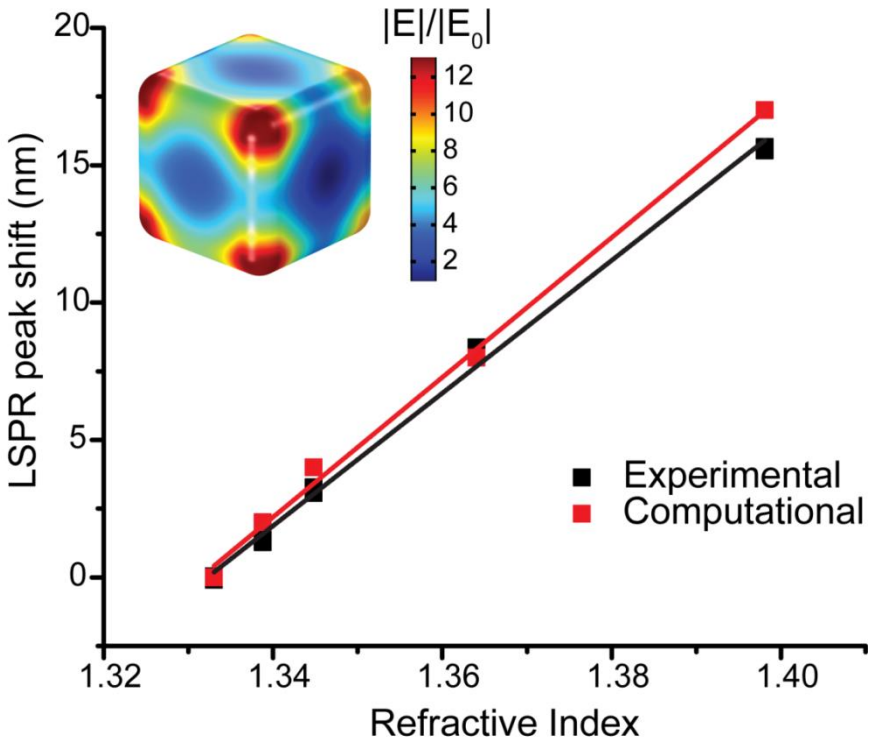

Figure 2: High quality nanocube synthesis and sensor sensitivity confirmed with single particle computational modeling. Refractive Index (RI) vs. change in quadrupole LSPR peak location using a single $Ag@SiO_2$ nanocube simulated in COMSOL Multiphysics and using $Ag@SiO_2$ nanocubes in various glycerol-water mixtures measured with a spectrophotometer. The experimental slope is 242 nm/RI unit ±4 (S.E. of the estimate, n=20). The computational slope is 254 nm/RI ± 9 (S.E., n=5). The details are in the Chapter II Methods Section. (Inset) A computational model of a single $Ag@SiO_2$ nanocube that was simulated in COMSOL Multiphysics® using the Radio Frequency module. Reprinted with permission from Worstell *et al.*[75]

Multivalent Binding Between CTB and GM1 Ganglioside

Cholera toxin subunit B (CTB) binding to the lipid bilayer was measured by observing the shift of the quadrupole LSPR scattering peak of our nanocube based sensor. All measurements were conducted with eight replicates for each protein concentration in a 384 well plate using a high-throughput microplate reader. We followed the protocol reported by Wu et al. to calibrate the correlation between the quadrupole LSPR shift and the protein density by titrating bound streptavidin onto the lipid bilayer containing biotin-PE.[74] (**Figure 22**) This correlation allowed quantification of an absolute bound CTB density on ganglioside presenting surfaces. Control experiments were also carried out on the lipid bilayer with 90 mol% DOPC and 10 mol% DOPS.

To measure the cooperativity of multivalent CTB binding, a classic multivalent binding model, the Hill-Waud binding model (**Equation 1**), was used to fit the equilibrium binding curves.[81]

Equation 1

$$C = \frac{C_{max}[P]^n}{K_h^n + [P]^n}$$

C is the concentration of bound CTB to the cell membrane surface and [*P*] is the concentration of unbound CTB in the solution. The fitted parameters are: C_{max}, the maximum binding capacity of membrane surface; K_h, the apparent dissociation constant; and *n*, the Hill coefficient of cooperativity. If there was no cooperativity between two bound gangliosides, *n* was equal to one. When *n* was larger or smaller than one, it represented positive or negative cooperativity, respectively.

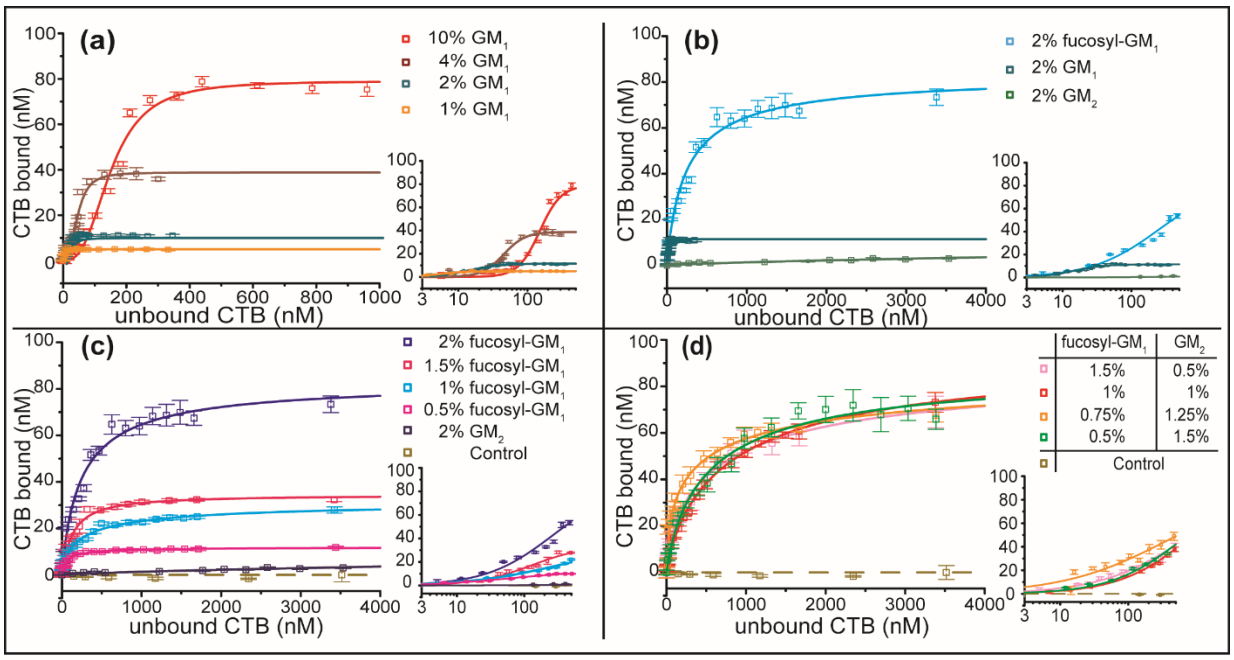

Figure 3: Equilibrium binding data for CTB binding with different gangliosides. The insets represent the same binding curves on semi-log scale to better show the data points at low concentrations**.** (a) CTB-GM1 binding data under differing surface densities. (b) Homogeneous receptor CTB-(GM1-like) ganglioside binding data with constant surface density. (c) CTB-fucosyl-GM1 & CTB-GM2 binding data under differing surface densities. (d) Heterogeneous CTB-ganglioside mixture binding data at constant surface density. A control of 90 mol% DOPC/ 10 mol% DOPS was used to verify the absence of non-specific binding. Data points are reported as mean ± S.D (n=8). Reprinted with permission from Worstell *et al.*[75]

In the GM1 binding experiments, the nanocube sensors were coated with lipid bilayers containing various surface densities of GM1 (1, 2, 4, and 10 mol%) separately for CTB binding. The binding curves were measured by titrating CTB in separate wells of a 384 well plate, with 8 replicates per titration, at each mol% GM1 (**Figure 3a**). The CTB-GM1 binding system provided a good comparison for our nanocube sensor with other established methods because its binding mechanism has been well studied.[63,69,81-85] The fitted parameters of the Hill-Waud equation are shown in **Table 1**. Intuitively, increasing GM1 density increased the binding capacity (C_{max}) of

the bilayer surfaces. We also observed that the K_h of CTB-GM1 binding increased with increasing GM1 mol%. Furthermore, Cremer and his coworkers observed the same phenomena on supported lipid bilayers using fluorescent microscopy.[81,82] They suggested the clustering effect of gangliosides in supported lipid bilayers at higher surface densities inhibits CTB binding.[82] In addition, the positive cooperativity of CTB-GM1 binding was observed from the fitted Hill's coefficients (*n*), and the measured coefficients were similar to the values reported in literature.[81,82]

Table 1: Hill-Waud Equation Fitting Parameters for various ganglioside compositions. Reprinted with permission from Worstell *et al.*[75]

Lipid composition (mol %)				Hill's equation fitting parameters				
DOPC%	DOPS%	GM1%	fucosyl-GM1%	GM2%	K_h±S.E. of the estimate (n=19) (nM)	C_{max} ±S.E. of the estimate (n=19) (nM)	n ±S.E. of the estimate(n=19)	R^2
89	10	1	0	0	5.6 ± 0.6	5.3 ± 0.1	2.25 ± 0.45	0.943
88	10	2	0	0	14.5 ± 1.0	11.5 ± 0.3	1.93 ± 0.25	0.968
86	10	4	0	0	48.0 ± 3.0	41.0 ± 1.8	2.79 ± 0.45	0.959
80	10	10	0	0	151.0 ± 7.0	79.0 ± 2.3	2.79 ± 0.31	0.986
89.5	10	0	0.5	0	59.4 ± 5.7	12.0 ± 0.3	0.78 ± 0.05	0.993
89	10	0	1	0	270.8 ± 56.8	32.5 ± 1.9	0.69 ± 0.06	0.992
88.5	10	0	1.5	0	129.1 ± 13.0	34.4 ± 1.1	1.06 ± 0.09	0.989
88	10	0	2	0	251.8 ± 47.1	83.5 ± 5.3	0.89 ± 0.10	0.985
88	10	0	0.5	1.5	563.4 ± 156.4	88.7 ± 8.5	0.85 ± 0.11	0.982
88	10	0	0.75	1.25	380.4 ± 159.1	91.0 ± 9.1	0.56 ± 0.07	0.978
88	10	0	1	1	830.5 ±114.6	96.6 ±4.9	0.82 ±0.04	0.998
88	10	0	1.5	0.5	682.7 ± 190.5	92.6 ± 7.9	0.69 ± 0.05	0.993

Multivalent Binding Between CTB and GM1-Like Gangliosides

Beyond GM1, other GM1-like gangliosides associated with CTB have been identified. Most of the previous studies identified GM1- and GM1-like ganglioside-CTB binding avidities

with isothermal titration calorimetry (ITC), mass spectrometry (MS), or immobilized receptors on solid substrates.[62-64,83,84,86] Some studies conducted the CTB-ganglioside binding measurements using fluidic lipid bilayers.[44,69,72,81,82,85,87-89] Regardless of measurement technique, these studies often reported the apparent association constants and thermodynamic parameters of CTB binding to various gangliosides, but few of them analyzed the cooperative actions between bound gangliosides. To further investigate cooperative interaction in multivalent CTB binding to GM1-like gangliosides, we selected two gangliosides, fucosyl-GM1 and GM2, which exhibit mild and weak binding avidity to CTB, respectively.

Masserini et al. [89] and Iwabuchi et al. [90] found the binding association constants of CTB with fucosyl-GM1 or GM1 ganglioside were comparable. Several studies reported diverse association binding constants of CTB with GM2, but the binding avidity of GM2 was generally much lower (10~10^5 times weaker) than GM1.[62,83,84,86] To investigate the multivalent binding of these two gangliosides, we measured the binding curves at 2 mol% surface density of each ganglioside and fitted the Hill-Waud equation to the curves. (**Figure 3b** and **Table 1**) The K_h of fucosyl-GM1 was approximately one order of magnitude higher than GM1. A very weak binding of CTB to GM2 was observed. However, we did not reach the plateau region for the GM2 binding curve, as the concentration of CTB was far beyond physiologically relevant conditions.[91] Regardless, this low binding avidity was not surprising because Lauer et al. and MacKenzie et al. could not detect any binding of CTB to fluidic bilayer surfaces with GM2 receptors.[69,85]

We observed the Hill coefficient is usually less than one for fucosyl-GM1, even when accounting for the standard error of the estimate. This indicated that the interaction between bound fucosyl-GM1 and its free counterpart is negatively cooperative. This implies the initially bound receptor lowers the binding avidity for future binding events. The fitted parameters, K_h

and C_{max}, of the GM2 binding curve were not very accurate as these two parameters depend highly on the plateau region of the binding curves. The lower CTB concentration range mainly determined the fitting of n value; hence, the negative cooperativity of GM2 binding was still convincing (n=0.70±0.04, mean ± S.E., n=19). To the best of our knowledge, such negative cooperativity of CTB with GM1-like gangliosides has not yet been reported.

The most surprising observation was that the binding capacity (C_{max}) of fucosyl-GM1 was more than 7 times greater than GM1 at the same surface density (2 mol%). This contrasted with the dissociation constant of GM1, which was more than 16 times lower. To exclude experimental error from degradation of GM1 reagents, we performed the same binding measurements with GM1 gangliosides acquired from three different vendors (Sigma-Aldrich, Avanti, and Matreya LLC). The binding curves of the three GM1 gangliosides across eight replicates were very consistent. (**Figure 23**) These experiments demonstrated that the degradation of GM1 reagent was not the cause of the lower binding capacity of the CTB- GM1 binding system. These data sets also indicated that the experimental variation of our binding measurements was low. The GM1 used for all the other experiments was obtained from Matreya LLC.

The Influence of Cooperativity on Binding Capacity

To the best of our knowledge, the unusually high binding capacity observed for fucosyl-GM1 has not been reported. Based on the fitting of the Hill-Waud model, we found that the major difference between GM1 and fucosyl-GM1 was the Hill coefficient of cooperativity, n. We suspected the reduced cooperativity of fucosyl-GM1 binding led to the higher observed binding capacity. To understand the binding mechanism, we explored a stepwise binding mechanism of CTB. Klassen and his coworkers used direct electrospray ionization mass

spectrometry (ESI-MS) to investigate the stepwise binding of GM1 to CTB. [64] They established a comprehensive stepwise binding model (**Figure 24**) and determined the apparent association constants for three different states (K_1, K_2, K_3), including zero, one, or two receptor-bound nearest neighbors.[64] The binding affinity was enhanced by a factor of approximately two when there was a bound GM1 next to the binding pockets. This comprehensive, single receptor binding model allowed us to explore the detailed binding mechanism by calculating the concentration of each binding state.

We modeled Klassen's stepwise binding and calculated the concentration of each CTB-GM1 bound state under different CTB concentrations. The equation we adapted from Klassen's model is summarized in APPENDIX A. The association constants of fucosyl-GM1 for each individual state were not measured, so we added a factor 'α' to estimate, from initial binding (K_1), the affinity of the CTB binding subunit when there are one (K_2) or two (K_3) bound gangliosides as the nearest neighbors. $\alpha > 1$ represented positively cooperative binding and $\alpha < 1$ represented negatively cooperative binding. Using the empirical values obtained by Klassen et al., $\alpha \approx 2$ for GM1, indicating positive cooperativity. This theoretical model demonstrated that receptors with reduced cooperativity compared with GM1 ($\alpha < 2$) could reach a higher binding capacity than GM1 ($\alpha \sim 2$), despite having the same initial binding affinity (K_1). (**Figure 4a**) Since the overall K_d was higher for fucosyl-GM1 (**Table 1)**, it was reasonable to conclude that K_1 of fucosyl-GM1 would be less than the K_1 for GM1. To reflect this qualitatively, we changed the value of K_1 to half of its original value to see if that altered our observation. (**Figure 25**) Despite this change, we observed that the binding capacity continued to be higher for receptors with lower cooperativity. To understand this unusual behavior, we calculated the concentration of CTB in each bound CTB state. (**Figure 26**) We found the model predicted that the number of

CTB molecules binding with two or more gangliosides was higher when the binding cooperativity was positive. For positive cooperativity, the bound gangliosides enhanced the binding affinity of unbound binding subunits, making the second and higher order binding events more favorable. In contrast, the average number of lipids per CTB was closer to one when the binding was negatively cooperative. As shown in plotted model data in **Figure 4b,** the average number of bound ganglioside receptors per CTB increased when cooperativity increased. This meant that the model predicted a single CTB bound more gangliosides and reduced the number of free gangliosides available on the lipid bilayer during positively cooperative binding. Therefore, the total binding capacity of positive cooperative binding was lower. Recently, Klassen and his coworkers reported a similar phenomenon using nanodisc-ESI-MS technology.[72] They found that the majority of CTB molecules bound to only one ganglioside when three gangliosides, GM1, GM2, and GM3, were incorporated in separate nanodiscs. If three gangliosides were mixed in a single nanodisc, most CTBs bound to two gangliosides. We believe the reduced cooperativity, relative to GM1, of GM1-like gangliosides led to their experimental findings. Our theoretical analysis of the stepwise binding model has demonstrated that cooperativity significantly influences binding capacity. Thus, the unusually high binding capacity of fucosyl-GM1 might be attributed to its lower cooperativity.

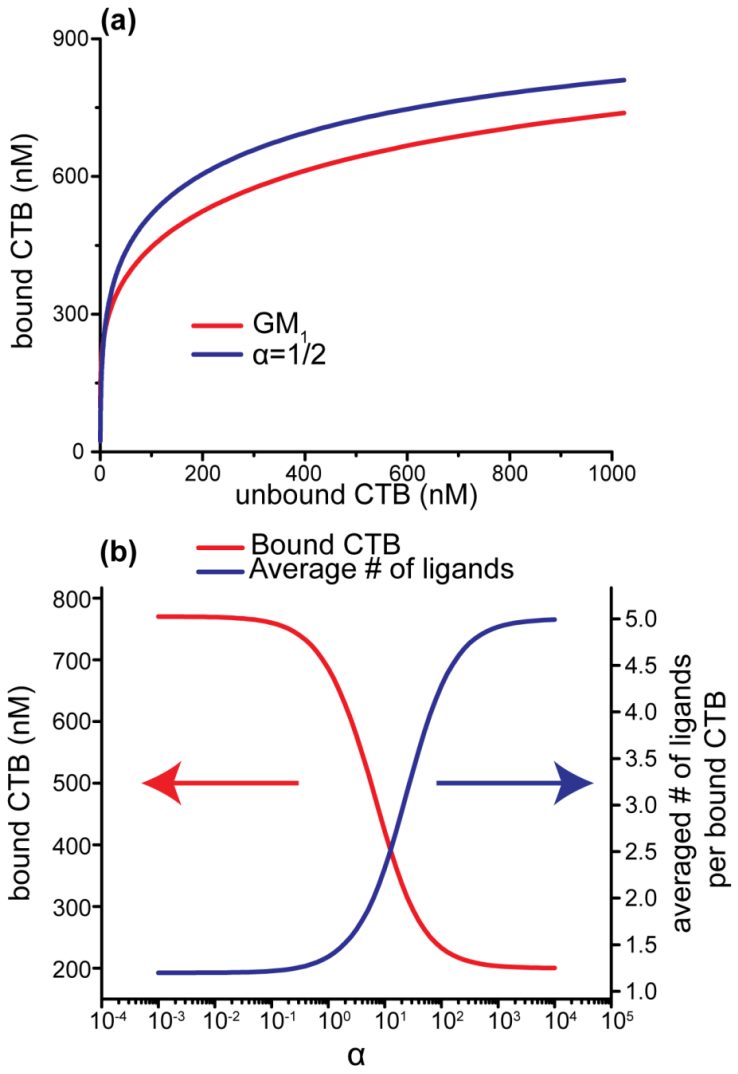

Figure 4: Simulated binding with varying cooperativity based on Klassen's theoretical model. (a) Total bound CTB as a function of unbound CTB for varying cooperativity ratios. The negative cooperativity ($\alpha = ½$) could reach a higher binding capacity than GM1 ($\alpha \sim 2$) (b) Bound CTB and average number of ganglioside receptors per bound CTB molecule as a function of the affinity scaling factor, α, with an unbound CTB concentration of 500 nM. Reprinted with permission from Worstell *et al.*[75]

The Influence of Mixed Gangliosides on Multivalent Binding

After demonstrating that cooperative interaction between molecules of a single ganglioside type significantly influences multivalent binding, we hypothesized that cooperative interaction between heterogeneous gangliosides might also play an essential role in CTB binding mechanisms. In order to test this hypothesis, we mixed weak and mild binding gangliosides, GM2 and fucosyl-GM1, under different surface densities to investigate their cooperative interactions. The total surface density of GM2 and fucosyl-GM1 was fixed at 2 mol% and we varied the ratio of these two gangliosides (0.5 mol%/1.5 mol%, 0.75 mol%/1.25 mol%, 1 mol%/1 mol%, and 1.5 mol %/0.5 mol % of GM2/fucosyl-GM1). For comparison, we also measured the binding curve of individual fucosyl-GM1 at 0.5, 1.0, 1.5, and 2.0 mol% surface density. The binding curves and the fitted Hill-Waud parameters were recorded in **Figure 3b** and **Table 1**. It is important to recognize that the K_h and n values do not carry the same physical meaning when commuted to the two-component binding model. This is because the Hill-Waud model was derived from single-receptor system (hemoglobin-oxygen binding). This means that a two-component fitted Hill-Waud model is an empirical model. Thus, K_h and n values must be considered apparent terms representing the combined effects of the two components; this limits any conclusions that could be drawn from a thermodynamic analysis of the fitted model. Due to these limitations, we do not refer to C_{max} when referencing the two-component system, but rather refer to the binding capacity observed at the highest tested concentration, 3.4 μM unbound CTB ($C_{3.4\mu M}$). By this measure, we can draw direct comparisons to the pure component systems.

As expected, without GM2, reducing fucosyl-GM1 surface density on the membrane surface reduced the maximum binding capacity (C_{max}). The dissociation constant also decreased at lower fucosyl-GM1 surface density. The same trend was observed in our GM1 measurements

and the GM1 measurements reported by Cremer and his coworkers.[81] Interestingly, the additional GM2 gangliosides compensated for the loss of fucosyl-GM1 (for the tested conditions) and the highest observed CTB binding ($C_{3.4\mu M}$) for GM2/fucosyl-GM1 mixtures reached values similar to $C_{3.4\mu M}$ for 2 mol% fucosyl-GM1. If CTB binding to GM2 and fucosyl-GM1 were independent, the $C_{3.4\mu M}$ for GM2/fucosyl-GM1 mixtures should equal the sum of the $C_{3.4\mu M}$ values for equivalent single-receptor bilayers containing GM2 or fucosyl-GM1. This is not the case. For instance, the total bound CTB at 3.4μM ($C_{3.4\mu M}$) on 1.5 mol% GM2/ 0.5 mol% fucosyl-GM1 surface is approximately 7 times higher than the summation of pure component systems. These data sets suggested the multivalent binding depends on the complex pattern of gangliosides.

Discussion

We performed direct measurements to demonstrate the essential nature of binding cooperativity in pentavalent CTB binding to gangliosides on lipid bilayer surfaces. Our stepwise reaction analysis confirmed the higher binding capacity of fucosyl-GM1 compared to GM1, and suggested that this might be induced by the reduced binding cooperativity of fucosyl-GM1. The observed binding capacity ($C_{3.4\mu M}$) of the membrane with the GM2/fucosyl-GM1 mixture also markedly increased compared to the summed total binding capacity of equivalent membranes with a single type of ganglioside. This change may indicate a conformational change induced by either fucosyl-GM1 or GM2 to alter binding preferences and/or inter-subunit distances. The other possible explanation is the reduction in membrane fluidity, which can improve CTB binding as observed by Terrell et al.[88] However, this seems less likely than cooperative interactions between fucosyl-GM1 and GM2 because the total ganglioside surface density was maintained at 2 mol% and both gangliosides have very similar molecular structures. Thus while

we cannot identify the exact mechanism, we are reasonably certain that cooperativity between fucosyl-GM1 and GM2 can significantly enhance the bound CTB concentration.

Biologists have also observed unexpected binding between CTB and mixed gangliosides.[22,23,92] In the past, CTB has been used to quantify the amount of GM1 that was present in a cell membrane [23,93], but the validity of this approach was refuted by Yanagisawa et al.[22] In the absence of GM1, Yanagisawa et al. observed strong reactivity between CTB and embryonic neuroepithelial cells and attributed this phenomenon to the expression of GM1- like ganglioside.[22] More recently, some studies have used local CTB concentration differences as a means to identify and/or quantify lipid rafts.[94,95] However, it was recommended that this approach be combined with other methods before asserting the presence of lipid rafts based on CTB binding to multiple gangliosides.[23,90] Thus, for CTB to be used in quantification and/or identification of GM1, the analysis must be combined with another analysis method, such as MS/MS or ITC, or a tool that can differentiate between binding of CTB to different gangliosides and account for cooperativity.

Similar cooperativity may appear in the other multivalent GBPs (e.g. lectins). Lectins, often consisting of multiple identical binding subunits, are widely used in glycomic analysis (e.g. lectin microarray or cell staining).[19,96-98] From conventional glycoarray analysis, it is known that some lectins preferentially bind to the same glycan structure; however, their binding specificities to a heterogeneous cell surface are very different. For instance, Galβ-GalNAc is the preferred glycan binding structure for *Amaranthus caudatus* lectin, *Agaricus bisporus* lectin, *Colchicum autumnale* lectin, *Maackia Amurensis* lectin I, and *Phytolacca americana* lectin, but these lectins exhibited varying binding specificities to different types of cells.[96] We hypothesize the cooperative efforts among heterogeneous glycans may contribute to lectin binding specificities.

Hence, in order to understand hetero-multivalent binding, a new analytical tool is of critical importance.

Cooperative binding between heterogeneous glycan structures is difficult to observe by conventional glycan microarray analysis because glycan microarrays often detect only the interactions with isolated glycans. Although some studies have printed mixed glycans on solid substrates[35,36], immobilized glycans cannot achieve optimal multivalent binding with proteins. Therefore, there is a need for our nanocube-based sensor with gangliosides inserted into a fluidic supported lipid bilayer that enables the detection of hetero-multivalent binding. Combined with glycolipid synthesis, such as neoglycolipid (NGL) technology[99], the nanocube-based lipid bilayer array can be an attractive tool for studying GBP-glycan recognition.

Our sensing platform greatly improves on traditional methods by taking advantage of supported lipid bilayer technology. Our platform is also an improvement on current fluidic bilayer methods in several ways. First, our nanocube-based sensor is inexpensive. Second, our assay is compatible with high-throughput analysis methods, allowing thorough study of complex binding systems. Third, our nanocube-based lipid bilayer array is compatible with common laboratory equipment, enabling widespread use while still maintaining sensitivity.

Chapter Conclusion

Using our nanocube-based system, we were able to experimentally elucidate the relationship between cooperativity and maximum CTB-ganglioside binding and the effects of mixing multiple recognized gangliosides in a single lipid bilayer system. Through experimental measurements and representative stepwise binding analysis, we demonstrated that binding cooperativity is essential in multivalent CTB binding. The attenuation or enhancement of CTB binding was shown not to simply be controlled by any one of the gangliosides; the reactivity

depended on cooperative interactions within the entire ganglioside complex. This analysis required many replicates and individual experimental conditions, despite only analyzing a single two component cross-reactivity test. We were able to obtain all of these data with replicates because of our highly accessible and high-throughput nanocube-based lipid bilayer array that can be leveraged by biological communities to dissect additional complex binding models of multivalent binding proteins.

CHAPTER III

HETERO-MULTIVALENT BINDING OF CHOLERA TOXIN SUBUNIT B WITH GLYCOLIPID MIXTURES*

Chapter Summary

GM1 has generally been considered as the major receptor that binds to cholera toxin subunit B (CTB) due to its low dissociation constant. However, using a unique nanocube sensor technology, we have shown that CTB can also bind to other glycolipid receptors, fucosyl-GM1 and GD1b. Additionally, we have demonstrated that GM2 can contribute to CTB binding if present in a glycolipid mixture with a strongly binding receptor (GM1/fucosyl-GM1/GD1b). This hetero-multivalent binding result was unintuitive because the interaction between CTB and pure GM2 is negligible. We hypothesized that the reduced dimensionality of CTB-GM2 binding events is a major cause of the observed CTB binding enhancement. Once CTB has attached to a strong receptor, subsequent binding events are confined to a two-dimensional membrane surface. Therefore, even a weak GM2 receptor could participate in second or higher order binding events because its surface reaction rate can be up to 10^4 times higher than the bulk reaction rate. To test this hypothesis, we altered the surface reaction rate by modulating the fluidity and heterogeneity of the model membrane. Decreasing membrane fluidity reduced the binding cooperativity between GM2 and a strong receptor. Our findings indicated a new protein-receptor binding assay, that can mimic the complex cell membrane environment more accurately, can be used to explore the inherent hetero-multivalency of the cell membrane. We have thus developed a new

*Reprinted with permission from "Hetero-multivalent Binding of Cholera Toxin Subunit B with Glycolipid Mixtures" by Krishnan, Pratik, Singla, Akshi, Lee, Chin-An, Weatherston, Joshua D., Worstell, Nolan C., Wu, Hung-Jen, 2017, *Colloids and Surfaces B: Biointerfaces*, 160,281-288, Copyright 2017 by Elsevier B.V.

membrane perturbation protocol to efficiently screen receptor candidates involved in hetero-multivalent protein binding.

Introduction

Many proteins recognize glycolipid receptors in cell membranes via multivalent binding mechanisms.[13] Such dynamic binding, driven by a series of binding domains, brings a protein to a membrane surface and initiates biological processes. Interactions between a single glycolipid receptor and a protein binding subunit are often weak, and therefore multivalency enhances the protein binding avidity and specificity to cell surfaces. Cholera toxin (CTx), the virulence factor of *Vibrio cholerae*, is a type of multivalent glycolipid binding protein. This AB_5 toxin consists of a single A subunit associated with five identical B subunits. The B pentamer binds to cell membranes and delivers the catalytic A subunit into the cytoplasm. A potential stepwise reaction of pentavalent cholera toxin subunit B (CTB) binding to the cell membrane[13,100] is shown in **Figure 5**. (1) CTB moves from the solution phase to the membrane surface, followed by one of its binding sites attaching to a glycolipid receptor; (2) Free glycolipids diffuse two dimensionally, encounter the bound CTB, and then enable subsequent binding. The synergistic effort amongst various binding pockets, membrane receptors, and membrane dynamics dramatically influences the overall association.[101]

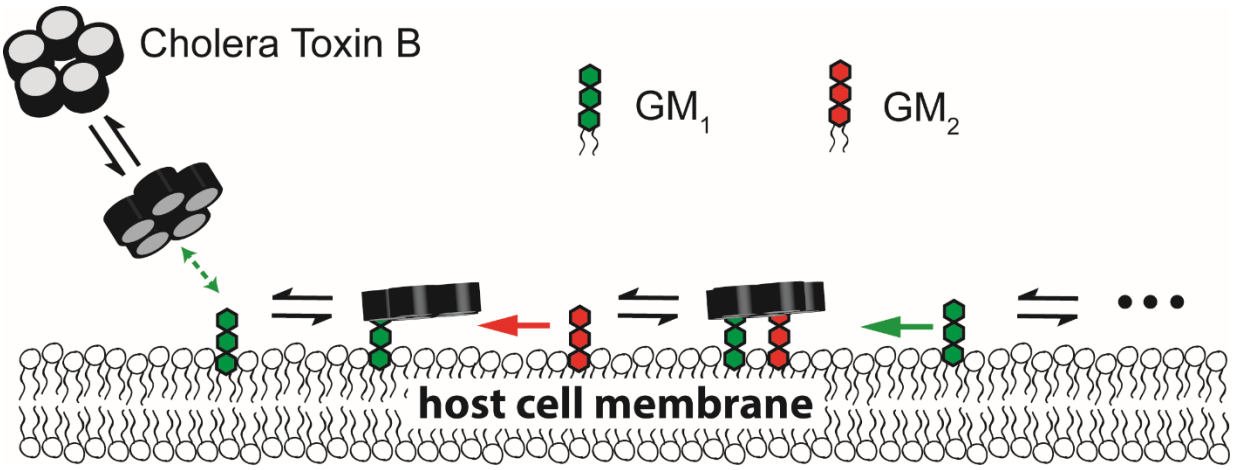

Figure 5: A schematic of the proposed CTB binding mechanism. CTB first diffuses from the solution phase to a membrane surface. One of its binding subunits finds a strongly binding receptor and then forms a relatively stable membrane bound state. Free glycolipid receptors diffuse two dimensionally, encounter the bound CTB, and then enable subsequent binding. The reaction rate on the two-dimensional membrane surface is significantly higher than the rate in three-dimensional bulk solutions. Thus, a weakly binding receptor, such as GM2, can participate in subsequent binding, leading to an enhanced binding capacity. Reprinted with permission from Krishnan *et al*.[18]

We recently developed a unique nanocube sensor by integrating supported lipid bilayer and plasmonic sensing technologies.[51] This new tool has enabled label-free detection of protein binding to model membrane surfaces using a standard laboratory spectrophotometer to observe the extinction spectrum shift of the quadrupolar localized surface plasmon resonance (LSPR) peak.[75] The nanocube sensor was used to investigate the multivalent binding principle of CTB interacting with various glycolipids.[75] We observed that the amount of CTB binding onto the surface containing fucosyl-GM1 was higher than GM1 although the dissociation constant of GM1 was an order of magnitude lower than that of fucosyl-GM1. This unintuitive result might be attributed to a reduced binding cooperativity between fucosyl-GM1 receptors leading to an

increased binding capacity.[75] Our previous findings indicated that dissociation constants cannot exclusively represent multivalent CTB bindings and that binding cooperativity also plays an essential role in determining CTB-cell membrane recognition.

Multivalent binding can be either homo-multivalent (i.e. a protein binds to multiple copies of the same type of receptor) or hetero-multivalent (i.e. a protein simultaneously binds to two or more different types of receptors).[102] Due to the complexity of hetero-multivalency, most studies have focused on homo-multivalency. However, homo-multivalent models neglect the inherent heterogeneity of cell membranes. We recently reported that adding a weak glycolipid receptor (GM2) to a model membrane containing fucosyl-GM1 significantly increased the total amount of bound CTB.[75] This was unexpected, as GM2 receptors have negligible binding avidity in bilayers with GM2 as the only glycolipid receptor. A few other studies have also reported that lectin binding to glycan mixtures is stronger than the binding to a single glycan.[34-37] However, the mechanism of such hetero-multivalency is not clear.

The goal of this study was to gain insight into the mechanism of hetero-multivalent CTB binding. We first investigated the binding cooperativity of CTB to various glycolipid mixtures. Positive cooperativity was observed when GM2 was mixed with any of the other three strongly binding receptors (GM1, fucosyl-GM1, and GD1b). We hypothesized that the increase of CTB binding is caused by a reaction rate enhancement mechanism, "reduction of dimensionality". (**Figure 5**) Once CTB has attached to a strong receptor, subsequent binding events are confined on the two-dimensional membrane surface. Therefore, even a weak GM2 receptor could now participate in second or higher order binding events because its surface reaction rate is around 10^4 times higher than the rate in the bulk solution. To test this hypothesis, we modulated the fluidity and heterogeneity of the model membrane by adding cholesterol or altering the fatty acid

composition of phospholipids and observed significant changes in the heterogeneous binding cooperativity. This complies with the surface reaction's strong dependence on the membrane environment. Our results indicated that the traditional protein binding assay, which detects protein interactions with a specific receptor one by one (e.g. microarray technology), is not appropriate to explore multivalent binding interactions. To discover all possible receptors that could participate in a binding process, we designed a new membrane perturbation protocol that can efficiently screen possible glycolipid receptors involved in multivalent protein binding.

Materials & Methods

Materials

Monosialoganglioside GM1 (NH_4^+salt) (Galβ1-3GalNAcβ1-4(Neu5Acα2-3)Galβ1-4Glc-Ceramide, GM1), monosialoganglioside GM2 (NH_4^+salt) (GalNAcβ1-4(Neu5Acα2-3)Galβ1-4Glc-Ceramide, GM2), monosialoganglioside GM3 (NH_4^+salt) (Neu5Acα2-3Galβ1-4Glc-Ceramide,GM3), fucosylated monosialoganglioside GM1 (NH_4^+salt) (Fucα1-2Galβ1-3GalNAcβ1-4(Neu5Acα2-3)Galβ1-4Glc-Ceramide, fucosyl-GM1) and disialoganglioside GD1b (NH_4^+salt) (Galβ1-3GalNAcβ1-4(Neu5Acα2-8)(Neu5Acα2-3)Galβ1-4Glc-Ceramide,GD1b) were purchased from Matreya LLC (State College, PA). 1,2-dioleoyl-sn-glycero-3-phosphocholine (DOPC), 1,2-dioleoyl-sn-glycero-3-phospho-L-serine - sodium salt (DOPS), 1,2-dimyristoyl-sn-glycero-3-phosphocholine (DMPC) and 1,2-dimyristoyl-sn-glycero-3-phospho-L-serine – sodium salt (DMPS) were obtained from Avanti Polar Lipids (Alabaster, AL). Cholera Toxin subunit B (CTB, lyophilized powder) from *Vibrio cholerae*, cholesterol and casein from bovine milk were purchased from Sigma-Aldrich. GM1 oligosaccharide (GM1os) (Galβ1-3GalNAcβ1-4(Neu5Acα2-3)Galβ1-4Glc) sugar was purchased from Elicityl (Crolles,

France). All the CTB binding experiments were performed in Tris-buffered saline-TBS (Sigma Aldrich).

Methods

Synthesis and calibration of the nanocube sensor

Silica coated silver nanocubes were prepared as reported in our previous publication.[75] The silver nanocube synthesis was based on the polyol method. The synthesis of the silica shell on the nanocubes was performed in a scaled-up synthesis batch using 2-propanol as the solvent. The quality of the nanocube sensor, including silica shell thickness, nanocube size and uniformity, was confirmed by transmission electron microscopy (FEI Technai G2 F20 FE-TEM). (**Figure 27**) The refractive index sensitivity of silica coated silver nanocubes was reported as peak shift (reported in nm) per refractive index unit (RIU). (**Figure 28**) Since the change in refractive index is directly proportional to the amount of bound proteins, LSPR peak shift allows an estimation of the amount of protein bound.[51]

Supported lipid bilayer preparation

Lipids stored in organic solvents (chloroform for DOPC, DOPS, DMPC, and DMPS or a chloroform/methanol/water mixture for glycolipids) were mixed to obtain the desired final composition. They were then dried using a rotary evaporator (Heidolph Hei-VAP Value®), followed by rehydration with Milli-Q® water. Small unilamellar vesicles (SUVs) were prepared by the standard extrusion protocol described in our prior publication.[75] A previously established modified vesicle fusion technique[75] was used to form supported lipid bilayers. The lipid bilayer coated nanocubes were incubated with 0.5 mg/ml casein in 1X TBS solution for 1 hour to prevent nonspecific binding of CTB.

CTB binding measurement

The lipid bilayer coated nanocubes were incubated with the required CTB concentration for 1.5 hours. Blank solutions were also prepared for each CTB concentration by mixing buffer and CTB corresponding to that composition. The extinction spectra of the solutions were measured in a 384 well plate with a UV/Vis microplate spectrophotometer equipped with a CCD (FLUOstar Omega®, BMG-Labtech). All measurements were carried out at room temperature, except the membrane fluidity experiment involving DMPC. The location of the quadrupolar LSPR peak was calculated by fitting the measured absorption spectra to a seventh order polynomial. Each protein binding measurement was repeated in eleven wells. Each data point is represented as the mean ± standard deviation (S.D.) where n = 11. The experimental conditions for each binding measurement are described below.

Combinatorial glycolipid array

To acquire binding curves for the pure glycolipid systems (1 mol% glycolipid along with 89 mol% DOPC and 10 mol% DOPS), the CTB concentration was varied from 0 to 1726 nM. For the binary mixture of glycolipids (1 mol% of each glycolipid along with 88 mol% DOPC and 10 mol% DOPS), the CTB concentrations used were 706 nM and 1726 nM.

GM1os pre-bound CTB binding experiment

345 nM CTB was incubated at various sugar (GM1os) concentrations (0 ~ 38.1 μM) prior to the binding measurement. The resulting GM1os-CTB complex was incubated with the bilayer containing 2 mol% glycolipid along with 88 mol% DOPC and 10 mol% DOPS.

Membrane perturbation protocol

The reference bilayer comprised of 0.25 mol% of each glycolipid (GM1, GM2, GM3, fucosyl-GM1 and GD1b), 10 mol% DOPS and 88.75 mol% of DOPC. For the perturbed membranes, one of the glycolipids was increased to 2 mol% while other glycolipids were maintained at 0.25 mol% along with 10 mol% DOPS and 87 mol% DOPC. Each experiment was treated with 0.5 mg/ml Casein in 1X TBS buffer to block non-specific binding and then incubated with 1726 nM CTB for 2 hours.

Results

CTB Binding to Glycolipid Pairs

Our previous study demonstrated that mixing GM2, a weak binding receptor, with fucosyl-GM1 could enhance the overall CTB binding.[75] In order to understand the mechanism of this hetero-multivalency, we constructed a combinatorial array of glycolipids to evaluate the cooperativity of CTB binding. The array was composed of glycolipids like GM1, GM2, GM3, fucosyl-GM1, and GD1b. (**Figure 6**) We first examined CTB binding to model membranes containing 1 mol% of a glycolipid. (**Figure 6b**) The shift in the location of the LSPR peak with respect to the control is directly proportional to the amount of CTB bound. CTB exhibited significant binding to the bilayers containing GM1, fucosyl-GM1, or GD1b. (**Figure 6b**) GM2 and GM3 showed negligible binding with CTB even at the highest CTB concentrations (1726 nM); this result was consistent with prior studies.[84,103,104] Thus, we categorized GM1/fucosyl-GM1/GD1b as strongly binding receptors and GM2/GM3 as weakly binding receptors.

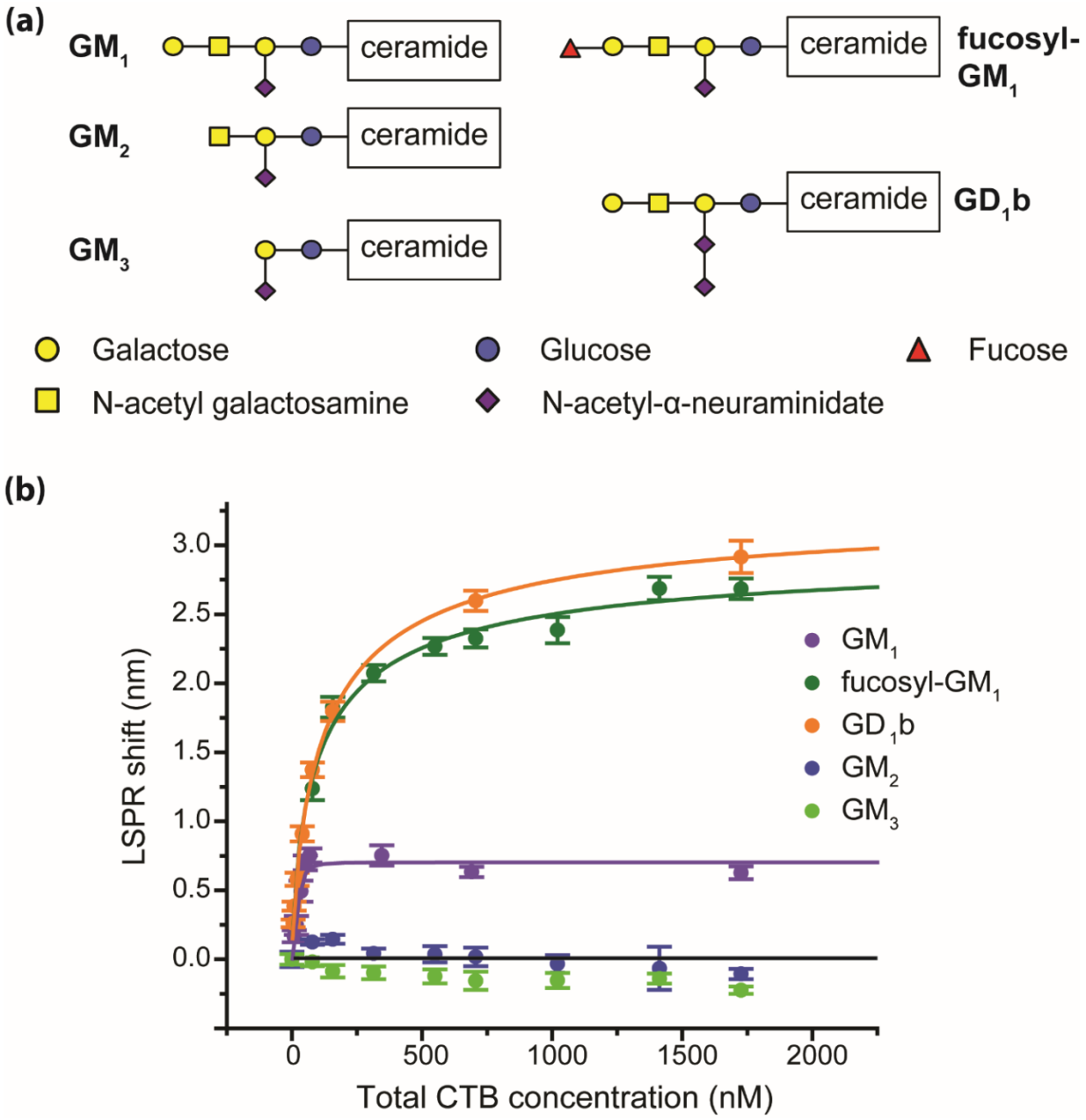

Figure 6: Homo-multivalent CTB binding. (a) Structures of glycolipids used in the study. (b) Equilibrium binding of CTB to pure glycolipids. The glycolipid composition in each case was 1 mol%. Data points are reported as mean ± S.D (n = 11). Reprinted with permission from Krishnan *et al.*[18]

The combinatorial array was prepared by mixing two glycolipids in a 1:1 ratio (1 mol% of each glycolipid). The amount of CTB bound to the glycolipid mixtures was measured at two different CTB concentrations (706 nM and 1726 nM). From the CTB-glycolipid binding curves (**Figure 6b**), we can see that CTB binding to the model membrane is approximately saturated at 1726 nM. Thus, we used this value to estimate the maximum binding capacity of the model membrane. We also measured the CTB binding at a lower CTB concentration (706 nM) to observe the influence of CTB concentration on binding cooperativity.

To quantify the binding cooperativity of hetero-multivalency, we have defined heterogeneous binding cooperativity (θ) as:

Equation 2

$$\theta = \frac{\text{LSPR shift when CTB binds to a bilayer containing paired glycolipids}}{\text{Sum of LSPR shift when CTB binds to a bilayer containing each individual glycolipid}}$$

If there is no cooperativity between two glycolipids, θ should equal 1. When θ is larger or smaller than 1, it represents positive or negative cooperativity, respectively. The calculated heterogeneous cooperativity was reported in **Table 2**. We observed positive cooperativity when GM2 was mixed with any of the strongly binding receptors (GM1, fucosyl-GM1, and GD1b) at both CTB concentrations. Since negligible CTB binding was observed with the model membrane surface containing GM2 as the only glycolipid receptor, the strongly binding receptors seemed to have activated GM2 receptors, which led to a higher CTB binding. However, no significant cooperativity was observed when GM3 was mixed with strongly binding receptors. In addition, cooperative action between strong receptors was negligible.

Table 2: Calculated heterogeneous binding cooperativity between two glycolipids. Column and row headings represent the mixture of two glycolipids. Each cell contains two values that represent the calculated cooperativity at the two CTB concentrations, 706 nM (top)/1726 nM (bottom). Cooperativity values are reported as mean ± S.D (n = 11). The raw data of CTB binding was reported in **Figure 29** and **Figure 30**. Reprinted with permission from Krishnan *et al*.[18]

GM1	fucosyl-GM1	GD1b	GM2	GM3	
	1.08 ± 0.03 1.12 ± 0.03	0.92 ± 0.02 1.05 ± 0.04	1.46 ± 0.17 1.99 ± 0.28	1.16 ± 0.26 0.92 ± 0.20	GM1
		0.94 ± 0.02 1.10 ± 0.03	1.57 ± 0.07 1.54 ± 0.09	1.19 ± 0.06 1.11 ± 0.04	fucosyl-GM1
			2.06 ± 0.08 1.96 ± 0.10	1.05 ± 0.05 0.98 ± 0.05	GD1b
				1.00 ± 0.77 1.00 ± 0.12	GM2
					GM3

Possible Causes of Heterogeneous Cooperativity

To the best of our knowledge, positive cooperativity between GM2 and other glycolipid receptors has not yet been reported. Several possible reasons may cause this heterogeneous cooperativity, including induced glycolipid cluster formation, allosteric regulation, and reduction of dimensionality. Each hypothesis is considered and discussed in the following paragraphs.

Cremer and his coworkers have demonstrated that increasing GM1 density in a model membrane induces the formation of GM1 clusters, leading to weaker CTB binding.[105] If mixing GM2 had induced the disturbance of glycolipid clusters leading to increased CTB binding, the addition of other glycolipids should have altered the clustering of glycolipid receptors as well and caused some change in binding cooperativity. However, we observed cooperative interactions only between GM2 and other strongly binding glycolipids. Furthermore, the

glycolipid concentration was kept relatively low (less than 2 mol%) to minimize any heterogeneous distribution of glycolipids on the membrane surface. Therefore, we believe that it is less likely for induced heterogeneity to be the major cause of positive cooperativity.

Allosteric regulation is another possible cause of positive cooperativity. The bound glycolipids (GM1/fucosyl-GM1/GD1b) could have enhanced the binding energy between GM2 and its adjacent binding sites, enabling GM2 to participate in the CTB binding process and leading to a higher binding capacity. (**Figure 7a**) To test this hypothesis, we modified the saturation binding assay developed by Leach et al. for detection of allosteric interactions.[106] Klassen and his coworkers have reported that at the equilibrium state CTB forms a binding complex with GM1 oligosaccharide (GM1os), an allosteric modulator that contains the same glycan structure as the GM1 glycolipid without its ceramide tail.[107] We first incubated CTB with various concentrations of GM1os oligosaccharide. Then, we measured the binding of the GM1os-CTB complex to a model membrane containing 2 mol% glycolipid (GM2 or fucosyl-GM1) at a fixed CTB concentration (345 nM). (**Figure 7b**) If the bound GM1os had altered the energetics of the adjacent CTB binding subunit, the allosteric effect should have initiated the attachment of the GM1os-CTB complex to the membrane containing GM2. Instead, negligible CTB binding to the lipid bilayer having GM2 was still observed. For the lipid bilayer containing 2 mol% of fucosyl-GM1, the amount of bound GM1os-CTB complex decreased with increased GM1os concentration. (**Figure 7b**) This is due to competitive binding between GM1os and fucosyl-GM1 receptors. In addition, three different research groups independently evaluated the allosteric effect of GM1os-CTB binding and found that the affinity constants increased by only twofold when the neighboring binding sites were occupied.[104,107,108] Turnbull et al. have estimated the dissociation constant for CTB binding with GM2 to be 2 mM.[104] Thus, even a

twofold enhancement of the affinity constant (leading to an ~1mM dissociation constant) is not sufficient to promote CTB binding to GM2 at physiological concentrations. Although we cannot completely exclude allosteric regulation between GM2 and other strong receptors, it is probably not the major cause for the observed positive cooperativity.

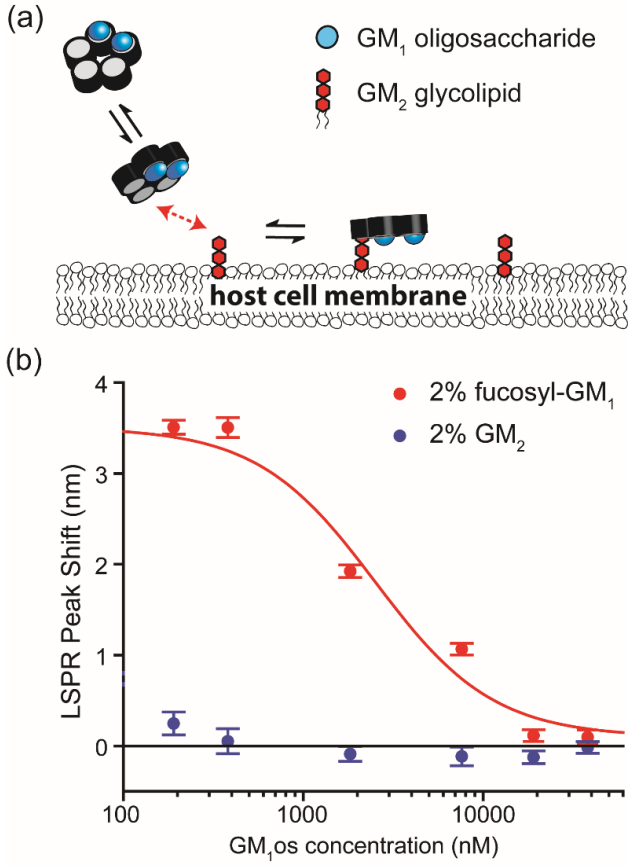

Figure 7: Evaluation of allosteric effect. (a) A schematic of the allosteric regulation hypothesis. CTB was incubated with GM1os to form a GM1os-CTB complex. Then, this GM1os-CTB complex was bound to a model membrane containing GM2. If GM1os modulated the energetics of the adjacent CTB binding pocket, the attachment of the GM1os-CTB complex to the membrane containing GM2 should be detectable. (b) Binding of the CTB-GM1os complex to membrane surfaces containing 2 mol% fucosyl-GM1 and 2 mol% GM2. Binding of the CTB-GM1os complex to the GM2 surface was still negligible; thus, allosteric regulation may not be a major cause of the enhanced CTB binding. Reprinted with permission from Krishnan *et al.*[18]

Another possible cause for positive heterogeneous cooperativity is the influence of reduced dimensionality. Searching for reaction partners is much more efficient on a two-dimensional membrane surface than in three-dimensional space. In 1968, Adam and Delbrück first proposed that organisms can shorten the diffusion time of dilute reactants by adsorption to cell membrane surfaces in order to enhance the reaction rates of the biological processes.[109] Many researchers have validated this concept and provided a comprehensive theory to describe this mechanism.[110-115] Recently, Sengers et al. also reported that reduced dimensionality can improve the binding efficiency of a bivalent monoclonal antibody interaction with membrane bound targets by about 10^4-fold.[116] Thus, it is possible that reduction of dimensionality enhanced CTB binding to GM2.

The Influence of Reduced Dimensionality

We hypothesized that CTB first moves from the solution phase to the membrane surface and attaches to one of the strongly binding receptors (GM1, fucosyl-GM1, and GD1b). Jobling et al. have shown that a single active binding site on the CTB pentamer is sufficient for cell binding and intoxication;[117] therefore, we expected CTB could form a relatively stable membrane-bound state with a single strongly binding receptor. (**Figure 5**) Once CTB is anchored to the surface, the effective concentration of GM2 on the two-dimensional membrane surface dramatically increases for subsequent bindings. Although the weak binding between GM2 and CTB implies a short lifetime of the CTB-GM2 complex, the enhanced effective concentration allows GM2 to continuously participate in the process of bind to CTB leading to an increase in binding capacity. This hypothesis requires the presence of a strongly binding receptor in order to anchor CTB to the membrane surface.

In order to verify this hypothesis, we first evaluated the two-dimensional and three-dimensional reaction rates using established theoretical models.[113-115] The reaction rate, ϕ, can be written as[114]:

Equation 3

$$\phi = k_{obs} C_A C_B$$

where C_A and C_B are the number densities of the two reactants, and k_{obs} is the empirical rate constant. In diffusion controlled reactions, k_{obs} is a function of diffusion coefficients ($D_{3D\ or\ 2D}$), the radius of diffusion spaces (b), and the encounter radius of the target receptor (a). Based on our experimental conditions, the bulk concentration of CTB (species A) and glycolipid (species B) were estimated as: $C_A = 3 \times 10^{-7}\ mol/L$, $C_B = 3 \times 10^{-7}\ mol/L$. Three-dimensional diffusivities of CTB and glycolipid containing liposomes were estimated using the Stokes-Einstein equation as $D_{A,3D} = 9.77 \times 10^{-11}\ m^2/s$ and $D_{B,3D} = 4.88 \times 10^{-12}\ m^2/s$. The measured diffusivity of bound CTB was acquired from literature ($D_{A,2D} = 2.5 \times 10^{-13}\ m^2/s$).[118,119] DOPC lipid diffusivity was $D_{B,2D} = 8.25 \times 10^{-12}\ m^2/s$.[120] Using different fluorescent labeling approaches, previous researchers have also reported the diffusivity of GM1 in DOPC bilayer to be around $3.6\sim8 \times 10^{-12}\ m^2/s$. [120-122] We estimated the three-dimensional reaction rate using Smoluchowski's relation which gives a steady-state rate constant for fast reactions,[114]

Equation 4

$$k_{obs,3D} = 4\pi a (D_{A,3D} + D_{B,3D})$$

Prior studies derived the approximate solution of k_{obs} for two-dimensional membrane reactions using Smoluchowski theory, mean-passage time theory, and statistical thermodynamic theory (the models are summarized in APPENDIX B).[113-115] Based on our experimental

conditions, we found that the two-dimensional reaction rate could be up to 10^4 higher than the three-dimensional reaction rate. The increased reaction rate implies that the effective concentration of reactants on the membrane surface is enhanced by about 10^4-fold. This calculated enhancement factor has the same order of magnitude as the value in the antibody system reported by Sengers et al.[116] In such a case, the reduction of dimensionality could raise the effective GM2 concentration close to or higher than the dissociation constant of CTB-GM2 (2mM). Thus, it is possible that this significant enhancement of reaction rate between bound CTB and GM2 led to higher CTB binding.

To further verify this hypothesis, we altered the diffusivity of glycolipids by replacing DOPC with DMPC that has a gel phase transition temperature near room temperature (24 °C). We conducted the measurements of CTB binding to DMPC model membranes with 1 mol% GM1 and GM1:GM2 mixture (1 mol%:1 mol%) at 15 °C and 45 °C. In the DOPC bilayer, which has transition temperature at -20 °C,[123] the cooperativity between GM1 and GM2 at 15 °C was quite similar to what we obtained at room temperature, which implies that such a temperature change does not alter CTB binding much (**Figure 8**). However, the diffusion of glycolipids in the DMPC gel phase is two orders of magnitude lower when compared to the fluidic DMPC membrane.[124,125] Goins et al. reported GM1 diffusivity to be approximately 1-2 x 10^{-13} m2/s in DMPC below 20 ℃.[126] Under this condition, the two-dimensional reaction rate is only 400-500 times higher than the three-dimensional reaction rate in the DMPC gel phase. Thus, we expected that the rate enhancement via reduced dimensionality would be minimized in the DMPC system at 15 °C. **Figure 8** shows that mixing GM2 with GM1 in a DMPC bilayer did not enhance the overall CTB binding at 15 °C; in contrast, binding enhancement was observed in the fluidic

DMPC bilayer at 45 °C. This result further corroborates our hypothesis that reduction in dimensionality is influencing the binding of CTB with heterogeneous mixtures of glycolipids.

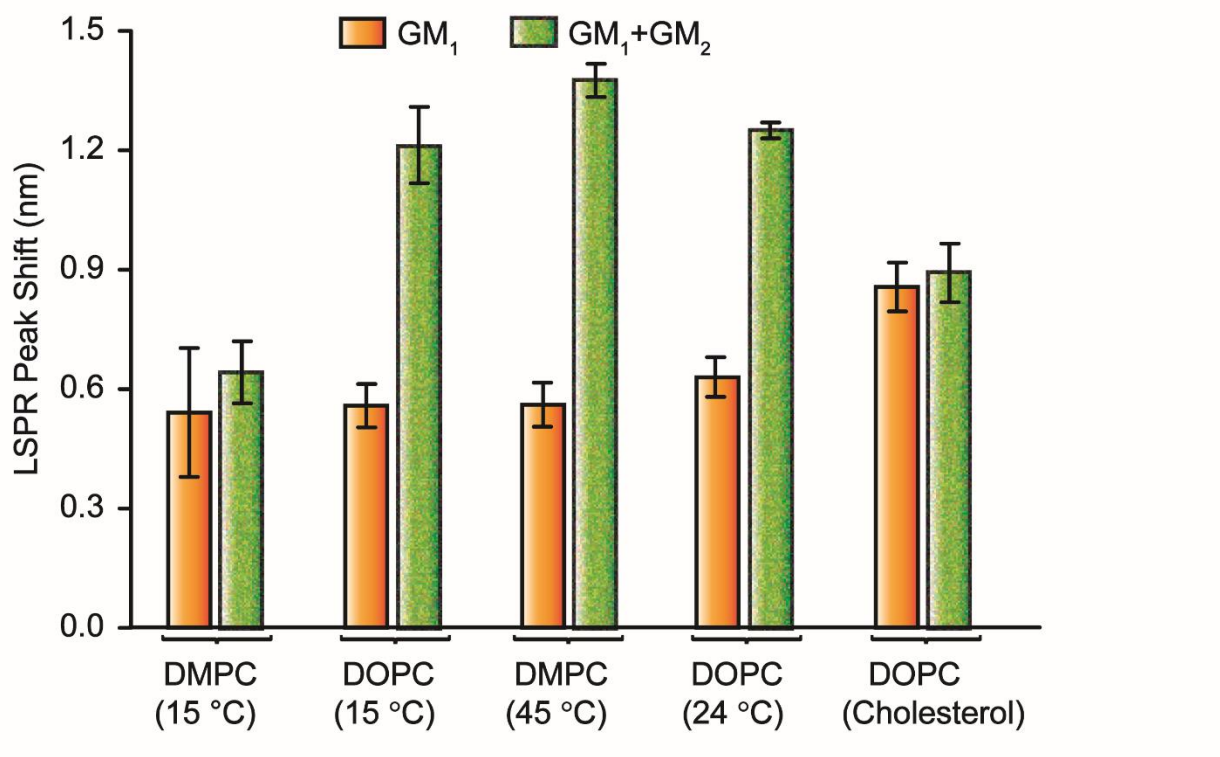

Figure 8: CTB binding to single glycolipid (orange) or paired glycolipids (green) in different membrane environments. (DMPC/DMPS (15 °C), DOPC/DOPS (15 °C), DMPC/DMPS (45 °C), DOPC/DOPS (room temperature) or DOPC/DOPS/cholesterol (room temperature)) The heterogeneous binding cooperativity between GM1 and GM2 depends on the fluidity and heterogeneity of the membranes. Data points are reported as mean ± S.D (n = 11). Reprinted with permission from Krishnan *et al*.[18]

In addition, 10 mol% of cholesterol was added to the DOPC bilayer in order to alter the fluidity and the heterogeneity of model membranes. Similar to the DMPC system, changing the membrane environment altered the heterogeneous binding cooperativity. (**Figure 8**) This result is not surprising because many studies have shown the compositions of fatty acids and cholesterol

in host cells can influence toxin potency.[127,128] Previous studies have also reported that surface diffusion and heterogeneity can influence the homo-multivalent CTB-GM1 binding.[129] Our result indicated that the membrane environment is also essential in the hetero-multivalent binding process.

The other question is why mixing GM3 with the other receptor did not enhance CTB binding. The only difference in the structure of GM2 and GM3 is that GM2 contains an additional N-acetyl galactosamine (GalNAc) in its glycan portion. The crystal structure of CTB-GM1 complex indicates that the sugar groups of galactose (Gal), GalNAc, and sialic acid (Neu5Ac) in GM1 were buried in the CTB binding subunit and contribute to 39%, 17%, and 43% of the contact surface area respectively.[130] CTB binding to GM3 that has only one Neu5Ac epitope should be weaker than to the GM2 receptor. In fact, Turnbull et al. estimated the dissociation constant for α-methyl sialoside, which contains only Neu5Ac epitope, to be 210 mM.[104] Even though the mechanism of reduced dimensionality could increase the reaction rate around 10^4-fold, the effective concentration of GM3 on the membrane surface is still far below the dissociation constant between CTB and the sialic acid residual. Therefore, it was not surprising that no cooperativity was found between GM3 and the other binding receptors.

A New Perturbation Protocol for Screening Glycolipid Receptors in Multivalent Interactions

One of the difficulties in observing hetero-multivalency is that some receptors, such as GM2, only exhibit significant binding when they form a partnership with other receptors. Traditional ligand-receptor binding assays (e.g. microarray technology) cannot reflect such hetero-multivalency because they screen only one specific receptor at a time. Thus, the contribution of GM2 was often ignored since CTB binding to pure GM2 was only detected at CTB concentrations far beyond physiologically relevant conditions. To address this issue,

previous studies have developed combinatorial arrays that mix two different receptors in a 1:1 ratio.[35] However, this labor-intensive method cannot observe hetero-multivalent binding involving more than two receptors.

In order to efficiently discover receptor candidates for multivalent binding proteins, we designed a new membrane perturbation protocol. This protocol first involves constructing a membrane that contains all receptor candidates with known compositions as a reference. The reference membrane is then perturbed by increasing the density of a single desired glycolipid receptor. If a specific receptor can either directly bind to the target protein or indirectly form a binding complex with the assistance of other glycolipids; the perturbation will alter the overall protein binding irrespective of the mechanism.

As a proof-of-concept, we constructed a reference membrane consisting of GM1, GM2, GM3, fucosyl-GM1, and GD1b (0.25 mol% of each glycolipid). We then perturbed the reference membrane by increasing one of the glycolipid receptors to 2 mol%. CTB binding to the reference membrane and each perturbed membrane is shown in **Figure 9**. As expected, CTB binding was significantly enhanced when the densities of GM1, fucosyl-GM1, and GD1b were increased. The positive binding cooperativity between GM2 and the other glycolipids present in the reference membrane also enhanced the overall CTB binding. In addition, increasing GM3 density did not enhance CTB binding. Thus, we could exclude GM3 as a CTB receptor candidate without conducting the entire combinatorial array measurement. In order to identify receptors of multivalent proteins from a large library of molecules, this perturbation method can be more efficient than combinatorial glycolipid arrays.

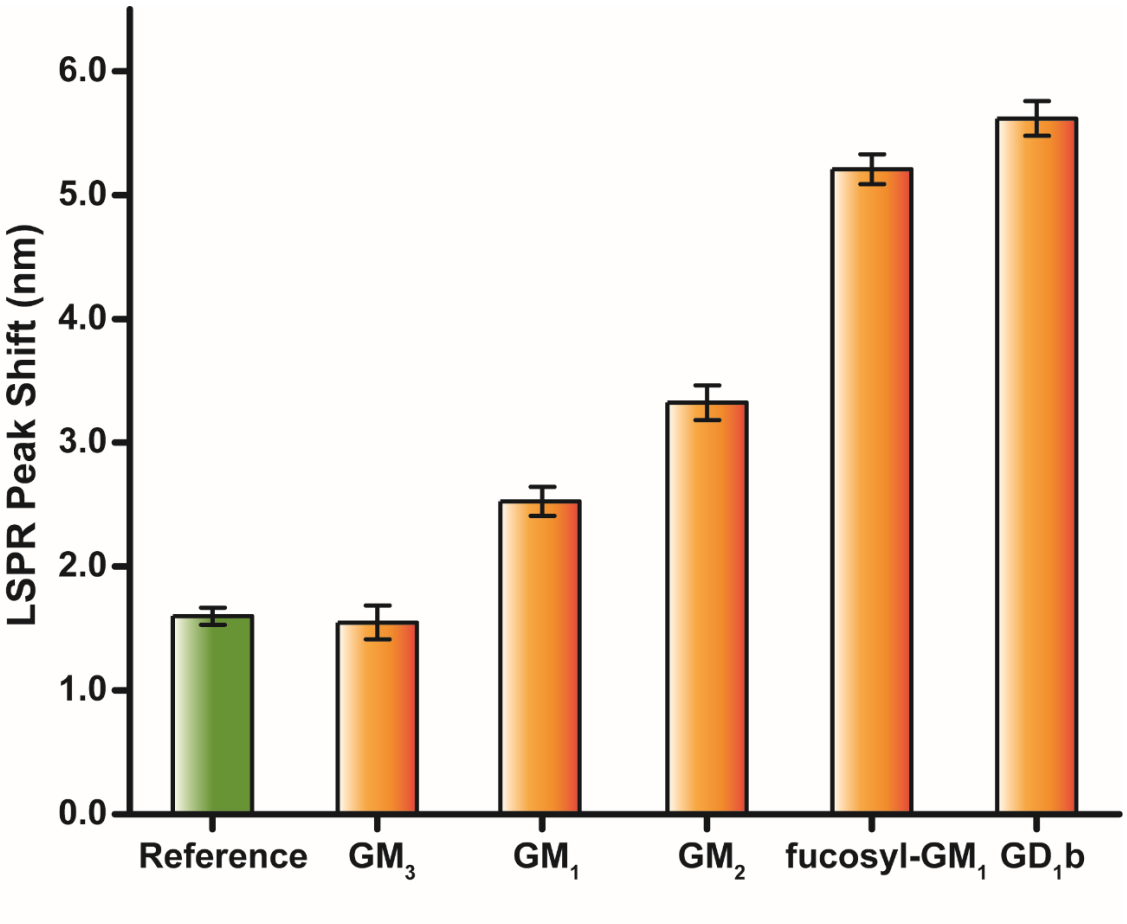

Figure 9: The demonstration of membrane perturbation protocol. 1726 nM CTB was bound to the reference and perturbed membranes that preserved all receptor candidates. The reference membrane contained 88.75 mol% DOPC, 10 mol% DOPS, 0.25 mol% each of GM1, GM2, GM3, GD1b and fucosyl-GM1. The reference membrane was perturbed by increasing the density of a specific glycolipid to 2 mol%. Data points are reported as mean ± S.D (n = 11). Reprinted with permission from Krishnan *et al*.[18]

Discussion

In this study, significant enhancement of CTB binding was observed when a strongly binding receptor was mixed with a weakly binding receptor (GM2). When investigated further, the reduction of dimensionality looks like the most likely cause. If this mechanism is valid, a fraction of the bound CTB should simultaneously bind to GM2 and other strong binding

receptors. Most recently, Klassen and his coworkers demonstrated the same heterogeneous binding cooperativity using a catch-and-release electrospray ionization-mass spectrometry (CaR-ESI-MS) assay.[131,132] Mass spectrometry allows for the identification of the types of receptors binding to CTB. Using CaR-ESI-MS assay, Klassen and his coworkers observed that CTB could bind to very weak binding receptors GM2 and GM3 when 7 different glycolipids (GM1, GM2, GM3, GD1a, GD1b, GD2, and GT1b) were mixed in either picodiscs or micelle systems, but no binding was observed when GM2 or GM3 was the only receptor. Their results provide evidence that CTB can directly bind to weakly binding receptors when they are mixed with strongly binding receptors. It is worth noting that we did not observe binding cooperativity between GM1 and GM3, but Klassen and his coworkers observed CTB binding to GM3. This is probably due to the difference of lipid bilayer conditions. In our experiment, surface density of glycolipid receptor was maintained at 1 mol%. The CaR-ESI-MS assay mixed 7 glycolipid receptors equally resulting in 14 mol% of each glycolipid. The reaction enhancement via reduced dimensionality was higher in the CaR-ESI-MS assay; thus, it is not surprising that Klassen and his coworkers observed CTB binding to GM3.

Reduction of dimensionality provided a potential mechanism to answer a long-standing question, why CTB binding does not correlate with GM1 level on cell surfaces.[133] Yanagisawa et al. observed strong reactivity between CTB and embryonic neuroepithelial cells in the absence of GM1.[24] Kirkeby stained GM1 with CTB and anti-GM1 antibody, and found that both labeling reagents were not co-localized.[29] In addition, GM1 is of very low abundance (0.0015-0.003 mol% of glycosphingolipids) in human small intestinal epithelial cells[31]; thus, a recent publication raised a question, whether GM1 is sufficient to induce cholera toxin attachment.[30] In the reduction of dimensionality model, high-affinity receptors can serve as initiators, and then

activate weak receptors, leading to higher retention of CTB on the cell surface. Thus, the overall CTB binding is not simply controlled by a single GM1 receptor; the weakly binding receptors can contribute to CTB binding via reduction of dimensionality. Surface diffusion and local density of membrane receptors can influence the two-dimensional reaction rate, membrane fluidity and heterogeneity (i.e. lipid raft) which can also play essential roles in the CTB binding process.

The mechanism of reduced dimensionality has also been used to explain unexpected phenomena in various multivalent binding studies.[34,100,116] For example, Mazor et al. observed that the binding avidity of a bispecific antibody to receptors confined in cell membrane surfaces were significantly higher than the binding avidity to free receptors in solution.[38] Sengers et al. established a mathematical model based on the reduced dimensionality hypothesis to describe the mechanism of bivalent antibody binding to heterogeneous membrane targets, and estimated that the effective affinity of the bivalently bound antibody can be enhanced by approximately 4 orders of magnitude.[116] These studies, combined with our own CTB binding measurements suggest the importance of the role of reduced dimensionality in multivalent protein-cell membrane recognition. Further kinetic studies are necessary in order to verify the hypothesis and establish a comprehensive model of hetero-multivalent recognition.

Since the complex interplay between multiple membrane receptors is critical, we also developed a new membrane perturbation protocol to efficiently screen receptor candidates. This protocol measured CTB binding to perturbed membranes that preserve all receptor candidates; therefore, the interplay between different receptors can be monitored. This new protocol is more efficient in screening the potential receptors than the combinatorial array, which detects proteins binding to the binary mixture of glycolipids. For example, if we plan to screen 20 receptor

candidates, the membrane perturbation protocol required only 21 measurements instead of 190 measurements in a combinatorial array.

Chapter Conclusion

In summary, we elucidated the essence of hetero-multivalency in CTB-cell membrane recognition using a high-throughput and easy-to-use nanocube sensors. We believe that the detection protocols presented here can provide a systematic and efficient strategy to investigate multivalent protein-cell membrane recognition.

CHAPTER IV

HETERO-MULTIVALENCY OF PSEUDOMONAS AERUGINOSA LECTIN LECA BINDING TO MODEL MEMBRANES

Chapter Summary

Multivalency is at the heart of lectin-glycan recognition. We demonstrated hetero-multivalency, a protein simultaneously binding to two or more different types of receptors, may play an essential role in LecA (a *Pseudomonas aeruginosa* adhesin)-glycolipid recognition. We observed that low-affinity receptors could be activated by high-affinity receptors, resulting in higher LecA binding capacity. Activation was probably mediated via a Reduction of Dimensionality (RD) mechanism. In this work, we investigated the binding cooperativity of LecA to various glycolipid receptors and mixtures of those same receptors. Interestingly, the strongly binding receptor, Gb3, could activate weaker binding receptors (i.e. LacCer, GalβCer, Gb4, AGM2, GM1, and AGM1) leading to higher LecA binding capacity. In addition, medium-affinity receptors, GM1 and AGM1, could also initiate LecA binding to each other and to weak receptors. Moreover, we identified specific requirements for hetero-multivalent binding. LecA concentration and the surface density of weak receptors must reach specific thresholds to trigger binding cooperativity.

Introduction

Pseudomonas aeruginosa is a ubiquitous and opportunistic bacterium. The increase of antibiotic resistance worldwide limits therapeutic options, leading to the high morbidity and mortality of *P. aeruginosa* infections.[134,135] One mechanism that *P. aeruginosa* uses to cause disease is adhesion to epithelial cells.[9-12] Adhesion of *P. aeruginosa* is mediated by surface

adhesins, including LecA (i.e. PA-IL), LecB (i.e. PA-IIL), and Type IV pilus (T4P), which bind to glycan receptors on epithelial cell surfaces.[136-140] In addition to their role in adhesion, LecA and LecB can influence host cell functions.[140-145] Thus, it is essential for us to understand the binding mechanisms used by *P. aeruginosa* adhesins to interact with host cell receptors in order to gain insight into strategies to combat infections.

In this article, we focus on LecA, a homotetrameric lectin, where each monomer has a single glycan binding site.[41] LecA contains two adjacent binding site pairs facing in opposite directions. (**Figure 10**) This configuration allows adhesion of *P. aeruginosa* to epithelial cells and may contribute to linkages between bacteria, subsequently leading to biofilm formation.[138,146] It is known that LecA prefers binding to α-D-galactose terminated glycans; typically, globotriaosylceramide (i.e. Gb3, Galα1-4 Galβ1-4 Glc ceramide) is considered to be a major receptor for LecA.[41,147-151] However, it is known that LecA can bind to other types of glycan receptors (e.g. β-galactose (Galβ) and N-acetylgalactosamine (GalNAc) terminated glycans), but the binding affinities are lower than that of binding to Gb3.[150,152]

We recently reported a hetero-multivalent binding phenomenon for cholera toxin subunit B (CTB) in an environment that mimics the natural cell membrane.[17,18] Interestingly, we found that strong binding receptors can activate weak binding receptors via a fundamental mechanism, Reduction of Dimensionality (RD).[18] We illustrate the concept of RD in **Figure 10**, which shows the stepwise process of LecA binding to a cell membrane containing two different glycolipid receptors. The binding mechanism includes: (1) a molecule diffuses from solution phase to a membrane surface and one of its binding sites attaches to a membrane receptor; (2) Free membrane receptors move two dimensionally, encounter the now bound molecule, and enable subsequent binding events. The reaction rates of these subsequent binding events are at least 10^4

times higher than the first binding event.[18] Thus, even a weak binding receptor can now participate in the second or higher order binding events resulting in greater protein attachment. This intrinsic mechanism suggests that the binding of multivalent proteins is not simply controlled by a single type of receptor; the cooperative actions between strong and weak receptors can greatly influence the overall attachment of proteins and bacteria.

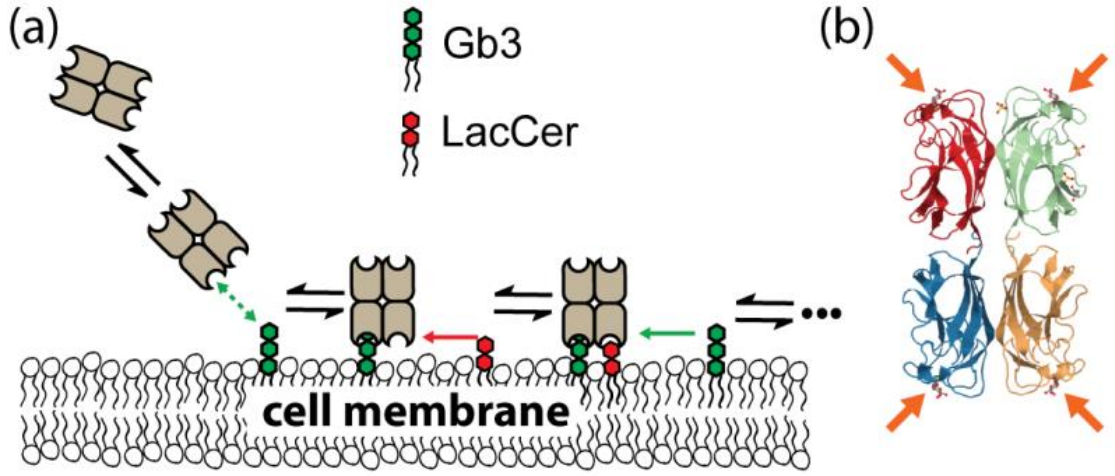

Figure 10: Schematic for the Reduction of Dimensionality (RD) model. (a) A schematic representation of RD influencing LecA interactions with the cellular membrane. LecA first diffuses from solution to a membrane surface and attaches to the high-affinity receptor, Gb3. Then, free membrane receptors move two dimensionally, enabling subsequent binding. The reduced dimensionality of diffusion enhances the effective concentrations of membrane receptors; thus, a weak receptor, such as LacCer, can contribute to LecA binding. (b) Graphical representation of LecA complexed with galactose as observed in the crystal structure (PDB code 1OKO).[147] The four binding sites are indicated by arrows. The protein and carbohydrate structures are displayed in a cartoon representation with coloring done by subunit using JSmol.

We hypothesized that the RD mechanism plays a key role in *P. aeruginosa* adhesion by influencing many different multivalent proteins, including LecA. Although Gb3 is the major LecA receptor, its surface concentration in different epithelial cells is not known. Gb3 is at low

levels in human intestinal epithelia cells and murine lungs.[31,153] We suspect that Gb3 can activate abundant but weaker glycolipid receptors, influencing LecA attachment via the RD mechanism. We examined hetero-multivalency in LecA binding through analysis of hetero-multivalent binding cooperativities between major and minor LecA binding receptors. We were excited to find that high-affinity receptors were able to activate weak binding receptors, leading to positive hetero-multivalent cooperativity. We performed colloid aggregation assays to evaluate the energetics involved in hetero-multivalent binding. We found that the RD mechanism leads to enhancement of LecA and *P. aeruginosa* adhesion through multivalent receptor interactions.

Methods & Materials

Materials

Ammonium hydroxide, bovine serum albumin Fraction V (BSA), copper (II) chloride dihydrate, ethanol, Pluronic F-127, polyvinylpyrrolidone (MW ~55,000) (PVP), tetraethyl orthosilicate (TEOS), silicone oil (useable range -50°C to +200°C) and tris-buffered saline (TBS) obtained as a 10x solution (1x working solution 20 mM Tris 0.9% NaCl pH ~7.4) were purchased from Sigma-Aldrich (St. Louis, Missouri). Silver(I) nitrate Premion grade was purchased from Alfa-Aesar (Tewksbury, Massachusetts). 2-Propanol (iPA) and Texas Red™ 1,2-dihexadecanoyl-sn-glycero-3-phosphoethanolamine, triethylammonium salt (TR-DHPE) was purchased from Fisher Scientific (Pittsburgh, Pennsylvania). 1,5-Pentanediol (PD) was purchased from Acros Organics (Geel, Belgium). PA-IL from *Pseudomonas aeruginosa* (also known as LecA) was purchased from Elicityl (Crolles, France). 5.04 μm silica beads were purchased from Bangs Laboratories Inc. (Fishers, Indiana). Calcium chloride was from BDH VWR Analytical (Radnor, Pennsylvania). Monosialoganglioside, GM1 (Galβ1-3GalNAcβ1-4(Neu5Acα2–3)Galβ1-4Glc-Ceramide), Gangliotetraosylceramide, AGM1,(Galβ1-3GalNAcβ1-

4Galβ1-4Glc-Ceramide), Gangliotriosylceramide, AGM2, (GalNAcβ1-4Galβ1-4Glc-Ceramide), Globotriaosylceramide, Gb3, (Galα1-4Galß1-4Glc-Ceramide), Globotetrahexosylceramide, Gb4, (GalNAcß1-3Galα1-4Galß1-4Glc-Ceramide), Lactosylceramide, LacCer, (Galβ1-4Glc-Ceramide) and Galactosylceramide, GalβCer, (Galß-Ceramide) were purchased from Matreya LLC (State College, PA). 1-palmitoyl-2-oleoyl-sn-glycero-3-phosphocholine (POPC) and 1-palmitoyl-2-oleoyl-sn-glycero-3-phospho-L-serine (sodium salt) (POPS) were purchased from Avanti Polar Lipids (Alabaster, AL).

Methods

Nanocube synthesis

The nanocube synthesis procedure is originally from Tao et al. [76] The silver nanocubes were synthesized via the polyol method which uses PVP as a structure-directing agent. In brief, the procedure was as follows. First, 0.2 g of $AgNO_3$ was dissolved into 10 mL of PD along with 30 µL of 8.2 g/L $CuCl_2$ in PD. Next, 20 mL of PD was added to a 100 mL round bottom flask that was then heated to 130°C with stirring in a 190°C silicon oil bath. After reaching 130 °C in the flask, 250 µL of the $AgNO_3$ solution along with 500 µL of a 20 g/L PVP in PD solution was added to the flask followed by a second addition of 500 µL from both the $AgNO_3$ and PVP solutions 35 seconds later. Then every following minute, 500 µL of each solution was added to the reactor until the solution turned a deep red color, about 15 minutes. After achieving a deep red color, the reaction was then allowed to cool and was washed by centrifugation using 200 proof ethanol.

The silica coating procedure was originally described in Wu et al.[74] and modified by Worstell et al.[17] First, 20 mL of the silver nanocube solution was washed into iPA via centrifugation and then added to a 250 mL round bottom flask along with 55 mL of iPA, 22.1

mL of MilliQ® water, 6.8 mL of TEOS, and 3.4 mL of 0.84 w/v% ammonium hydroxide. Next, the mixture was stirred at room temperature for 60 minutes before 50 mL of ethanol was added to stop the reaction. After stopping the reaction, the silica coated cubes were centrifuged and reconstituted in 75 mL of iPA. The solution was then returned to the round bottom flask along with 22.1 mL of MilliQ® water, and 6.8 mL of TEOS. This solution was incubated at 60 °C for 10 hours before being washed with MilliQ® water. The silica coated nanocubes were stored in MilliQ® water at room temperature until use.

Vesicle preparation

Small unilamellar vesicles (SUVs) were prepared via extrusion.[17] The procedure in brief is as follows. First, the desired compositions of lipids in chloroform solutions, prepared as per manufacturers recommendations, were mixed in a 25 mL round bottom flask and, then, dried using a rotary evaporator (Heidolph Hei-VAP Value®). Next, the dried lipids were reconstituted using MilliQ® water and extruded through a 100 nm polycarbonate filter (Whatman®) using a mini-extruder (Avanti Polar Lipids) resulting in a 3 g/L SUV solution.

Supported lipid bilayer formation on Ag@SiO_2 nanocubes

Supported lipid bilayers were formed on the nanocubes using a modified vesicle fusion method.[17] 100 µL of the 3 g/L SUV solution was added to a 0.5 mL Eppendorf® tube and vortex mixed for 20 seconds. Then, 10 µL of a concentrated nanocube solution was added to the tube and the tube was vortex mixed for 1 second. Following this, 110 µL of 2x TBS was added to the tube and vortex mixed for one second. These last two steps were repeated pipetting 10 µL of concentrated nanocube solution and 10 µL of 2x TBS each time until 100 µL of the nanocube solution were consumed. Then, the tube was vortex mixed for an additional 10 seconds and diluted with 1x TBS with 100 µM $CaCl_2$ to the desired nanocube concentration.

Supported lipid bilayer formation on silica beads

Supported lipid bilayers were formed on the silica beads using a vesicle fusion method.[154] Initially, the stock silica bead solution was sonicated for 10 minutes and 5 µL of the solution was pipetted into a 0.5 mL Eppendorf® tube. The beads were then washed three times with MilliQ® water and the beads were resuspended in a final volume of 25 µL. In a separate 0.5 mL Eppendorf® tube, 25 µL of the SUV solution was added to 50 µL of 1x TBS and vortex mixed. Then, 25 µL of the washed beads were added to the SUV buffer solution and vortex mixed for 10 seconds and incubated for 10 minutes. Then, the beads were blocked with BSA for 1 hour followed by washing with 1x TBS resulting in a final volume of 100 µL of bilayer coated beads.

Nanocube protein binding measurement

Bilayer coated nanocubes were incubated for 1 hour with 31.3 µL of 0.5 g/L BSA per 1250 µL of nanocube solution to reduce nonspecific binding. Then, the desired amount of LecA was added. For these experiments, 10 mol% POPS/90 mol% POPC lipid bilayer was used as a control. After addition of LecA, the test, control, and blank solutions were vortex mixed for 10 seconds and pipetted as 20 µL aliquots into wells of a 384 well plate, 8 wells for the test, 4 wells for the control, and 4 wells for the blank solutions for each LecA concentration tested. Finally, the plate was read using a UV/Vis microplate reader spectrophotometer equipped with a CCD (FLUOstar Omega®, BMG-Labtech) to collect the extinction spectra every 13.3 minutes for a total of 80 minutes at room temperature. The resulting spectra were the results of averaging 200 flashes per well at a 1 nm resolution. The location of the quadrupole LSPR (Localized Surface Plasmon Resonance) peak (LSPR peak) was determined by 5^{th} order polynomial fitting. The resulting LSPR peak shift was calculated from the average LSPR peak location of the 8 wells and then subtracted by the LSPR shift of the control lipid bilayer.

Video microscopy for silica particle aggregation

Wells of a 96 well-plate (Costar® 3370) were coated with polyethylene glycol (PEG) using Pluronic F-127. Initially, each well was rinsed four times by ethanol and 250 µL ethanol was left to incubate in the wells for 30 minutes. Then, the wells were rinsed extensively with ethanol followed by five successive rinses of MilliQ® water. Following the cleaning steps, 250 µL of 5 g/L F-127 was added to each of the wells and left overnight. The next day, each well was rinsed five times with 250 µL of 1x TBS with 100 µM $CaCl_2$ while ensuring that none of the wells dried out when removing the solution. After the final rinse, the volume of solution left in each PEG-coated well was 96 µL of 1x TBS with 100 µM $CaCl_2$.

The procedure for video microscopy was adapted from Duncan et al.[155] 5 µL of 0.0324 g/L LecA solution in 1x TBS with 100µM $CaCl_2$ was added to a PEG-coated well and allowed to mix for at least 5 minutes. After LecA addition, 4 µL of the bilayer coated silica beads were added to the well and images were collected for 1.5 hours at an average frame rate of 12.8 frames/min. Imaging was performed using an inverted optical microscope (Axiovert® 200M , Carl Zeiss, Germany) with a 20x objective (Plan-NeoFluar, NA is 0.5, Carl Zeiss). Images were collected with a 14 bit CCD Camera (AxioCam HRc®, Carl Zeiss) operated in binning mode 1 (pixel size is 308nm/pixel, image area is 1388 X 1040 $pixels^2$ = 427 X 320 μm^2) . An image analysis algorithm coded in MatLab 2016a® was used to locate and track the centers of each particle.[156,157] Particles were considered associated when the distance between particles centers was less than or equal to ≈2a+2 pixels (a is the particle radius).

Statistical analysis and regression

The data comprising each binding curve is given as a mean ± standard deviation (S.D.) where n = 8. The Hill-Waud model was then fit to the data for each binding curve via the

Levenberg Marquardt algorithm in OriginPro 9.1® (OriginLab). This returned the calculated value, standard error, and R^2 value as well as the residuals, studentized residuals, and studentized deleted residuals. The parameter values and standard errors were reported in **Table 5**.

Colloid Aggregation Kinetic Theory

Duncan and Bevan measured Concanavalin A (ConA) binding to dextran by analyzing the aggregation kinetics of dextran-coated silica particles.[155] Here, we adapted the same analysis to monitor interactions between LecA and glycolipids. Compared to the nanocube protein binding measurement, this aggregation kinetic analysis allowed us to directly observe the energetic differences of LecA binding to different glycolipid mixtures. The analysis was conducted by measuring the rate of single particle disappearance using video microscopy.[155] The aggregation rate at short time scales was defined as:

Equation 5

$$\theta_1^{-1} = \frac{\phi_{1,0}}{\phi_1} = 1 + 4k_{11}\phi_{1,0}t$$

where t is time in seconds and θ_1 is the fraction of single particles remaining over time. θ_1^{-1} was determined by taking the ratio of the number density of single particles at a certain time (ϕ_1) and at time = 0 ($\phi_{1,0}$). k_{11} is the rate constant for the self-aggregation of single particles. We obtained k_{11} by fitting θ_1^{-1} vs. time data to **Equation 5**. This aggregation kinetic model is valid for short time scales; thus, we fit the experimental data between $t = 0$ and $t = \tau$.[155] The definition of diffusion time (τ) is described in APPENDIX C. k_{11} is only a function of pair potential between two particles, u_{pp}. As $k_{11} \gg 0$, it indicates strong binding between LecA and glycolipids. For weak interactions, $k_{11} \to 0$. By comparing k_{11} values, we can observe the energetic differences of LecA binding to different glycolipid mixtures.

Results

According to the RD model, we hypothesize that high-affinity receptors can activate weak binding receptors, leading to increased overall binding capacities. We focused the current study on LecA from *P. aeruginosa*. We expected the primary LecA receptor, Gb3, could effectively facilitate other lower affinity receptors' ability to bind LecA, leading to greater LecA attachment to the lipid bilayer. Here, we used the nanocube sensing platform to observe LecA binding to lipid bilayers.[17,18] The quadrupole LSPR shift in the absorption spectra represents LecA binding. The data point at each protein concentration represents an average over 8 replicates. The saturation binding curves were fit by the Hill-Waud binding model[81]

Equation 6

$$\Delta\lambda_{LSPR} = \frac{V_m[LecA]^n}{K_h^n + [LecA]^n}$$

where K_h is the Hill's equation apparent dissociation constant, n is the Hill cooperativity coefficient, [LecA] is the concentration of LecA, and V_m is the maximum $\Delta\lambda_{LSPR}$ of the fully bound state. $\Delta\lambda_{LSPR}$ is the observed LSPR peak shift, which corresponds to the attachment of LecA to the lipid bilayer surface. To quantify the cooperative binding effect, we modified the heterogeneous cooperativity defined in our recent paper[18]:

Equation 7

$$\text{heterogeneous cooperativity } (\phi) = \Delta\lambda_{mix} - \sum_i \Delta\lambda_{pure,i}$$

where $\Delta\lambda_{mix}$ is the LSPR shift when LecA binds to a bilayer containing two different glycolipids, and $\Delta\lambda_{pure,i}$ is the LSPR shift when LecA binds to a bilayer containing the correspondent individual glycolipid, i. If no enhancement is observed between two different glycolipids, the ϕ value should be approximately zero. A positive (or negative) ϕ value indicates positive (or negative) cooperativity.

Potential Glycolipid Receptors

Prior glycoarray studies have shown αGal terminated glycans are LecA's preferred receptors but LecA can also bind to βGal terminated glycans with lower affinity.[150,152,158] Here, we measured LecA binding to the common galactose terminated glycolipids, including Gb3, GM1, AGM1, LacCer, and GalβCer. (**Figure 31**) As shown in **Figure 11**, LecA significantly bound to the bilayer containing 1 mol% Gb3. At the same density, LecA-AGM1 binding was much weaker, and LecA binding to GM1 was not measurable. When we increased the glycolipid density to 5 mol%, LecA binding to both AGM1 and GM1 became significant. At 5 mol% density, the dissociation constant (K_h) of GM1 is slightly higher than AGM1. We also noted that the weaker affinity GM1 had a higher V_m than AGM1. This phenomenon is similar to CTB binding; the homo-multivalent binding cooperativity, *n*, can influence the binding capacity.[17] LacCer and GalβCer were observed to be highly abundant in intestinal epithelium, and LacCer was noted as abundant in murine lungs.[31,159] However, their binding avidities are much lower than GM1 and AGM1. We could not observe LecA binding to LacCer surfaces unless the LacCer density was increased to 8 mol%. For GalβCer, LecA binding is still not measureable at an 8 mol% surface density. Based on these results, we rank these glycolipids in order of affinity, Gb3 $\gg$ GM1 $\approx$ AGM1 $\gg$ LacCer $>$ GalβCer, and categorize them into three groups: (1) Strong receptors: Gb3; (2) Moderate receptors: GM1 and AGM1; (3) Weak receptors: LacCer and GalβCer.

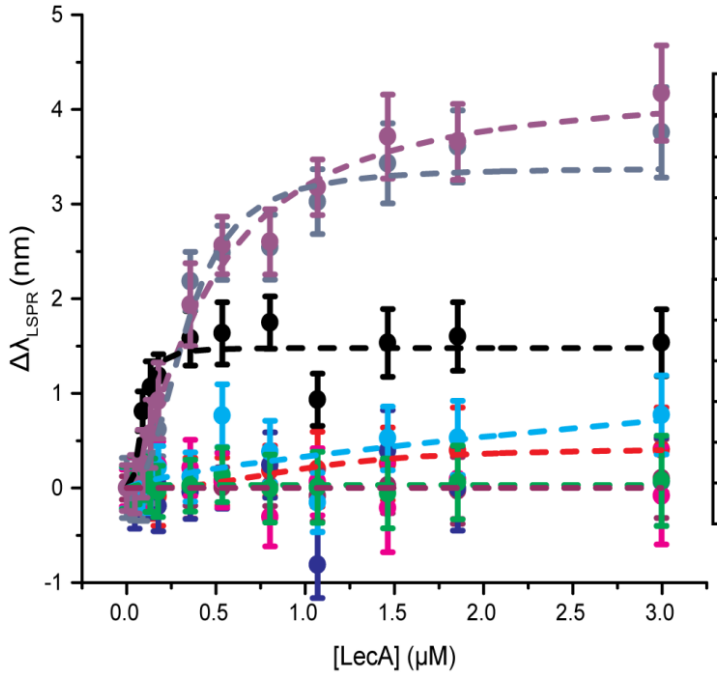

	Lipid Compositions (mol%)				
	Gb3	GM1	AGM1	LacCer	GalβCer
●	0	5	0	0	0
●	0	0	5	0	0
●	1	0	0	0	0
●	0	0	0	8	0
●	0	0	1	0	0
●	0	1	0	0	0
●	0	0	0	0	4
●	0	0	0	0	8
●	0	0	0	4	0

Figure 11: The saturation binding curves of LecA binding to common galactose terminated glycolipids. The dash lines represent the curve fits to Hill's equation. Data points are reported as mean ± S.D (n = 8). To better show the data points at low concentrations, the same binding curves on a semi-log scale are shown in APPENDIX C.

Positive Binding Cooperativity Between Strong and Weak Receptors (Gb3 & LacCer)

Based on the RD model, we expected that strong receptors would activate weak receptors, leading to higher binding capacity for LecA. To demonstrate this concept, we measured LecA binding to the mixtures of Gb3 and LacCer. Keeping the mol% of Gb3 in the bilayer fixed at 1 mol%, we performed measurements at telescoping concentrations of LacCer (8, 4, 2 and 1 mol%) in the bilayer (**Figure 12a**). LecA binding to pure 4 mol% surface density LacCer was not measureable, and the maximum binding (at 3μM LecA) to pure 8 mol% LacCer is minimal. After mixing LacCer with 1 mol% of Gb3, we saw increased LecA binding to mixtures of Gb3 and LacCer.

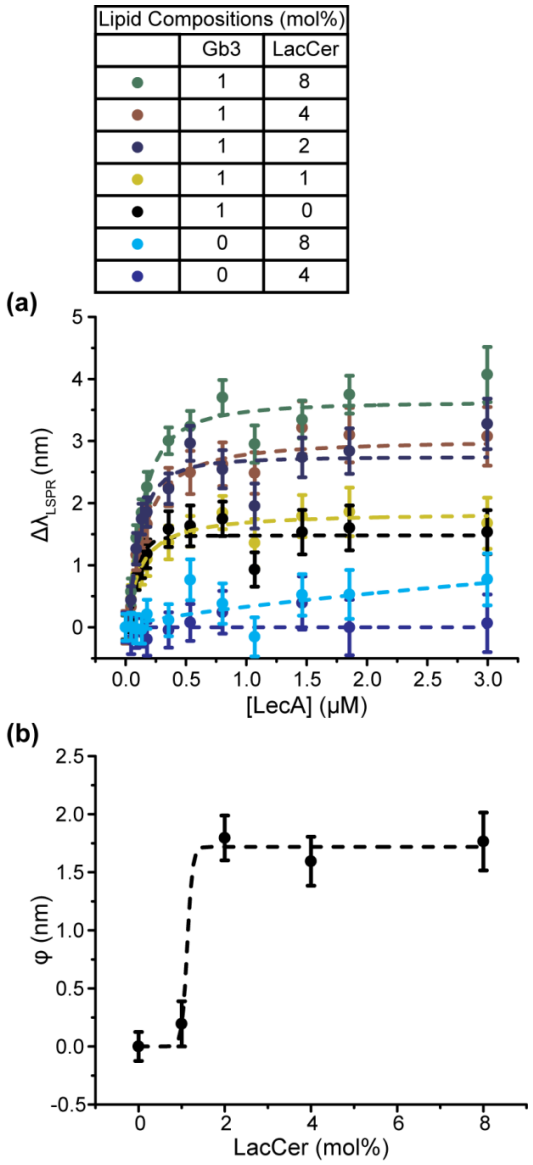

Figure 12: LecA binding to Gb3/LacCer mixtures shows positive cooperativity. (a) Saturation binding curves of LecA binding to bilayers containing Gb3/LacCer mixtures. The dashed lines are the Hill equation fits to the data (represented as mean±S.D. (n=8)). To better show the data points at low concentrations, the binding curves on a semi-log scale are shown in APPENDIX C. (b) ϕ values for 1 mol% of Gb3 mixed with different densities of LacCer. ϕ was calculated based on the LSPR shift at the highest LecA concentration (3 μM). Dash line representing the fit of ϕ to the sigmoidal function is a guide to the eye.

As described above, we can use hetero-multivalent cooperativity (ϕ in **Equation 7** to quantify the enhanced binding capacity. In **Figure 12b**, no obvious positive cooperativity was observed when 1 mol% Gb3 was mixed with 1 mol% LacCer, but cooperativity drastically increased at 2 mol% of LacCer. This result seems to be indicating that the surface density of the weak receptor has to reach a threshold value in order to contribute in LecA binding.

Figure 35 shows the changes in cooperativity under different LecA concentrations. The average cooperativity is minimal below 0.1 μM LecA, but then increases until beginning to level off around 2 μM LecA. In the RD model, LecA has to first anchor to Gb3 in order to change from three-dimensional to two-dimensional diffusion, leading to an increased effective concentration of the weak receptor for the subsequent binding events. Thus, this hetero-multivalent binding process is limited by the first binding step, which corresponds to the dissociation constant, K_h, of Gb3 (0.1 μM). This is probably the reason why the observed cooperativity significantly increased above the K_h value.

It is important to recognize that the cooperativity defined in **Equation 7** should refer to the change of the number of bound LecA (i.e. binding capacity) molecules. Besides the increased binding capacities of Gb3+LacCer mixtures, we observed that the K_h values also increased. (**Table 5**) In a simple monovalent binding model, the molar Gibbs free energy (i.e. binding avidity) is related to the dissociation constant[160]:

Equation 8

$$\Delta G = -RTln(K_d)$$

Although this function is not applicable to multivalent binding systems, we expect that the increase in dissociation constant (K_h) is associated with the decrease in binding energy (avidity) between LecA and membrane surfaces.[81] This phenomenon is consistent with the CTB

binding system. When the weak receptor GM2 was mixed with other strong receptors, the dissociation constants also increased.[17,18]

Alternative Measurement of LecA Binding Avidity to Gb3 & LacCer Mixtures

As described above, after mixing Gb3 with LacCer, we observed an increase in K_h, which may refer to a decrease in LecA binding avidity. As an additional confirmation of this argument, we used a nascent video microscopy technique developed by Duncan and Bevan to directly measure the binding avidity of LecA. Duncan and Bevan measured ConA and dextran interactions by observing the aggregation process of dextran-coated colloidal particles. ConA, an agglutinating lectin, has a similar configuration to LecA. The paired glycan binding sites of ConA facing opposite directions linked the dextran-coated silica beads, leading to colloid aggregation. Duncan and Bevan developed a theoretical model to describe the correlation of aggregation kinetics and the pair potential energy between two particles. This video microscopy technique not only offers us an alternative measurement of LecA binding avidity but also allows for direct visualization of LecA-glycolipid receptor interactions.

To implement this technique, we first deposited lipid bilayers containing the desired glycolipid receptors onto 5 μm silica beads. Then, LecA was bound to glycolipid receptors thereby linking two silica particles. (**Figure 13**) The aggregation rate is associated with the binding energy between LecA and glycolipid receptors. Supplemental videos show the aggregation kinetics of lipid bilayer coated particles. If the binding avidity was strong, the aggregation occurred immediately after two particles touch. (**Movie 1 & 2**) In contrast, if the binding avidity is weak, we observed a fraction of particles that could collide and bounce apart. (**Movie 3**) This aggregation process can be quantified by measuring the rate of single particle disappearance. We calculated the aggregation rate (k_{11}) by following the analysis developed by

Duncan and Bevan. (see Chapter IV Materials and Methods section). When $k_{11} \gg 0$, it indicates strong binding. For weak interactions, $k_{11} \to 0$. By comparing k_{11} values, we can observe the energetic differences of LecA binding to different glycolipid mixtures.

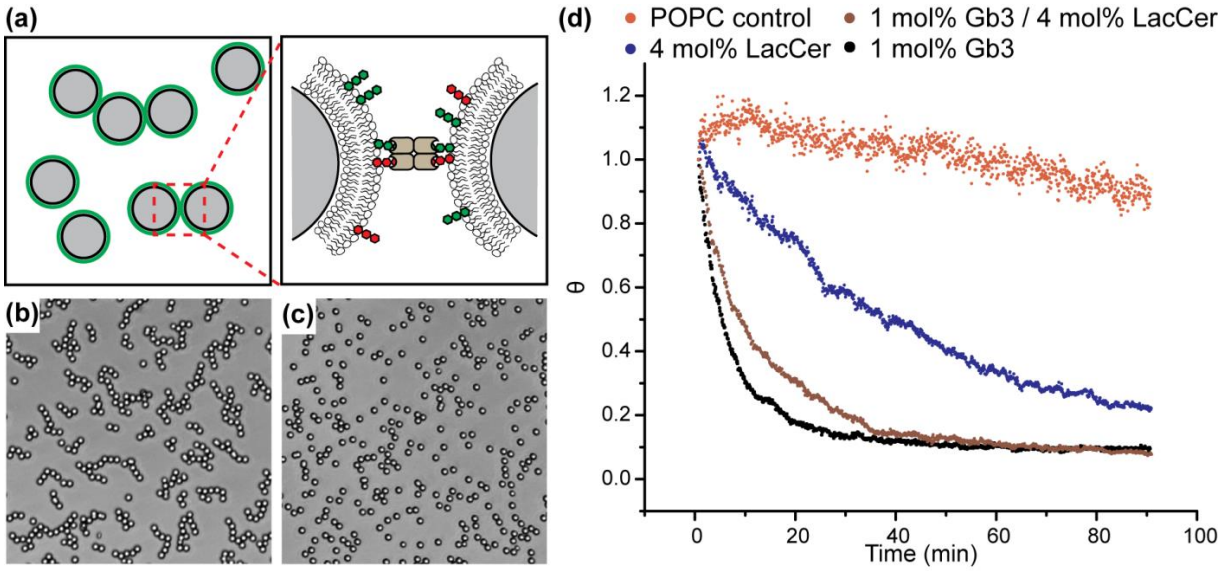

Figure 13: Colloid aggregation kinetics. (a) A schematic drawing of silica particle aggregation induced by LecA-glycolipid binding. (b) A snapshot of particle aggregation mediated by LecA tethering. (c) A snapshot of particle dispersion without LecA. (d) Particle aggregation under different conditions. The decay rate of the singlet ratio (θ) is associated with the binding avidity between LecA and membrane receptors.

The calculated aggregation rate (k_{11}) at various membrane compositions is reported in the **Table 3**. The k_{11} value significantly decreased after adding 4 mol% LacCer to the lipid bilayer containing 1 mol% Gb3, indicating the binding avidity reduced in the Gb3+LacCer mixture. This observation is interesting. If LecA only interacts with the major receptor, Gb3, additional LacCer should not significantly change the binding avidity because the surface density of Gb3 remained at 1 mol%. This phenomenon can be explained by the RD mechanism. When LecA interacts with

pure 1 mol% Gb3 bilayers, a LecA could bind to maximum of four Gb3 receptors, forming a strong linkage between the silica beads. When LecA interacts with lipid bilayers containing a LacCer and Gb3 mixture, due to the increased effective concentration of LacCer, LacCer could compete with Gb3 receptors in LecA binding. In this situation, a portion of LecA might bind to both Gb3 and LacCer simultaneously, leading to a weaker linkage between two silica beads.

Table 3: Aggregation rate (k11) of Gb3, LacCer, Gb3+LacCer, and control bilayers. k11 is represented as mean ± S.D. (n =2). N/A indicates that the S.D. was not determined.

Lipid Compositions (mol %)				**Fitted**
Gb3	**LacCer**	**POPS**	**POPC**	**k_{11} (μm^2/(bead*s)**
1	0	10	89	0.20 ± 0.03
0	4	10	86	0.03 ± N/A
1	4	10	85	0.13 ± 0.01
0	0	10	90	0.01 ± N/A

This result is consistent with the dissociation constants measured by the nanocube sensor experiments. Based on colloid aggregation theory, the aggregation rate (k_{11}) and the dissociation constants (K_h) are proportional to the logarithmic avidity[155]. Comparing pure 1 mol% Gb3 and 1 mol% Gb3+4 mol% LacCer, the binding avidity reduced around half in both nanocube measurements (K_h in **Table 5**) and colloidal aggregation data (k_{11} in **Table 3**). This independent measurement of LecA binding avidity supports our hypothesis of the RD model.

Positive Cooperativity Between Gb3 and Other Weak Receptors (Galβ/GalNAc Terminated Glycolipids)

Besides LacCer, we explored hetero-multivalent binding cooperativity between Gb3 and other weak glycolipid receptors. We first mixed Gb3 with the simplest glycolipid, galactosylceramide (GalβCer), which consists of a single β–galactose residue attached to a ceramide tail. GalβCer is highly abundant in the brain and intestinal epithelial cells;[14,31] thus, it may play a role in the LecA binding process. At pure 8 mol% GalβCer, we did not observe significant LecA binding. This indicated that the binding affinity of GalβCer is weaker than LacCer. As expected, we observed possible positive cooperativity when 8 mol% GalβCer was mixed with 1 mol% Gb3. (**Figure 14** and **Table 4**) However, the degree of enhancement is lower than the Gb3+LacCer combination. This is probably due to the weaker interaction between LecA and GalβCer.

Table 4: Binding enhancement, ϕ, calculated using Equation 7 with 3 μM LecA LSPR shifts. The values are the mean ± S.E. (n=8).

Lipid compositions (mol%)							
Gb3	**GM1**	**AGM1**	**LacCer**	**GalßCer**	**Gb4**	**AGM2**	**ϕ**
1	1	0	0	0	0	0	1.9 ± 0.3
1	0	1	0	0	0	0	1.6 ± 0.3
1	0	0	1	0	0	0	0.2 ± 0.2
1	0	0	2	0	0	0	1.8 ± 0.2
1	0	0	4	0	0	0	1.6 ± 0.2
1	0	0	8	0	0	0	1.8 ± 0.2
1	0	0	0	8	0	0	0.8 ± 0.2
1	0	0	0	0	8	0	0.5 ± 0.2
1	0	0	0	0	0	8	0.7 ± 0.2
0	1	1	0	0	0	0	1.6 ± 0.3
0	1	0	4	0	0	0	1.4 ± 0.2
0	1	0	8	0	0	0	2.0 ± 0.3
0	1	0	0	8	0	0	0.6 ± 0.2
0	0	1	4	0	0	0	1.7 ± 0.2
0	0	1	8	0	0	0	1.8 ± 0.2
0	0	1	0	4	0	0	0.2 ± 0.3
0	0	1	0	8	0	0	0.4 ± 0.2

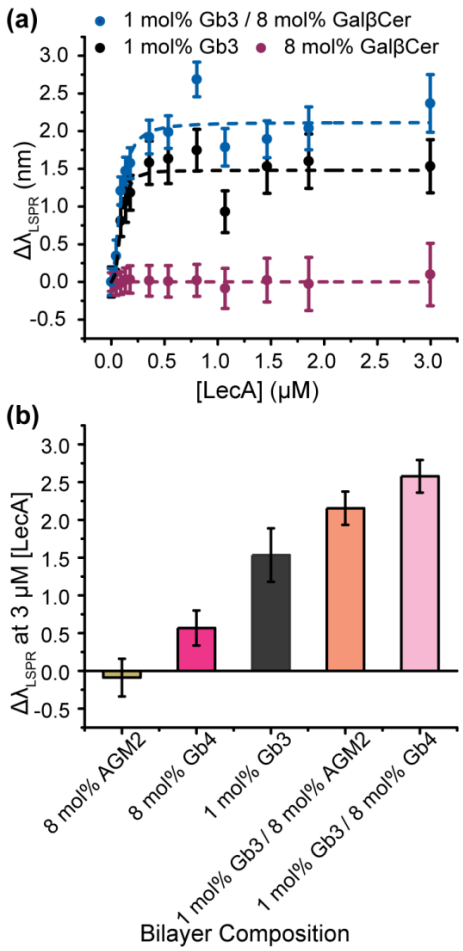

Figure 14: Cooperativity between Gb3 and other weak receptors. (a) Saturation binding curves of LecA to the bilayers containing Gb3, GalßCer, and Gb3+GalßCer. The dashed lines represent Hill equation fits to the data (represented as average ± S.D. (n=8)). To better show the data points at low concentrations, the binding curves on a semi-log scale are shown in APPENDIX C (b) 1 mol% Gb3 mixed with GalNAc terminated glycolipids at 3 μM LecA. (average ± S.D. (n=8)).

Prior glycoarray data showed that LecA has weak binding affinity to N-acetylgalactosamine (GalNAc) terminated glycans.[149,150,152] Thus, we also investigated the binding cooperativities of two GalNAc terminated glycolipids, Gb4, and AGM2. In this case, we only conducted LecA binding experiments at 3 μM, which is the highest concentration in the

previous binding curves. At 8 mol% of pure AGM2, no significant LecA binding was observed. The degree of LecA binding to 8 mol% pure Gb4 is similar to the 8 mol% pure LacCer system. When AGM2 was mixed with 1 mol% Gb3, we again observed potential positive cooperativity between strong and weak binding receptors. This shows that Gb3 could form a partnership with GalNAc terminated glycolipids, leading to positive cooperativity.

Gb3, GM1, and AGM1 Bilayers

After seeing various levels of cooperativity for Gb3 mixed with a variety of weak receptors, we became interested in observing the cooperativity between Gb3 and the moderate receptors (AGM1 and GM1). Weak receptors were activated by increasing the effective concentration via the RD mechanism. Therefore, it is reasonable to assume the moderate receptors could be activated via the same RD mechanism. As expected, in **Figure 15**, we observed that 1 mol% Gb3 receptors could activate either 1 mol% AGM1 or GM1, leading to higher LecA attachment. In addition to testing cooperativity between Gb3 and moderate receptors, we compared the cooperativity amongst the moderate receptors themselves. In the mixture of 1 mol% of GM1 and 1 mol% of AGM1, we observed much greater LecA attachment than the values in bilayers containing 1 mol% of either GM1 or AGM1. The increase of available receptors in the lipid bilayer is probably the reason for the increased cooperativity among moderate receptors.

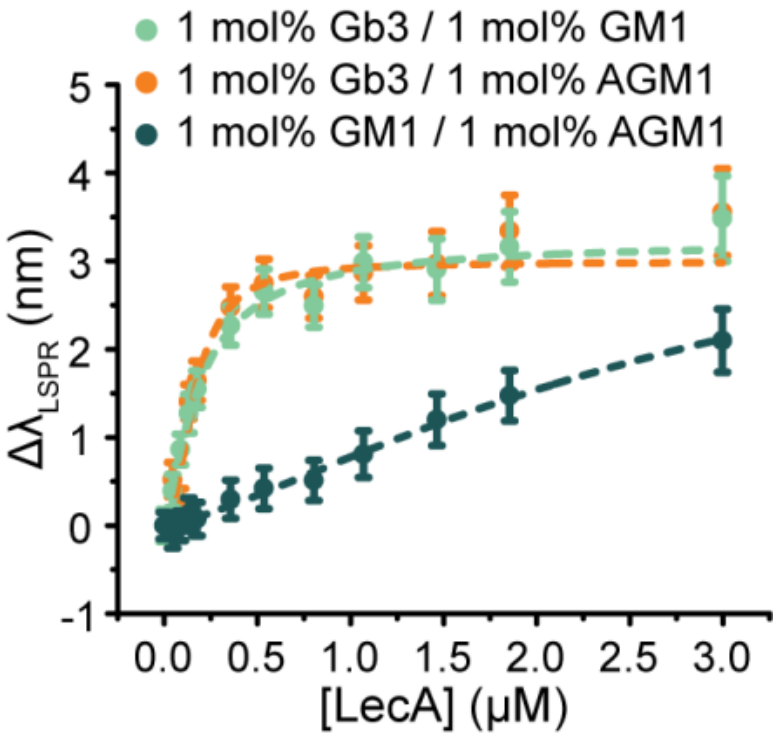

Figure 15: Cooperativity amongst Gb3, GM1, and AGM1 binary mixtures. Saturation curves for LecA binding to the bilayers containing mixtures of Gb3 and moderate receptors show positive cooperativity. The data are represented as mean ± S.D. (n=8). The dashed lines represent Hill equation fits to the data. To better show the data points at low concentrations, the binding curves on a semi-log scale are shown in APPENDIX C.

Binding Cooperativity Amongst Moderate and Weak Receptors

In addition to the strong receptor (Gb3), we wondered if the moderate receptors (AGM1 and GM1) were sufficient to activate weak receptors (i.e. LacCer and GalβCer), leading to higher LecA attachment. First, we investigated the binding cooperativity between LacCer and the moderate receptors. (**Figure 16a**) We observed positive cooperativity between 1 mol% of each moderate receptor, individually, with 4 or 8 mol% of LacCer. This observation indicated that the moderate receptors were able to activate LacCer, leading to the increased LecA attachment. We

also examined the change of cooperativity under different LecA concentrations. (**Figure 35**) Similar to Gb3+LacCer system, the cooperativity became significant when the LecA concentration reached a threshold value. However, the threshold concentration of the moderate receptors (~0.5 μM) was higher than the threshold of Gb3 (0.1μM). As discussed above, LecA has to first bind to high affinity receptors, leading to an increased effective concentration of the weak receptor for subsequent binding. The threshold LecA concentration is probably dominated by the first binding step, which is associated with the K_h of the higher affinity receptor. Thus, we observed cooperativity significantly increased after the LecA concentration reached the K_h value of the moderate receptors (~0.5 μM).

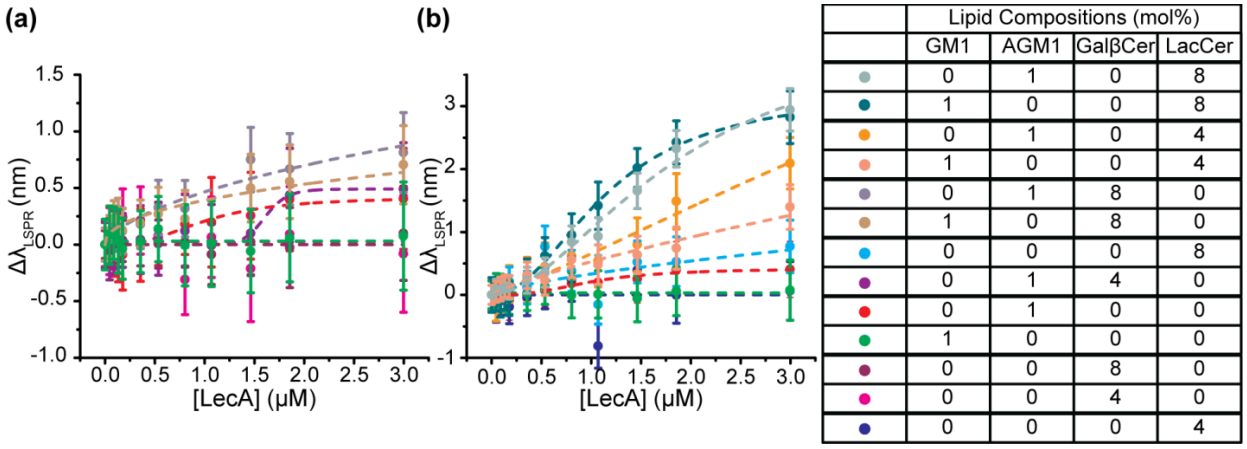

	Lipid Compositions (mol%)			
	GM1	AGM1	GalβCer	LacCer
●	0	1	0	8
●	1	0	0	8
●	0	1	0	4
●	1	0	0	4
●	0	1	8	0
●	1	0	8	0
●	0	0	0	8
●	0	1	4	0
●	0	1	0	0
●	1	0	0	0
●	0	0	8	0
●	0	0	4	0
●	0	0	0	4

Figure 16: Cooperativity between moderate and weak receptors. Saturation curves for LecA binding to GM1 and AGM1 show cooperativity with (a) LacCer and (b) GalβCer. The dashed lines represent Hill equation fits to the data (represented as average ± S.D. (n=8)). To better show the data points at low concentrations, the binding curves on a semi-log scale are shown in APPENDIX C.

The cooperativity between the moderate receptors and GalβCer is not as significant as LacCer. (**Figure 16b**) The calculated heterogeneous cooperativity for GalβCer with GM1 is

slightly higher than AGM1; however, the cooperativity values for both GM1 and AGM1 systems are below two standard deviations. (**Table 4**) As a result, it is not clear whether there is positive cooperativity between GalβCer and moderate receptors.

Regardless, we have confirmed that LecA binding capacity enhancement is not necessarily limited to just the highest affinity receptor, Gb3, but can also be observed with GM1 and AGM1 mixtures. This is similar to the case with CTB in which positive cooperativity is observed with both GM1 (a strong receptor) and fucosyl-GM1 (a moderate receptor).[18]

Discussion

We demonstrated that mixing high-affinity receptors with weaker binding receptors leads to increased LecA binding capacity on model membranes. This phenomenon can be accurately described using the RD model.[17,18] Furthermore, in order to initiate cooperative binding, we found two conditions must be satisfied. First, there is a minimum LecA concentration required before observing significant cooperativity. The minimum concentration corresponds to the dissociation constants (K_h) of the highest affinity receptors present in the model membrane. This is evidenced by cooperativity increasing above 0.1 μM LecA for Gb3+LacCer mixture and above 0.5 μM LecA for GM1+LacCer and AGM1+LacCer mixtures. This criterion is predicted by the RD mechanism. In the RD model, the first binding event brings a ligand from solution phase to the model membrane; then, the effective receptor concentrations increase for the subsequent binding events due to the reduced dimensionality of diffusion. Therefore, it is logical to expect the occurrence of hetero-multivalent binding is limited by the first binding event, which corresponds to the dissociation constant between LecA and the highest affinity receptor.

The second criterion is that the weaker receptor has to reach a minimum density. This threshold density seems associated with the affinity of the weaker receptor. For Gb3+LacCer

mixtures, no obvious cooperativity was observed at 1 mol% of LacCer, but the cooperativity drastically increased at 2 mol% of LacCer. When Gb3 was mixed with the moderate receptors (GM1 & AGM1), we observed significant cooperativity at 1 mol% of the moderate receptor. This observation is similar to the CTB binding system. When comparing two weak CTB receptors (dissociation constants of GM2 & GM3: 2mM & 210mM), we observed significant cooperativity when a high-affinity receptor was mixed with 1 mol% of GM2, but 1 mol% of GM3 was not sufficient to induce hetero-multivalent binding.[18] However, after raising GM3 to 14 mol%, the cooperativity was observed.[33]

The threshold density of LacCer, approximately 2 mol%, is a noticeable portion of the total model membrane. This raises the question of whether LacCer in epithelial cells is present in sufficient quantities to play a role in LecA binding. To address this concern, we note that glycolipids are highly enriched in the apical plasma membrane of polarized epithelial cells.[7,161,162] Additionally, it has been shown that the glycolipid content can reach up to 30% of the total membrane lipids in microvilli.[163] This is significant as the typical total glycolipid fraction of the entire membrane for mammalian cells is ~5%.[164] Furthermore, Parkin et al. observed the microvillar membranes in porcine kidney cortex contain 3.53 mass% of LacCer, and LacCer was further enriched up to 7.26 mass% in detergent-resistant domains of microvilli.[165] Besides cell polarization, Gb3 can also cluster with galactosyl ceramide, glucosyl ceramide, and LacCer in cholesterol enriched domains.[166] These clustering processes could further concentrate local glycolipid abundance. Therefore, it is reasonable to expect that the threshold density of LacCer is biologically relevant on a local scale.

According to the RD hypothesis, the activation of weak receptors increases the total amount of available binding sites on membrane surfaces, resulting in increased binding

capacities. In the same situation, when a LecA molecule simultaneously binds to Gb3 and LacCer receptors, we expected its binding avidity would be lower than that of LecA binding to four Gb3 receptors. This hypothesis was supported by our experimental observations. When Gb3 was mixed with weak and moderate receptors, the K_h value increased. In addition, the colloid aggregation measurement exhibited the deceased binding avidity of Gb3+LacCer mixtures. The changes of binding capacity and binding avidity may affect downstream processes of LecA. For instance, Eierhoff et al. showed that LecA-Gb3 interaction is critical to induce *P. aeruginosa* invagination of giant unilamellar vesicles (GUVs) and H1299 cells.[145] Based on their theoretical model, a higher number of LecA-Gb3 binding events and higher adhesion energy enhance membrane engulfment of *P. aeruginosa*. Therefore, it is reasonable to expect that the potential hetero-multivalent binding of LecA influences the invagination process. Another example is that Gb3 serves as a signaling receptor for LecA to induce CrkII phosphorylation.[140] The participation of weak receptors, such as LacCer, may change the signaling response. Moreover, it has been reported that ligand binding to LacCer can activate Src family kinase Lyn.[167] Thus, the hetero-multivalent binding of lectins introduces a possible secondary role of lectins in the Lyn signaling pathway. Further investigation is required to understand the potential role of hetero-multivalency in various biological systems.

Besides demonstrating a LecA binding mechanism, we demonstrated the potential of using hetero-multivalent binding to improve targeted drug delivery. Traditionally, targeted drug delivery schemes have tended to decorate the drug carrier with the highest affinity receptors[168,169]; however, this strategy often leads to higher off-target binding. A recent computational study suggests that using a combination of multiple weaker affinity ligands can improve selectivity, and that selectivity can be further optimized by varying the ligand surface

densities.[170] This theoretical study brings to light a new aspect of targeted drug delivery. However, using a set of low affinity ligands may reduce the targeting efficiency of drug carriers. A potential solution is to decorate weak-affinity ligands on a fluidic liposome surface along with a moderate ligand that can facilitate weak ligand-receptor binding via the RD mechanism. Thus, we believe liposomal carriers are an attractive approach for the design of multivalent-targeted drug delivery systems.

In our recent work with collaborators, liposome-bacterium studies demonstrate the applicability of glycolipid mixtures to achieve improved liposome targeting to *P. aeruginosa*.[171] Specifically, our results yielded two main conclusions. First, adding multiple types of glycolipids can significantly improve liposome binding beyond single glycolipid liposomes.[171] Given the observed binding pattern, LecA is probably not the only actor at work in liposome binding to *P. aeruginosa*. We believe other galactose binding adhesins, such as T4P, contribute to the observed liposome targeting. Second, the binding between *P. aeruginosa* and liposomes containing only LacCer receptor was negligible.[171] Therefore, LacCer has to form a partnership with the Gb3 receptor in order to exhibit improved liposome retention. This phenomenon is consistent with the LecA and CTB binding systems. Weak receptors need the assistance of high-affinity receptors to initiate hetero-multivalent binding. This phenomenon presents an issue to conventional ligand-receptor screening assays (e.g. microarray technology) because they screen receptors one by one. As a result, conventional methods may miss the essential weak binding receptors, which exhibit high binding selectivity to the target pathogens. Thus, our previously published membrane perturbation protocol could provide a more efficient strategy to screen potential weak receptors involving *P. aeruginosa* in binding.[18] However, there is much work to

be done to create a rational basis for *a priori* targeting design in terms of both affinity and selectivity.

Chapter Conclusion

Using model membranes, we have shown positive cooperativity of hetero-multivalency in LecA and the experimental observations support the RD hypothesis. Furthermore, we found that protein concentration and the density of weak receptors in model membranes are critical parameters to trigger hetero-multivalent binding. Based on our observations, we expect that the localized enrichment of membrane receptors induced by phase separation, dynamics of the cell cytoskeleton, cell polarization, and lipid asymmetry can influence the effect of the RD mechanism. Further studies are required to dissect the role of the RD mechanism in biological systems.

CHAPTER V

SEMI-QUANTITATIVE EVALUATION OF HETEROGENEOUS GLYCOLIPID MIXTURE HETERO-MULTIVALENCY USING A TURBIDITY-BASED EMULSION AGGLUTINATION (TEA) ASSAY

Chapter Summary

Lectin hetero-multivalency, binding to two or more different types of receptors, has been demonstrated to play a role in both LecA (a *Pseudomonas aeruginosa* adhesin) and Cholera Toxin subunit B (a *Vibrio cholerae* toxin) binding to glycolipids. This work has been done using nanocube sensors. While the nanocube sensors are one of the most high-throughput methods that also provide quantitative data, it is preferable to sacrifice some data quality in favor of efficiency when screening large molecular libraries. In order to complement the nanocube sensor, we present a semi-quantitative turbidity-based emulsion agglutination (TEA) assay for efficiently screening lectin binding capacities to heterogeneous lipid surfaces. The benefit of this assay is that it relies on the use of emulsions that can be formed in a continuous manner to enable semi-quantitative high-throughput screening without the bottleneck of functionalization. The TEA assay utilizes the lectin-induced aggregation rate of glycolipid stabilized oil droplets to determine hetero-multivalency. We demonstrate the correlation of the initial dτ/dt from UV\Vis turbidity data and increasing particle size as determined by Dynamic Light Scattering (DLS) to the aggregation rate. The aggregation rate in both systems followed the trend observed in our prior hetero-multivalent binding capacity results using a nanocube sensor. Therefore, the developed TEA assay can be used as a high-throughput tool to screen for hetero-multivalency before turning to the batch functionalized quantitative nanocube sensor.

Introduction

The exterior surface of cell membranes is densely populated with sugars in what is known as the "glycocalyx".[13] This glycocalyx forms the foundation for interactions as diverse as cell-cell recognition, host-pathogen recognition, and cell signaling.[13,172-174] The proteins that mediate this interaction by binding to glycans are called lectins.[13] As the affinity between a glycan and a single binding site in a lectin is typically low, lectins utilize multiple subunits to bind several glycans simultaneously.[13,172-174] These multivalent interactions give rise to not only stronger overall binding, but also enable modulation of affinity and selectivity of the binding lectin.[175-178]

We recently demonstrated that hetero-multivalency (i.e. a lectin simultaneously interacting with different types of receptors) could enhance the binding capacity of lectins to model membranes via an inherent Reduction of Dimensionality (RD) mechanism.[17,18,171] The evidence of hetero-multivalency presents a critical issue to conventional ligand-receptor screening assays because they do not account for the nature of multivalency and the fluidity of cell membranes. To address the issue, we recently introduced a novel nanocube sensor that enables label-free detection of protein binding to cell membrane mimicking surfaces using a standard laboratory spectrophotometer.[17,18,171] Although, the nanocube system encompasses many unique advantages (e.g. high-throughput utility, absolute quantification without daily calibration, easy-to-use, high sensitivity, etc.), a few drawbacks remain.[17,18,171] The primary drawback is that the formation of supported lipid bilayers has to be conducted in a batch process, which slows down the overall screening process. This limits the scientific community's ability to screen receptor candidates for hetero-multivalency from a large molecular library.[18] Therefore, a

high-throughput screening system for determining potential receptors involved in hetero-multivalent binding is desirable.

A promising system for the high-throughput screening of lectin interactions with glycolipids is the agglutination assay.[179] Lectin-glycan interactions are detected by monitoring the lectin-induced aggregation of glycan-coated particles. Classically, this assay was a hemagglutination assay in which the lectins that induced red blood cell aggregation indicated the donors' blood group type.[180-183] Several groups have used oil in water (O/W) emulsion to replace the red blood cells in the hemagglutination assay.[184-188] Oil droplets are superior to other types of agglutination assays in several aspects. First, in contrast to red blood cells, the types and densities of receptors on oil droplet are controllable. Second, glycolipids presented at the oil-water interface maintain the same two dimensional fluidity as on native cell membranes.[189] Third, compared to liposome agglutination assays, the higher refractive index of oil droplets improves the sensitivity of agglutination measurements at smaller particle sizes.[190] Fourth, the preparation of these emulsions can be done via high-throughput ultrasonication or high-pressure homogenization.[191] Both well-established emulsion methods can generate stable nano-sized droplets, typically about 100 nm in diameter.[191-194] Thus, nano-sized emulsion aggregation represents a high-throughput customizable system for hetero-multivalent screening.

In this paper, we present a turbidity-based emulsion agglutination (TEA) assay to rapidly determine potential glycolipid candidates involved in lectin hetero-multivalency. We have demonstrated that LecA from *Pseudomonas aeruginosa* could induce aggregation of glycolipid decorated particles at certain glycolipid compositions;[171] thus, we used LecA to validate the TEA assay. The emulsion aggregation results in changes in solution turbidity. These changes in turbidity were measured by a UV/Vis spectrophotometer as graphically represented in **Figure**

17.[184-188,195,196] Prior studies have determined the relationship between the turbidity of the solution at various wavelengths and the particle size, allowing us to quantify the degree of agglutination using turbidity.[197,198] The hetero-multivalency candidates identified by the emulsion agglutination assay correlated well with the nanocube experiments performed in our recent publication.[171] In addition, we validated our particle aggregation results using kinetic measurements of particle size by DLS and found excellent agreement between these two techniques.

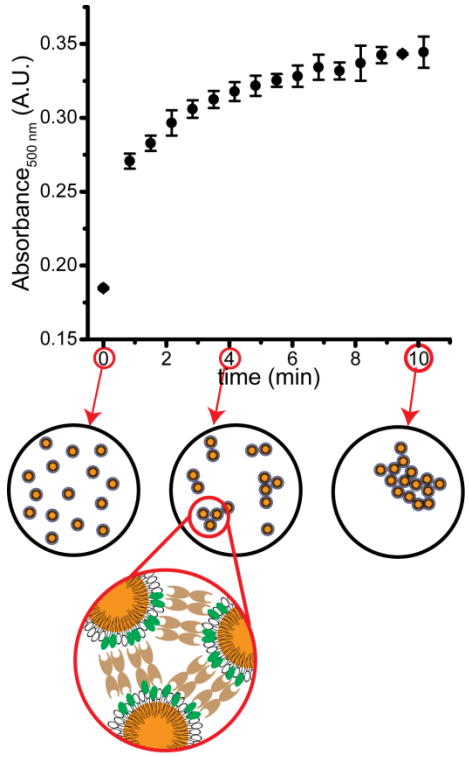

Figure 17: Schematic of particle aggregation relative to observed changes in absorbance at 500 nm.

Emulsion Turbidity Theory

In this article we rely on the analysis of Timasheff.[198] Using a UV/Vis spectrophotometer, we measure the absorbance of the solution as shown in **Figure 17**. The turbidity can be expressed as a function of emulsion concentration and particle size: [197]

Equation 9

$$\tau = \frac{\ln\left(\frac{I_0}{I}\right)}{l} = K\pi a^2 N$$

where τ = the turbidity; I_0 = intensity of the incident light; I = intensity of the transmitted light; l = scattering path length; a = the particle radius; N = the concentration of particles; and K = the total scattering coefficient which typically varies between 0 and 5.[190] K is defined as

Equation 10

$$K = K_0\left(\frac{a}{\lambda}\right)^y$$

where K_o = the size-independent component of the scattering coefficient and y is the exponent of the wavelength, λ, dependent on the particle size and refractive index. In our analysis, the measured absorbance represents the turbidity; thus a 1/2.303 factor is included in K_o. While, the y exponent typically varies between -2.2 and 4.0 (Rayleigh scattering) and is given by Timasheff as:[198]

Equation 11

$$\left(\frac{\partial \ln \tau}{\partial \ln \lambda}\right)_a = -y$$

For a polydisperse system, turbidity is defined as:

Equation 12

$$\tau = K_0 \sum_i V_i^{\frac{2}{3}} N_i \left(\frac{V_x^{\frac{1}{3}}}{\lambda}\right)^y$$

where $V_i = 4/3\pi a_i^3$, N_i is the number of particles of radius a_i, and:

Equation 13

$$V_i = xV_0$$

where x is the degree of polymerization. When the total mass of the associating species is constant then:

Equation 14

$$N_i = N_0(1-p)^2 p^{x-1}$$

where N_0 is the initial number of particles and p is the fraction of all functional groups reacted after a given time, t. Combining this with **Equation 12** gives

Equation 15

$$\tau = \frac{KN_0 V_0^{\frac{y+2}{3}}}{\lambda^y} \sum_i p^{x-1}(1-p)^2 x^{\frac{y+2}{3}}$$

and

Equation 16

$$\frac{d\tau}{dt} = \frac{KN_0 V_0^{\frac{y+2}{3}}}{\lambda^y}(1-p)^2 \frac{d}{dt}\sum_i p^{x-1} x^{\frac{y+2}{3}}$$

where $p = \frac{\frac{1}{2}kt}{1+\frac{1}{2}kt}$ and k is the rate constant of the second-order condensation polymerization/coagulation rate. For the case of Rayleigh scattering, these equations become, as given by Oster:

Equation 17

$$\tau = \frac{1}{2.303}\frac{24\pi^3}{\lambda^4} n_0^4 \left(\frac{m^2-1}{m^2+2}\right)^2 V_0^2 N_{0,c}(1+kt)$$

and

Equation 18

$$\frac{d\tau}{dt} = \frac{1}{2.303}\frac{24\pi^3}{\lambda^4} n_0^4 \left(\frac{m^2-1}{m^2+2}\right)^2 V_0^2 N_{0,c} k$$

where $N_{0,c}$ is the initial number of particles per unit volume, n_0 is the refractive index of the solvent, and m is the ratio of solute to solvent refractive indices.[196] From these equations, it is clear that dτ/dt is a function of the aggregation rate, k (called the coagulation rate above and by Timasheff).[198]

To ensure that sufficient time was given to allow for particle aggregation, we calculated the mean first pass time using the Stokes-Einstein equation:

Equation 19

$$D = \frac{k_b T}{6\pi\mu a}.$$

where: D is the droplet diffusivity; k_b is the Boltzmann constant; T is temperature; and μ is the viscosity. Following the analysis of Smoluchowski, the diffusion limited mean first pass time is then:[113]

Equation 20

$$t_{diffusion} = \frac{1}{4\pi a N D}$$

Therefore, we can calculate $\tau_{diffusion}$ be sure that the aggregation rate that we observe from the DLS and the turbidity measurements are not diffusion limited aggregation rates.

Methods and Materials

Materials

Silicone oil (refractive index of 1.403), PA-IL from *Pseudomonas aeruginosa* (also known as LecA), and tris-buffered saline (TBS) obtained as a 10x solution (1x working solution

20 mM Tris 0.9% NaCl pH ~7.4) were purchased from Sigma-Aldrich (St. Louis, Missouri). Calcium chloride was from BDH VWR Analytical (Radnor, Pennsylvania). Globotriaosylceramide, Gb3, (Galα1-4Galß1-4Glc-Ceramide), and Lactosylceramide, LacCer, (Galβ1-4Glc-Ceramide) were purchased from Matreya LLC (State College, PA). 1-palmitoyl-2-oleoyl-sn-glycero-3-phosphocholine (POPC) was purchased from Avanti Polar Lipids (Alabaster, AL).

Methods

Preparation of O/W emulsion

The desired compositions of lipids in chloroform solutions were mixed in a 25 mL round bottom flask and, then, dried using a rotary evaporator (Heidolph Hei-VAP Value®). The dried lipids were reconstituted using 1X TBS with 100 μM $CaCl_2$, forming multillamellar vesicles (MVs) in an aqueous solution. The emulsions were prepared by mixing 5 μL of silicone oil, 474.18 μL of 1X TBS with 100 μM $CaCl_2$, and 220 μL of MV solution. The mixture was then sonicated with a Qsonica Q125 tip sonicator used at 60% amplitude for 1 hour cycling 10 seconds on and 10 seconds off in an ice bath. The size distributions of oil droplets were determined by DLS.

Kinetic turbidity measurement

The emulsion was diluted as 20 μL of emulsion into 80 μL of 1X TBS with 100 μM $CaCl_2$ in each of six wells of a 96 well plate (Costar® 3370) to maintain turbidity in a range of 0.5 to 0.8 A.U. This was done in order to ensure that the UV/Vis was in the linear response region. The turbidity of the emulsions was detected by an ultra-fast UV/Vis microplate spectrophotometer equipped with a CCD camera (FLUOstar Omega®, BMG-Labtech). Because biological analytes do not significantly absorb light at a wavelength of 500 nm, the turbidity was

determined at this wavelength. 10 μL of 3.227 g/L LecA was added to three wells of the emulsion to induce agglutination. 10 μL of the buffer was added to the remaining three wells as the negative controls. All of the solutions were mixed by pipetting in the well plate. After mixing, the turbidity of the emulsions was detected using the microplate spectrophotometer. The extinction spectra were collected in the range of 300-1000 nm wavelengths every ~40-60 s for 60 minutes and then every 30 minutes for 2 more hours at room temperature. Each spectrum was the result of averaging 200 flashes per well at a 1 nm resolution. The time from LecA addition to the start of turbidity detection was 50 s. The absorbance at 500 nm over the course of 2 min was fit with a line to obtain the change in turbidity vs time, $d\tau/dt$.

Kinetic DLS measurements

Batch mode hydrodynamic size (diameter) measurements were performed on a Malvern Zetasizer Nano ZS90® (Malvern Instruments, Southborough, Massachusetts) at 90°. The emulsion was diluted as 10 μL of emulsion into 90 μL of 1X TBS with 100 μM $CaCl_2$ followed by equilibration (typically 2 minutes) in the DLS at 25°C before a minimum of three measurements per sample were made. After dilution, the system was checked for multi-particle scattering by testing 10 μL of emulsion diluted into 190 μL of 1x TBS with 100 μM $CaCl_2$ to ensure that it gave the same particle diameter. Then 5 μL of 3.227 g/L LecA was added to the cuvette of the 10 μL emulsion into 90 μL of 1X TBS with 100 μM $CaCl_2$ dilution and mixed by pipetting the solution 10 times. A measurement of hydrodynamic size (determined by cumulants average or Z- average) via three measurements was then taken every 10 minutes for 2 hours. Only results with a polydispersity index (PDI) less than 0.3 were used for fitting to minimize errors in calculating particle diameter by method of cumulants.

Statistical analysis

The turbidity testing for each lipid composition was repeated on 3 different days with 3 technical replicates on each day for a total of 9 replicates. The turbidity data sets were tested for normality using the Kolmogorov-Smirnov test in OriginPro 9.1®. In all cases, we could not reject the null hypothesis that the data came from normal distributions. Therefore, it was reasonable to apply the equal variances and Welch's unequal variances t-test to the data. For data across lipid compositions, the unequal variance t-test was used. For interday data, the population data was compared to each individual day's data of the same lipid composition using the equal variance t-test and the coefficient of variance for each lipid composition was calculated. The DLS data set is represented as mean ± SE (n=3 runs over each 10 min interval) per lipid composition.

Results and Discussion

Figure 18 provides example curves of turbidity as a function of time for each bilayer composition tested. Initially, the turbidity increases proportionally to particle size as the particles exhibit Rayleigh scattering, $y \approx 4$ in **Equation 11**.[198] As the particles continue to aggregate, y goes from ≈ 4 to -2 indicating a shift from $a < \lambda$ ($y \approx 4$ to 2, Rayleigh scattering region) to $a \approx \lambda$ ($y = 2$ to -1, Mie scattering region) and finally to $a > \lambda$ ($y = -1$ to -2.2, Airy theory region).[190,198] It should be noted that the plateau region of the turbidity data should not be assumed to be the steady state value. Timasheff explains that the plateau region is special case that occurs when $y = 1$ and causes scattering to be independent of particle radius yielding a maximum value.[198] If we continue the experiment to longer times, we see an inversion in the dependence of the turbidity with particle size and observe a decrease in turbidity when $y < 0$.[198] Therefore, the changes in the turbidity data are adequately predicted by Timasheff's theory.

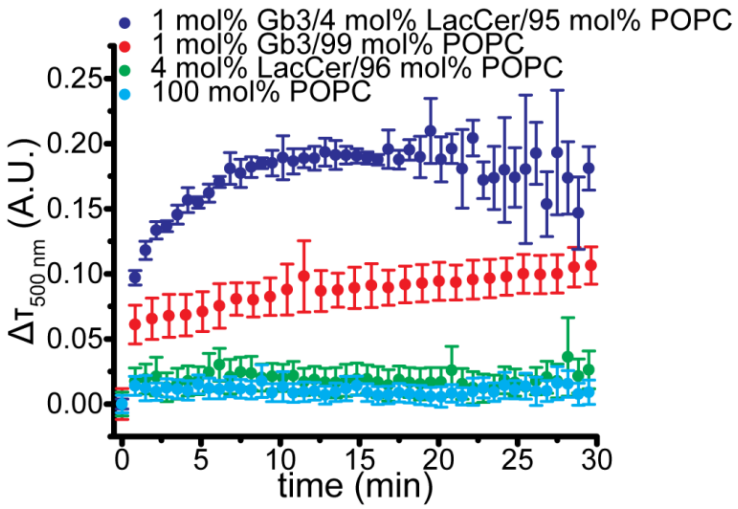

Figure 18: Example baseline subtracted turbidity data for each bilayer composition. Data is given as a dot plus error bars where the dot is the mean and the error bars are a standard deviation, n = 3, D.F. = 2).

Given the complexity of calculating the population distribution required for using **Equation 15**, the analysis is greatly simplified by using only the initial linear region of the turbidity data. This initial region should follow the predictions of Rayleigh scattering. We validated the use of Rayleigh scattering for the initial time points (particle diameter ≤ 275 nm and y = 2 to 2.5 for t < 2 min) using the parameters given by Kerker *et al*. with the cutoff criteria as defined by Rahn-Chique *et al*.[188,199,200] Kerker *et* al. defined two parameters, α (the dimensionless size parameter) and C_{RGD} (a measure of phase shift), to evaluate the Rayleigh scattering, where both are given as[188,199,200]:

Equation 21

$$\alpha = 2\pi a/\lambda$$

and

Equation 22

$$C_{RGD} = \left(\frac{4\pi a}{\lambda}\right)(m-1).$$

when $\alpha < 2.0$, there is a less than 10% error in using Rayleigh scattering. For our system, $\alpha \leq 1.7$ and $C_{RGD} \leq 0.19$ when using 1.338 as the refractive index of 1x TBS buffer.[201] Our C_{RGD} value is less than the Rayleigh scattering threshold (C_{RGD} = 0.22) given by Rahn-Chique *et al.*[188] Therefore, we could use **Equation 17** and **Equation 18** to interpret the turbidity data. Thus, $d\tau/dt$ value calculated from the initial slope (t < 2 min) of the turbidity data should be proportional to the particle aggregation rate, excluding the influence of multiple scattering.

There are two primary advantages to performing the analysis in the Rayleigh scattering region. First, particle aggregates can induce greater changes in turbidity in the Rayleigh scattering region than in the Mie scattering or Airy theory regions, leading to higher sensitivity of the turbidity measurement. Second, the initial slope, $d\tau/dt$, of the turbidity data is sufficient for relative aggregation rate comparisons. This is because only k will vary in **Equation 18** if m, N_0, V_0, and λ are constant. Thus, to ensure that the Rayleigh scattering equations were applicable, the analysis was conducted using data for 0-2 minutes, i.e. when the particle diameter is less than 275 nm, giving $\alpha < 2.0$ and $C_{RGD} < 0.22$ for all lipid compositions.

Although we can use α and C_{RGD} to evaluate the applicability of Rayleigh scattering, the particle size is required to determine the parameters. Therefore, a particle size measurement, provided by techniques such as DLS, is needed. Another approach to determine whether the system is in the Rayleigh scattering region is measuring the y value using turbidity data. For Rayleigh scattering, y should be greater than or equal 2. This becomes a useful criterion to substitute for DLS measurements as y has been linked to the particle size.[202-204] However, y is only a valid approximation of particle size in regions where there is no significant light

absorption from the molecules, such as the surfactant (lipids, in this case), aqueous phase, and oil phase.[202-208] To ensure the selected wavelengths incident light obeys Rayleigh scattering, we used turbidity data over the range of 500-800 nm wavelength to calculate *y* as given by **Equation 11**.[198] This alternative approach can be useful for scientific communities because only UV\Vis measurements are needed to calculate the wavelength exponent, *y*, in order to determine if we are in the Rayleigh scattering region. However, there are a few potential pitfalls to using this method. One pitfall is that the $y \geq 2$ criterion assumes the oil and aqueous phases are the silicone oil and 1x TBS buffer solutions used in this work. If this is not the case, the Rayleigh scattering region is only certain if $y = 4$. Another pitfall is that the TEA assay should be conducted under different droplet concentrations until the turbidity measurements give a consistent initial slope in order to avoid multiple scattering.[188] Thus, the work presented here will simplify future analysis with the same system by eliminating the need for subsequent DLS measurements.

Kinetic DLS Results

To validate the TEA assay, we first conducted a binding experiment with DLS. The results are shown in **Figure 19**. In each case, a two-fold dilution of the emulsion gave the same diameter as before dilution ensuring that our observations were not altered by multiple scattering. 1 mol% Gb3 + 4 mol% LacCer aggregated the fastest at 5.8 ± 0.3 nm/min (n=6, DF=4). 1 mol% Gb3 aggregated about five times slower at 1.16 ± 0.05 nm/min (n=14, DF =12). 4 mol% LacCer aggregated at 0.084 ± 0.0045 nm/min (n=8, DF =6), approximately half the rate of 1 mol% Gb3. This was greater than the base line aggregation of 100 mol% POPC that corresponds to essentially constant particle size. Given the addition of LecA does not induce a change in the 100 mol% POPC emulsion particle size, we can conclude that any observed increase in particle size

is due to the specific interaction of LecA with a glycolipid receptor resulting in droplet aggregation.

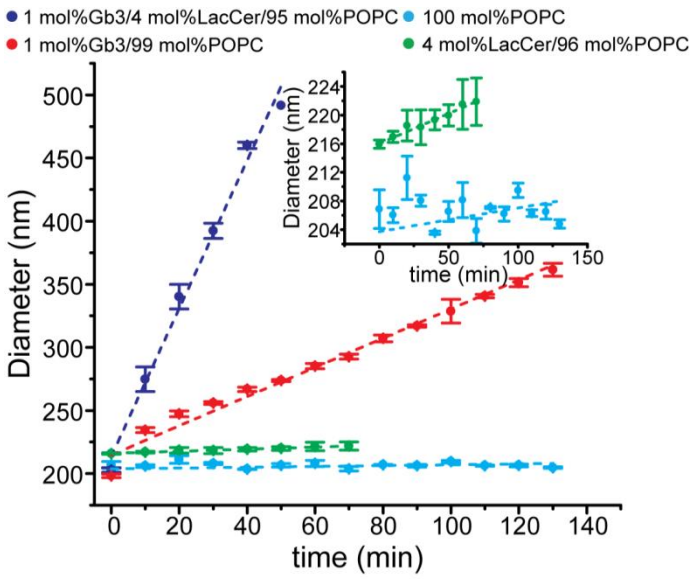

Figure 19: DLS data of average diameter as a function of time since LecA addition. Dots with bars represent the average diameter determined from cumulants Z-ave mean ± S.E. (n = 3) of three tests for each 10 minute time interval with a PDI < 0.3. The dashed line represents the fitted slope for each bilayer composition. Inset is a zoomed in view of 4 mol%LacCer and 100 mol% POPC bilayers.

In our prior work with LecA, we observed that lipid surfaces containing both Gb3 and LacCer bound more LecA than either Gb3 or LacCer individually.[171] This indicated that hetero-multivalency, a protein simultaneously binding to two or more different types of receptors, may play an essential role in LecA-glycolipid recognition.[171] Interestingly, the aggregation rate in the DLS seems to exhibit the same behavior as the binding capacity we observed using our nanocube system indicating that the DLS aggregation rate can be used to observe hetero-multivalency.[171]

Kinetic Turbidity Results

After noting that the emulsions' DLS aggregation rate was correlated to our prior binding capacity results, we focused on relating $d\tau/dt$ for the Gb3 and LacCer system to the DLS results and prior binding capacity data.[171] The results of this testing across three different days are shown in **Figure 20**. What was immediately obvious is that each day's three data points were part of the same cluster as each other day's proving the reproducibility of this method. This was confirmed in that the data from each day was not significantly ($p < 0.05$) different from the total population and that the coefficients of variation of 9%, 14%, 52%, and 58% for 1 mol% Gb3 + 4 mol % LacCer, 1 mol% Gb3, 4 mol% LacCer, and 100 mol% POPC, respectively. The slope of 1 mol% Gb3 ($d\tau/dt = 6.6*10^{-4}\pm0.3*10^{-4}$ ($n = 9$, $DF = 8$)) was significantly greater ($p < 0.001$) than both 4 mol% LacCer ($d\tau/dt = 2.2*10^{-4}\pm0.4*10^{-4}$($n = 9$, $DF = 8$)) and 100 mol% POPC($d\tau/dt = 1.7*10^{-4}\pm0.3*10^{-4}$($n = 9$, $DF = 8$)). Furthermore, the slope of 1 mol% Gb3 + 4 mol % LacCer ($d\tau/dt = 1.33*10^{-3}\pm0.04*10^{-3}$ ($n = 9$, $DF = 8$)) was significantly greater ($p < 0.001$) than 1 mol% Gb3. Therefore, we again saw the same behavior as the nanocube binding capacity in that 1 mol% Gb3 + 4 mol% LacCer aggregates faster than 1 mol% Gb3 indicating that the TEA assay can be used to observe hetero-multivalency.

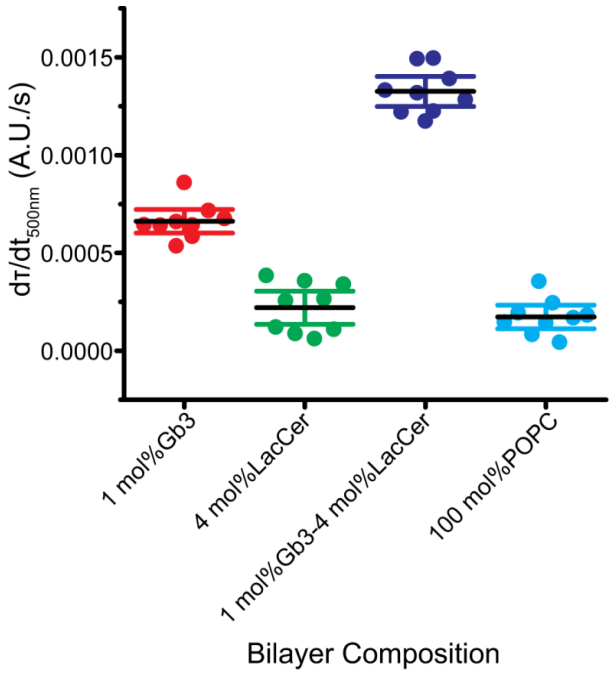

Figure 20: Bilayer reproducibility for four different bilayer compositions. Dots represent individual data points across 3 days. Solid black lines represent the mean slope of each bilayer. Colored lines represent two SE (n=9) of each bilayer.

From **Equation 18**, we can see that dτ/dt is changing due to a change in the aggregation rate, *k*. Combining this with the DLS result, we can say that dτ/dt is the result of LecA induced droplet aggregation that has been correlated to the hetero-multivalency observed in our nanocube system.[171] Furthermore, the ranking given in **Figure 20** agrees with the DLS measurement ranking for 1 mol% Gb3 + 4 mol% LacCer, 1 mol% Gb3, and 100 mol% POPC. Taken together, the data demonstrate that the linear region emulsion turbidity slope, dτ/dt, over longer times is strongly correlated to our expectations of hetero-multivalency from the nanocube system.[171]

TEA Assay Limitations

Both nanocube sensor data and the DLS results are in close agreement with dτ/dt data. This demonstrates the feasibility of using the TEA assay to study hetero-multivalency. However,

a few limitations remain with the TEA assay. First, the sensitivity is lower than the DLS and nanocube assays. Although the affinity between LacCer and LecA is weak, we could detect LecA binding to 4 mol% LacCer lipid surfaces using the DLS and nanocube sensor but not using the TEA assay. To improve the sensitivity, we could increase the droplet size. Increasing droplet size would result in greater changes in $d\tau/dt$, as turbidity is proportional to a^3, resulting in improved sensitivity. However, increasing the droplet size will make the TEA assay approach the Mie scattering region, leading to lower sensitivity. In order to minimize this tradeoff, oil droplets with higher refractive indices could be used. This is why oil droplet agglutination is preferred over liposome agglutination.[209]

A second limitation is that the TEA assay is semi-quantitative. This is inherent to the system as the values of $d\tau/dt$ are dependent on the working conditions and are therefore sensitive to droplet concentrations and droplet size. The number of droplets is important as it alters the mean first pass time. By altering the mean first pass time, you change the fastest aggregation rate that can be determined using the system, i.e. the diffusion limited reaction rate. Changing the diffusion limited reaction rate modulates the system's sensitivity range as only aggregation rates below the diffusion limit can be differentiated from each other.[196] The number of droplets is also proportional to droplet size, which is important for the reasons stated above. For the current system, the data is also statistically limited to being semi-quantitative. Only 1 mol% Gb3 + 4 mol% LacCer has a S/N ratio of greater than 10, a typical *a priori* limit of quantitation threshold.[210] While both 1 mol% Gb3 and 1 mol% Gb3 + 4 mol% LacCer have S/N ratios greater than 3, a typical a priori limit of detection threshold.[210] Thus, using $d\tau/dt$ is limited to semi-quantitative analysis.

A third limitation is that the current method only works for Rayleigh scattering below the diffusion limited aggregation rate. The limitation of Rayleigh scattering is a choice made in the design of the TEA assay so that it is unnecessary to determine the population distribution and so that hetero-multivalency can be determined without needing additional measurements of particle size.[198] This enables measurements using only the UV/Vis. On the other hand, the ceiling imposed by the diffusion limited rate is inherent to any aggregating system as the particles cannot aggregate faster than the time it takes for the particles to diffuse.[113] This can be worked around by increasing droplet concentration thereby lowering the mean first pass time, but the observable aggregation rate is eventually limited by the UV/Vis instrument's detection rate. Therefore, the current assay has limitations, but by altering experimental conditions or introducing additional measurements those limitations can be mitigated or removed.

TEA Assay Benefits

Despite some drawbacks, the TEA assay solves current problems with the tools used to study multivalent proteins. First, the TEA assay solves the problem of high-throughput screening of hetero-multivalency. For example, if we intend to screen 40 unknown receptors potentially involved in hetero-multivalent binding, approximate 800 conditions have to be examined in a binary combinatory binding assay. The intrinsic complexity of hetero-multivalency presents an issue for all existing assays. The TEA assay is compatible with a microwell plate reader enabling quick detection of multiple formulations simultaneously. Furthermore, nano-sized emulsions can be formed using continuous methods via sonication or high-pressure homogenization removing a key limitation of our nanocube sensor.[191] Second, the TEA assay provides a second way to determine relative hetero-multivalent binding that is easy to use, utilizes only inexpensive and widely available reagents, and uses only common laboratory equipment. The result of this is that

the TEA assay can easily be adopted in a wide range of biological laboratories. Thus, combined with its established reproducibility, the TEA assay is a tool that is amenable to screening of large molecular libraries without requiring specialized equipment.

Chapter Summary

We have applied emulsion aggregation theory to develop the TEA assay for studying complex hetero-multivalency of agglutinating lectins. The TEA assay was shown to correlate well with the DLS measured particle size changes induced by the addition of LecA. Furthermore, the TEA assay followed the expected results from our prior work reiterating the concept of hetero-multivalency in LecA binding to lipid mixtures of Gb3 with LacCer. In conclusion, our TEA assay enables the semi-quantitative detection of multivalent protein binding to heterogeneous lipid surfaces. Its high-throughput utility will significantly accelerate the receptor screening process for hetero-multivalency.

CHAPTER VI

CONCLUSIONS AND FUTURE WORK

In this work, we demonstrated the fundamentals of multivalent lectin binding, proposed a two-step binding mechanism (Reduction of Dimensionality, RD), and designed a semi-quantitative turbidity-based TEA assay for efficient screening of lectin hetero-multivalency. The initial demonstration of the fundamentals of multivalent lectin binding was given in Chapter II. Following up on this work, a two-step binding mechanism was proposed and validated for the binding of CTB to glycolipids in Chapter III. Chapter IV began the validation of the RD mechanism for LecA binding. Finally, Chapter V demonstrated and validated the use of emulsion turbidity as an efficient way to study lectin hetero-multivalency using droplet

Besides demonstrating CTB binding fundamentals, Chapter II explored two additional points. First, we used a theoretical model developed by Klassen *et al* to show that homogeneous cooperativity (Hill's coefficient, n) is inversely linked to homogeneous binding capacity.[17] This explained how CTB could have a higher binding capacity to fucosyl-GM1 as opposed to GM1 even though GM1 has a higher binding affinity.[17] Second, we provided a possible explanation to the question of why CTB does not correlate with GM1 binding *in vivo* as posed by Yanagisawa et al.[22] This question could be addressed by both the homogeneous and heterogeneous cooperativity observed in CTB binding to glycolipids. Together, these additional points supplement the conclusions of Chapter II by providing a theoretical explanation of CTB binding to homogeneous lipid bilayers.

In addition to proposing and providing initial validation of RD for CTB, we introduce two further points in Chapter III. First, we demonstrated that heterogeneous cooperativity is not

limited to fucosyl-GM1 + GM2.[18] This is important because it confirms the importance of the RD mechanism and the study of heterogeneous mixtures. Second, we established a membrane perturbation protocol.[18] This protocol enables the efficient screening of heterogeneous cooperativity receptor candidates by minimizing the number of experimental conditions compared to prior binary mixture arrays.[18] Therefore, Chapter III does more than propose and validate the RD model. Chapter III confirms the importance of the RD model by showing it applies more generally than a single case and developing a novel method of identification of additional systems affected by RD.

Chapter IV extends beyond the confirmation of the RD mechanism in LecA. We demonstrate additional rules governing heterogeneous cooperativity. Namely, there are threshold values of LecA concentration and the weak affinity receptor density that must be achieved before heterogeneous cooperativity will be observed.[171] Thus, Chapter IV extends the RD mechanism to introduce important lectin and lipid specific criteria for activating heterogeneous cooperativity.

In providing an TEA assay amenable to high-throughput emulsion formation and screening, Chapter V provides a way to efficiently identify glycolipid mixtures that exhibit hetero-multivalency. We provide evidence that LecA induces aggregation in glycolipid stabilized oil droplets that is correlated to the lipid surface binding capacity.[211] This was confirmed by measuring particle size as a function of time via DLS. Besides providing an additional system to assess hetero-multivalency, the turbidity-based assay enables easy modulation of oil phase viscosity to assess the impacts of the RD mechanism in lectin binding. In addition, the assay has potential to allow assessment of hetero-multivalency in molecules, such long chain glycolipids, that are difficult to incorporate into supported lipid bilayers.[212] Therefore, Chapter V introduces a

TEA assay for lectin binding that allows for the facile screening of receptors for hetero-multivalency without the functionalization limitations of the nanocube.

Taken together, Chapters II-V provide an initial framework for understanding and utilizing multivalent, especially hetero-multivalent, lectin binding. Initially, this was done by highlighting the necessity of understanding how heterogeneous environments alter lectin binding in previously unexpected ways. Secondly, this work provided evidence for RD as a central mechanism in multivalent binding systems. Third, we provide evidence of lectins binding to mixtures of multiple types of receptors. In the LecA system, the binding occurred between lactosyl ceramide (LacCer) and Gb3, each of which can trigger signaling pathways.[140,167] Therefore, it is possible for heterogeneous multivalent binding to link signaling pathways. Lastly, we introduced the option of improving selectivity of lectin systems. This is a result of lectins' ability to bind to receptor mixtures enabling tuning of a lectin inhibitor using two or more receptor types. This is in contrast to prior lectin inhibitor optimization that typically focused solely on tuning lectin binding with a single receptor type.[25,40,213] Thus, we developed an initial framework for understanding multivalent lectin binding with consideration to elucidating biologically relevant phenomena and improving lectin inhibition.

Building upon the work presented here, a future direction of this work is to establish a method to theoretically predict heterogeneous cooperativity from monovalent binding affinity and capacity. Successful development of a theoretical prediction method would be beneficial to the scientific community in several ways. First, such a method would enable the *a priori* design of drug delivery schemes based on mixed receptor bilayers and facilitate the tuning of relevant parameters, such as binding affinity, capacity, and selectivity.[171] Second, a theoretical method should greatly simplify the identification of new systems that exhibit hetero-multivalency. This

would be accomplished by limiting the number of tests required to only the most likely conditions as determined by theoretical prediction of heterogeneous cooperativity. The development of a theoretical prediction method also seems feasible. One reason is that the RD model does not necessarily require measurements of the mixture meaning that individual binding data and physical properties should be sufficient.[18,171] Another reason is that we have already established that heterogeneous cooperativity activation is correlated to receptor binding affinity. Thus, the development of a theoretical prediction method would be beneficial to the scientific community and seems feasible based on preliminary evidence.

A second future direction of this work is to expand the membrane perturbation protocol to extracted cell membranes. Development of this method should enable quick assessment of host-pathogen interactions for cooperativity. This would detect relevant binding receptors that are missed by current techniques.[17] Furthermore, the facile doping of the bilayer with additional glycolipids should also work in concert with the aforementioned theoretical prediction method to confirm any predictions of hetero-multivalency. This expansion of the membrane perturbation protocol could be quickly applied to the TEA assay as it only requires incorporation of the membranes with the oil and buffer. Furthermore, this expansion should also be compatible with the nanocube system, albeit with a bit more work than the TEA assay. The primary reason is that coating of epithelial and bacterial outer cell membranes has been demonstrated for planar supported lipid bilayers.[212,214,215] Therefore, the coating of nanocubes using analogous methods should be achievable. A secondary reason is the ability to co-adsorb doping glycolipids vesicles along with the extracted cell membranes providing an easy way to modulate glycolipid densities required for the membrane perturbation protocol. As a result, the expansion of the membrane

perturbation protocol should be an achievable future direction and greatly influence analysis of heterogeneous lectin binding especially in less understood lectins.

A third future direction of this work is to further validate the RD mechanism. In Chapter III and Chapter IV, we demonstrated strong support for the RD mechanism. However, we did not establish the relative contributions of allosteric regulation and the RD mechanism to the enhanced binding capacity caused by hetero-multivalency. Elucidating the relative contributions may be beneficial as it can assist in the development of a theoretical prediction method for hetero-multivalency. This elucidation may be possible by cross-linking the lectin subunits to keep their native state before binding to any glycolipids.[216] Once cross-linked, the lectin can be bound to a mixed glycolipid receptor membrane and the binding capacity evaluated. If hetero-multivalency is observed, then we can compare its relative amount to that observed with uncross-linked lectins to determine the contribution of allosteric regulation. This effect can be confirmed by crosslinking the lectin subunits after binding to glycolipids to establish any conformational changes.[217] Thus, the difference between the native state cross-linked lectin and the unmodified lectin binding would give the relative contribution of allosteric regulation to hetero-multivalency and provide additional insights into how to theoretically predict when hetero-multivalency will occur and the extent of binding capacity enhancement.

In conclusion, this work has achieved its stated goal. Namely, in this work, we demonstrated the fundamentals of multivalent lectin binding, proposed a two-step binding mechanism (RD), showed that the RD mechanism applies in a second multivalent lectin system, and developed a TEA assay amenable to high-throughput emulsion formation and screening. This work can be readily expanded in three primary ways. First, a method to theoretically predict -multivalency could be developed. Second, the membrane perturbation protocol can be extended

to extracted cell membranes. Third, the relative contributions of allosteric regulation and the RD mechanism to hetero-multivalency could be quantified. Thus, the work presented here provides the foundation for a rational basis of understanding and utilizing hetero-multivalency and its effects on lectins binding to glycolipids.

REFERENCES

1 Feynman, R. & Wilczek, F. *The character of physical law*. 127-128 (MIT press, 1965).

2 Anderson, N. L. & Anderson, N. G. The Human Plasma Proteome: History, Character, and Diagnostic Prospects. *Molecular & Cellular Proteomics* **1**, 845-867 (2002).

3 Bhalla, U. S. Signaling in Small Subcellular Volumes. I. Stochastic and Diffusion Effects on Individual Pathways. *Biophysical Journal* **87**, 733-744, doi:http://dx.doi.org/10.1529/biophysj.104.040469 (2004).

4 Dickinson, B. C. & Chang, C. J. Chemistry and biology of reactive oxygen species in signaling or stress responses. *Nat Chem Biol* **7**, 504-511 (2011).

5 Kholodenko, B. N., Brown, G. C. & Hoek, J. B. Diffusion control of protein phosphorylation in signal transduction pathways. *Biochemical Journal* **350**, 901 (2000).

6 Zerial, M. & McBride, H. Rab proteins as membrane organizers. *Nature reviews. Molecular cell biology* **2**, 107 (2001).

7 van Meer, G. & Simons, K. The function of tight junctions in maintaining differences in lipid composition between the apical and the basolateral cell surface domains of MDCK cells. *The EMBO Journal* **5**, 1455-1464 (1986).

8 Steck, T. L. & Dawson, G. Topographical Distribution of Complex Carbohydrates in the Erythrocyte Membrane. *Journal of Biological Chemistry* **249**, 2135-2142 (1974).

9 Chi, E., Mehl, T., Nunn, D. & Lory, S. Interaction of *Pseudomonas aeruginosa* with A549 pneumocyte cells. *Infection and Immunity* **59**, 822-828 (1991).

10 Fleiszig, S. M., Zaidi, T. S., Fletcher, E. L., Preston, M. J. & Pier, G. B. *Pseudomonas aeruginosa* invades corneal epithelial cells during experimental infection. *Infection and Immunity* **62**, 3485-3493 (1994).

11 Fleiszig, S. M. *et al.* Relationship between cytotoxicity and corneal epithelial cell invasion by clinical isolates of *Pseudomonas aeruginosa*. *Infection and Immunity* **64**, 2288-2294 (1996).

12 Mewe, M. *et al. Pseudomonas aeruginosa* lectins I and II and their interaction with human airway cilia. *The Journal of Laryngology & Otology* **119**, 595-599, doi:10.1258/0022215054516313 (2006).

13 Varki, A., Etzler, M., Cummings, R. D. & Esko, J. D. *Essentials of Glycobiology*. 2 edn, (Cold Spring Harbor Laboratory Press, 2009).

14 Varki, A. *et al.* in *Essentials of Glycobiology* (eds A. Varki *et al.*) (2009).

15 Zhang, R.-G. *et al.* The Three-dimensional Crystal Structure of Cholera Toxin. *Journal of Molecular Biology* **251**, 563-573, doi:http://dx.doi.org/10.1006/jmbi.1995.0456 (1995).

16 Karaveg, K. *et al.* Crystallization and preliminary X-ray diffraction analysis of lectin-1 from *Pseudomonas aeruginosa*. *Acta Crystallographica Section D* **59**, 1241-1242, doi:10.1107/S0907444903008710 (2003).

17 Worstell, N. C., Krishnan, P., Weatherston, J. D. & Wu, H.-J. Binding Cooperativity Matters: A GM1-Like Ganglioside-Cholera Toxin B Subunit Binding Study Using a Nanocube-Based Lipid Bilayer Array. *PLOS ONE* **11**, e0153265, doi:10.1371/journal.pone.0153265 (2016).

18 Krishnan, P. *et al.* Hetero-multivalent Binding of Cholera Toxin Subunit B with Glycolipid Mixtures. *Colloids and Surfaces B: Biointerfaces*, doi:https://doi.org/10.1016/j.colsurfb.2017.09.035 (2017).

19 Schwarz, A. & Futerman, A. H. Determination of the Localization of Gangliosides Using Anti-ganglioside Antibodies: Comparison of Fixation Methods. *Journal of Histochemistry & Cytochemistry* **45**, 611-618, doi:10.1177/002215549704500413 (1997).

20 Lanne, B., Cîopraga, J., Bergström, J., Motas, C. & Karlsson, K.-A. Binding of the galactose-specific *Pseudomonas aeruginosa* lectin, PA-I, to glycosphingolipids and other glycoconjugates. *Glycoconjugate Journal* **11**, 292-298, doi:10.1007/bf00731201 (1994).

21 Bauwens, A. *et al.* Facing glycosphingolipid–Shiga toxin interaction: dire straits for endothelial cells of the human vasculature. *Cellular and Molecular Life Sciences* **70**, 425-457, doi:10.1007/s00018-012-1060-z (2013).

22 Yanagisawa, M., Ariga, T. & Yu, R. K. Letter to the Glyco-Forum: Cholera toxin B subunit binding does not correlate with GM1 expression: a study using mouse embryonic neural precursor cells. *Glycobiology* **16**, 19G-22G, doi:10.1093/glycob/cwl003 (2006).

23 Dawson, G. Measuring brain lipids. *Biochimica et Biophysica Acta (BBA) - Molecular and Cell Biology of Lipids* **1851**, 1026-1039, doi:http://dx.doi.org/10.1016/j.bbalip.2015.02.007 (2015).

24 Yanagisawa, M., Ariga, T. & Yu, R. K. Cholera toxin B subunit binding does not correlate with GM1 expression: a study using mouse embryonic neural precursor cells. *Glycobiology* **16**, 19G-22G, doi:10.1093/glycob/cwl031 (2006).

25 Bernardi, A. *et al.* Multivalent glycoconjugates as anti-pathogenic agents. *Chemical Society Reviews* **42**, 4709-4727, doi:10.1039/C2CS35408J (2013).

26 Cecioni, S., Imberty, A. & Vidal, S. Glycomimetics versus multivalent glycoconjugates for the design of high affinity lectin ligands. *Chemical reviews* **115**, 525-561, doi:10.1021/cr500303t (2015).

27 Cecioni, S. *et al.* Rational Design and Synthesis of Optimized Glycoclusters for Multivalent Lectin–Carbohydrate Interactions: Influence of the Linker Arm. *Chemistry - A European Journal*, 6250-6263 (2012).

28 Jung, H., Robison, A. D. & Cremer, P. S. Multivalent ligand-receptor binding on supported lipid bilayers. *Journal of structural biology* **168**, 90-94, doi:10.1016/j.jsb.2009.05.010 (2009).

29 Kirkeby, S. Cholera toxin B subunit-binding and ganglioside GM1 immuno-expression are not necessarily correlated in human salivary glands. *Acta Odontologica Scandinavica* **72**, 694-700, doi:10.3109/00016357.2014.898090 (2014).

30 Wands, A. M. *et al.* Fucosylation and protein glycosylation create functional receptors for cholera toxin. *eLife* **4**, e09545, doi:10.7554/eLife.09545 (2015).

31 Breimer, M. E., Hansson, G. C., Karlsson, K.-A., Larson, G. & Leffler, H. Glycosphingolipid composition of epithelial cells isolated along the villus axis of small intestine of a single human individual. *Glycobiology* **22**, 1721-1730, doi:10.1093/glycob/cws115 (2012).

32 Li, J. *et al.* Screening Glycolipids Against Proteins in Vitro Using Picodiscs and Catch-and-Release Electrospray Ionization-Mass Spectrometry. *Analytical Chemistry* **88**, 4742-4750, doi:10.1021/acs.analchem.6b00043 (2016).

33 Han, L., Kitova, E. N. & Klassen, J. S. Detecting Protein–Glycolipid Interactions Using Glycomicelles and CaR-ESI-MS. *Journal of The American Society for Mass Spectrometry* **27**, 1878-1886, doi:10.1007/s13361-016-1461-6 (2016).

34 Shen, L. *et al.* Membrane Environment Can Enhance the Interaction of Glycan Binding Protein to Cell Surface Glycan Receptors. *ACS Chemical Biology* **9**, 1877-1884, doi:10.1021/cb5004114 (2014).

35 Rinaldi, S. *et al.* Analysis of lectin binding to glycolipid complexes using combinatorial glycoarrays. *Glycobiology* **19**, 789-796, doi:10.1093/glycob/cwp049 (2009).

36 Gallegos, K. M. *et al.* Shiga toxin binding to glycolipids and glycans. *Plos One* **7**, e30368, doi:10.1371/journal.pone.0030368 (2012).

37 Ortega-Muñoz, M. *et al.* Click Multivalent Heterogeneous Neoglycoconjugates – Modular Synthesis and Evaluation of Their Binding Affinities. *European Journal of Organic Chemistry* **2009**, 2454-2473, doi:10.1002/ejoc.200801169 (2009).

38 Mazor, Y. *et al.* Insights into the molecular basis of a bispecific antibody's target selectivity. *mAbs* **7**, 461-469, doi:10.1080/19420862.2015.1022695 (2015).

39 Sengers, B. G. *et al.* Modeling bispecific monoclonal antibody interaction with two cell membrane targets indicates the importance of surface diffusion. *mAbs* **8**, 905-915, doi:10.1080/19420862.2016.1178437 (2016).

40 Imberty, A., Mitchell, E. P. & Wimmerová, M. Structural basis of high-affinity glycan recognition by bacterial and fungal lectins. *Current Opinion in Structural Biology* **15**, 525-534, doi:http://doi.org/10.1016/j.sbi.2005.08.003 (2005).

41 Imberty, A., Wimmerová, M., Mitchell, E. P. & Gilboa-Garber, N. Structures of the lectins from *Pseudomonas aeruginosa*: insights into the molecular basis for host glycan recognition. *Microbes and Infection* **6**, 221-228, doi:http://doi.org/10.1016/j.micinf.2003.10.016 (2004).

42 Rodrigue, J. *et al.* Aromatic thioglycoside inhibitors against the virulence factor LecA from *Pseudomonas aeruginosa*. *Organic & Biomolecular Chemistry* **11**, 6906-6918, doi:10.1039/C3OB41422A (2013).

43 Pukin, A. V. *et al.* Strong Inhibition of Cholera Toxin by Multivalent GM1 Derivatives. *ChemBioChem* **8**, 1500-1503, doi:10.1002/cbic.200700266 (2007).

44 Sly, K. L. & Conboy, J. C. c. c. u. e. Determination of Multivalent Protein-Ligand Binding Kinetics by Second-Harmonic Correlation Spectroscopy. *Analytical Chemistry* **86**, 11045-11054, doi:10.1021/ac500094v (2014).

45 Munoz, E. M., Correa, J., Riguera, R. & Fernandez-Megia, E. Real-Time Evaluation of Binding Mechanisms in Multivalent Interactions: A Surface Plasmon Resonance Kinetic Approach. *Journal of the American Chemical Society* **135**, 5966-5969, doi:10.1021/ja400951g (2013).

46 Kikkeri, R., Hossain, L. H. & Seeberger, P. H. Supramolecular one-pot approach to fluorescent glycodendrimers. *Chemical Communications*, 2127-2129, doi:10.1039/B802177E (2008).

47 Percec, V. *et al.* Modular Synthesis of Amphiphilic Janus Glycodendrimers and Their Self-Assembly into Glycodendrimersomes and Other Complex Architectures with Bioactivity to Biomedically Relevant Lectins. *Journal of the American Chemical Society* **135**, 9055-9077, doi:10.1021/ja403323y (2013).

48 Zhang, S. *et al.* Unraveling functional significance of natural variations of a human galectin by glycodendrimersomes with programmable glycan surface. *Proceedings of the National Academy of Sciences* **112**, 5585-5590 (2015).

49 Xiao, Q. *et al.* Onion-like glycodendrimersomes from sequence-defined Janus glycodendrimers and influence of architecture on reactivity to a lectin. *Proceedings of the National Academy of Sciences* **113**, 1162-1167 (2016).

50 Sherman, S. E., Xiao, Q. & Percec, V. Mimicking Complex Biological Membranes and Their Programmable Glycan Ligands with Dendrimersomes and Glycodendrimersomes. *Chemical reviews* **117**, 6538-6631, doi:10.1021/acs.chemrev.7b00097 (2017).

51 Wu, H. J. *et al.* Membrane-protein binding measured with solution-phase plasmonic nanocube sensors. *Nat. Methods* **9**, 1189-U1181, doi:10.1038/nmeth.2211 (2012).

52 Laurent, N., Voglmeir, J. & Flitsch, S. L. Glycoarrays-tools for determining protein-carbohydrate interactions and glycoenzyme specificity. *Chemical Communications*, 4400-4412, doi:10.1039/B806983M (2008).

53 Köhn, M., Benito, J. M., Ortiz Mellet, C., Lindhorst, T. K. & García Fernández, J. M. Functional Evaluation of Carbohydrate-Centred Glycoclusters by Enzyme-Linked Lectin Assay: Ligands for Concanavalin A. *ChemBioChem* **5**, 771-777, doi:10.1002/cbic.200300807 (2004).

54 McCoy, J. P., Varani, J. & Goldstein, I. J. Enzyme-linked lectin assay (ELLA): Use of alkaline phosphatase-conjugated Griffonia simplicifolia B4 isolectin for the detection of α-d-galactopyranosyl end groups. *Analytical Biochemistry* **130**, 437-444, doi:http://dx.doi.org/10.1016/0003-2697(83)90613-9 (1983).

55 Tanaka, M. & Sackmann, E. Polymer-supported membranes as models of the cell surface. *Nature* **437**, 656 (2005).

56 Castellana, E. T. & Cremer, P. S. Imaging large arrays of supported lipid bilayers with a macroscope. *Biointerphases* **2**, 57-63, doi:10.1116/1.2732312 (2007).

57 Yamazaki, V. *et al.* Cell membrane array fabrication and assay technology. *BMC Biotechnology* **5**, 18, doi:10.1186/1472-6750-5-18 (2005).

58 Zhu, X. Y. *et al.* Quantitative Glycomics from Fluidic Glycan Microarrays. *Journal of the American Chemical Society* **131**, 13646-13650, doi:10.1021/ja902783n (2009).

59 Ma, Y., Sobkiv, I., Gruzdys, V., Zhang, H. & Sun, X.-L. Liposomal glyco-microarray for studying glycolipid–protein interactions. *Analytical and Bioanalytical Chemistry* **404**, 51-58, doi:10.1007/s00216-012-6096-2 (2012).

60 Zippel, B. & Neu, T. R. Characterization of Glycoconjugates of Extracellular Polymeric Substances in Tufa-Associated Biofilms by Using Fluorescence Lectin-Binding Analysis. *Applied and Environmental Microbiology* **77**, 505-516 (2011).

61 Gorelick, F. S., Sarras, M. P. & Jamieson, J. D. Regional differences in lectin binding to colonic epithelium by fluorescent and electron microscopy. *Journal of Histochemistry & Cytochemistry* **30**, 1097-1108, doi:10.1177/30.11.6897257 (1982).

62 Schoen, A. & Freire, E. Thermodynamics of intersubunit interactions in cholera toxin upon binding to the oligosaccharide portion of its cell surface receptor, ganglioside GM1. *Biochemistry* **28**, 5019-5024, doi:10.1021/bi00438a017 (1989).

63 Turnbull, W. B., Precious, B. L. & Homans, S. W. Dissecting the Cholera Toxin−Ganglioside GM1 Interaction by Isothermal Titration Calorimetry. *Journal of the American Chemical Society* **126**, 1047-1054, doi:10.1021/ja0378207 (2004).

64 Lin, H., Kitova, E. & Klassen, J. Measuring Positive Cooperativity Using the Direct ESI-MS Assay. Cholera Toxin B Subunit Homopentamer Binding to GM1 Pentasaccharide. *Journal of The American Society for Mass Spectrometry* **25**, 104-110, doi:10.1007/s13361-013-0751-5 (2014).

65 Sheikh, K. A., Deerinck, T. J., Ellisman, M. H. & Griffin, J. W. The distribution of ganglioside-like moieties in peripheral nerves. *Brain* **122**, 449-460, doi:10.1093/brain/122.3.449 (1999).

66 Willison, H. J. & Yuki, N. Peripheral neuropathies and anti-glycolipid antibodies. *Brain* **125**, 2591-2625, doi:10.1093/brain/awf272 (2002).

67 Park, S., Gildersleeve, J. C., Blixt, O. & Shin, I. Carbohydrate microarrays. *Chem Soc Rev* **42**, 4310-4326, doi:10.1039/c2cs35401b (2013).

68 Wang, L. *et al.* Cross-platform comparison of glycan microarray formats. *Glycobiology* **24**, 507-517, doi:10.1093/glycob/cwu019 (2014).

69 Lauer, S., Goldstein, B., Nolan, R. L. & Nolan, J. P. Analysis of Cholera Toxin−Ganglioside Interactions by Flow Cytometry†. *Biochemistry* **41**, 1742-1751, doi:10.1021/bi0112816 (2002).

70 Ma, Y., Sobkiv, I., Gruzdys, V., Zhang, H. & Sun, X. L. Liposomal glyco-microarray for studying glycolipid-protein interactions. *Anal Bioanal Chem* **404**, 51-58, doi:10.1007/s00216-012-6096-2 (2012).

71 Zhu, X. Y. *et al.* Quantitative Glycomics from Fluidic Glycan Microarrays. *Journal of the American Chemical Society* **131**, 13646-13650, doi:10.1021/ja902783n (2009).

72 Leney, A. C., Fan, X., Kitova, E. N. & Klassen, J. S. Nanodiscs and Electrospray Ionization Mass Spectrometry: A Tool for Screening Glycolipids Against Proteins. *Analytical Chemistry* **86**, 5271-5277, doi:10.1021/ac4041179 (2014).

73 Yamazaki, V. *et al.* Cell membrane array fabrication and assay technology. *BMC biotechnology* **5**, 18, doi:10.1186/1472-6750-5-18 (2005).

74 Wu, H.-J. *et al.* Membrane-protein binding measured with solution-phase plasmonic nanocube sensors. *Nat Meth* **9**, 1189-1191, doi:http://www.nature.com/nmeth/journal/v9/n12/abs/nmeth.2211.html#supplementary-information (2012).

75 Worstell, N. C., Krishnan, P., Weatherston, J. D. & Wu, H. J. Binding cooperativity matters: A GM1-like ganglioside-cholera toxin B subunit binding study using a nanocube-based lipid bilayer array. *PLoS ONE* **11**, e0153265, doi:10.1371/journal.pone.0153265 (2016).

76 Tao, A., Sinsermsuksakul, P. & Yang, P. Polyhedral Silver Nanocrystals with Distinct Scattering Signatures. *Angewandte Chemie International Edition* **45**, 4597-4601, doi:10.1002/anie.200601277 (2006).

77 Wang, R., Tang, J., Liu, J., Wang, Y. & Huang, Z. Preparation of Ag@SiO2Dispersion in Different Solvents and Investigation of its Optical Properties. *Journal of Dispersion Science and Technology* **32**, 532-537, doi:10.1080/01932691003757082 (2011).

78 Niitsoo, O. & Couzis, A. Facile synthesis of silver core - silica shell composite nanoparticles. *Journal of colloid and interface science* **354**, 887-890, doi:10.1016/j.jcis.2010.11.013 (2011).

79 Sun, Y., Mayers, B., Herricks, T. & Xia, Y. Polyol Synthesis of Uniform Silver Nanowires: A Plausible Growth Mechanism and the Supporting Evidence. *Nano Letters* **3**, 955-960, doi:10.1021/nl034312m (2003).

80 Mornet, S., Lambert, O., Duguet, E. & Brisson, A. The Formation of Supported Lipid Bilayers on Silica Nanoparticles Revealed by Cryoelectron Microscopy. *Nano Letters* **5**, 281-285, doi:10.1021/nl048153y (2005).

81 Shi, J. *et al.* GM1 Clustering Inhibits Cholera Toxin Binding in Supported Phospholipid Membranes. *Journal of the American Chemical Society* **129**, 5954-5961, doi:10.1021/ja069375w (2007).

82 Jung, H., Robison, A. D. & Cremer, P. S. Multivalent ligand–receptor binding on supported lipid bilayers. *Journal of structural biology* **168**, 90-94, doi:http://dx.doi.org/10.1016/j.jsb.2009.05.010 (2009).

83 Kim, C. S., Seo, J. H. & Cha, H. J. Functional Interaction Analysis of GM1-Related Carbohydrates and Vibrio cholerae Toxins Using Carbohydrate Microarray. *Analytical Chemistry* **84**, 6884-6890, doi:10.1021/ac301511t (2012).

84 Kuziemko, G. M., Stroh, M. & Stevens, R. C. Cholera Toxin Binding Affinity and Specificity for Gangliosides Determined by Surface Plasmon Resonance. *Biochemistry* **35**, 6375-6384, doi:10.1021/bi952314i (1996).

85 MacKenzie, C. R., Hirama, T., Lee, K. K., Altman, E. & Young, N. M. Quantitative analysis of bacterial toxin affinity and specificity for glycolipid receptors by surface plasmon resonance. *Journal of Biological Chemistry* **272**, 5533-5538 (1997).

86 Schengrund, C. L. & Ringler, N. J. Binding of Vibrio cholera toxin and the heat-labile enterotoxin of *Escherichia coli* to GM1, derivatives of GM1, and nonlipid oligosaccharide polyvalent ligands. *Journal of Biological Chemistry* **264**, 13233-13237 (1989).

87 Winter, E. M. & Groves, J. T. Surface Binding Affinity Measurements from Order Transitions of Lipid Membrane-Coated Colloidal Particles. *Analytical Chemistry* **78**, 174-180, doi:10.1021/ac0514927 (2006).

88 Terrell, J., Yadava, P., Castro, C. & Hughes, J. Liposome Fluidity Alters Interactions Between the Ganglioside GM1 and Cholera Toxin B Subunit. *Journal of Liposome Research* **18**, 21-29, doi:10.1080/08982100801893929 (2008).

89 Masserini, M., Freire, E., Palestini, P., Calappi, E. & Tettamanti, G. Fuc-GM1 ganglioside mimics the receptor function of GM1 for cholera toxin. *Biochemistry* **31**, 2422-2426, doi:10.1021/bi00123a030 (1992).

90 Iwabuchi, K. *et al.* Membrane microdomains in immunity: Glycosphingolipid-enriched domain-mediated innate immune responses. *BioFactors* **38**, 275-283, doi:10.1002/biof.1017 (2012).

91 Molander-Melin, M. *et al.* Structural membrane alterations in Alzheimer brains found to be associated with regional disease development; increased density of gangliosides GM1 and GM2 and loss of cholesterol in detergent-resistant membrane domains. *Journal of Neurochemistry* **92**, 171-182, doi:10.1111/j.1471-4159.2004.02849.x (2005).

92 Giuliani, A. *et al.* The different inhibiting effect of cholera toxin on two leukemia cell lines does not correlate with their toxin binding capacity. *Mol Cell Biochem* **152**, 103-112, doi:10.1007/BF01076072 (1995).

93 Yanagisawa, M. & Yu, R. K. The expression and functions of glycoconjugates in neural stem cells. *Glycobiology* **17**, 57R-74R, doi:10.1093/glycob/cwm018 (2007).

94 Mikhalyov, I. & Samsonov, A. Lipid raft detecting in membranes of live erythrocytes. *Biochimica et Biophysica Acta (BBA) - Biomembranes* **1808**, 1930-1939, doi:http://dx.doi.org/10.1016/j.bbamem.2011.04.002 (2011).

95 Tuosto, L. *et al.* Organization of plasma membrane functional rafts upon T cell activation. *European Journal of Immunology* **31**, 345-349, doi:10.1002/1521-4141(200102)31:2<345::AID-IMMU345>3.0.CO;2-L (2001).

96 Tao, S. C. *et al.* Lectin microarrays identify cell-specific and functionally significant cell surface glycan markers. *Glycobiology* **18**, 761-769, doi:10.1093/glycob/cwn063 (2008).

97 Arnaud, J., Audfray, A. & Imberty, A. Binding sugars: from natural lectins to synthetic receptors and engineered neolectins. *Chem Soc Rev* **42**, 4798-4813, doi:10.1039/c2cs35435g (2013).

98 Hu, S. & Wong, D. T. Lectin microarray. *Proteomics. Clinical applications* **3**, 148-154, doi:10.1002/prca.200800153 (2009).

99 Palma, A. S., Feizi, T., Childs, R. A., Chai, W. & Liu, Y. The neoglycolipid (NGL)-based oligosaccharide microarray system poised to decipher the meta-glycome. *Current opinion in chemical biology* **18**, 87-94, doi:10.1016/j.cbpa.2014.01.007 (2014).

100 Fishman, P. H. & Atikkan, E. E. Mechanism of action of cholera toxin: effect of receptor density and multivalent binding on activation of adenylate cyclase. *The Journal of membrane biology* **54**, 51-60 (1980).

101 Fasting, C. *et al.* Multivalency as a chemical organization and action principle. *Angewandte Chemie* **51**, 10472-10498, doi:10.1002/anie.201201114 (2012).

102 Muller, C., Despras, G. & Lindhorst, T. K. Organizing multivalency in carbohydrate recognition. *Chemical Society Reviews* **45**, 3275-3302, doi:10.1039/C6CS00165C (2016).

103 Lauer, S., Goldstein, B., Nolan, R. L. & Nolan, J. P. Analysis of cholera toxin−ganglioside interactions by flow cytometry. *Biochemistry* **41**, 1742-1751, doi:10.1021/bi0112816 (2002).

104 Turnbull, W. B., Precious, B. L. & Homans, S. W. Dissecting the cholera toxin-ganglioside GM1 interaction by isothermal titration calorimetry. *J Am Chem Soc* **126**, 1047-1054, doi:10.1021/ja0378207 (2004).

105 Shi, J. J. *et al.* GM(1) clustering inhibits cholera toxin binding in supported phospholipid membranes. *Journal of the American Chemical Society* **129**, 5954-5961, doi:10.1021/ja069375w (2007).

106 Leach, K., Sexton, P. M. & Christopoulos, A. in *Current Protocols in Pharmacology* (John Wiley & Sons, Inc., 2001).

107 Lin, H., Kitova, E. N. & Klassen, J. S. Measuring positive cooperativity using the direct ESI-MS assay. Cholera toxin B subunit homopentamer binding to GM1 pentasaccharide. *J Am Soc Mass Spectrom* **25**, 104-110, doi:10.1007/s13361-013-0751-5 (2014).

108 Schafer, D. E. & Thakur, A. K. Quantitative description of the binding of GM1 oligosaccharide by cholera enterotoxin. *Cell Biophysics* **4**, 25-40, doi:10.1007/bf02788553 (1982).

109 Adam, G. & Delbruck, M. in *Structural chemistry and molecular biology* (eds A. Rich & N. Davidson) 198–215 (W. H. Freeman and Co., 1968).

110 Axelrod, D. & Wang, M. Reduction-of-dimensionality kinetics at reaction-limited cell surface receptors. *Biophysical journal* **66**, 588 (1994).

111 McCloskey, M. A. & Poo, M. Rates of membrane-associated reactions: reduction of dimensionality revisited. *The Journal of cell biology* **102**, 88-96 (1986).

112 Berg, H. C. & Purcell, E. M. Physics of chemoreception. *Biophys J* **20**, 193-219, doi:10.1016/S0006-3495(77)85544-6 (1977).

113 Hardt, S. L. Rates of diffusion controlled reactions in one, two and three dimensions. *Biophysical Chemistry* **10**, 239-243, doi:http://dx.doi.org/10.1016/0301-4622(79)85012-7 (1979).

114 Keizer, J. Diffusion effects on rapid bimolecular chemical reactions. *Chemical reviews* **87**, 167-180, doi:10.1021/cr00077a009 (1987).

115 Szabo, A., Schulten, K. & Schulten, Z. First passage time approach to diffusion controlled reactions. *The Journal of Chemical Physics* **72**, 4350-4357, doi:10.1063/1.439715 (1980).

116 Sengers, B. G. *et al.* Modeling bispecific monoclonal antibody interaction with two cell membrane targets indicates the importance of surface diffusion. *MAbs* **8**, 905-915, doi:10.1080/19420862.2016.1178437 (2016).

117 Jobling, M. G., Yang, Z., Kam, W. R., Lencer, W. I. & Holmes, R. K. A single native ganglioside GM1-binding site is sufficient for cholera toxin to bind to cells and complete the intoxication pathway. *mBio* **3**, e00401-00412, doi:10.1128/mBio.00401-12 (2012).

118 Hsieh, C.-L., Spindler, S., Ehrig, J. & Sandoghdar, V. Tracking single particles on supported lipid membranes: multimobility diffusion and nanoscopic confinement. *The Journal of Physical Chemistry B* **118**, 1545-1554, doi:10.1021/jp412203t (2014).

119 Day, C. A. & Kenworthy, A. K. Mechanisms underlying the confined diffusion of cholera toxin B-subunit in intact cell membranes. *PLoS ONE* **7**, e34923, doi:10.1371/journal.pone.0034923 (2012).

120 Lindblom, G. & Orädd, G. Lipid lateral diffusion and membrane heterogeneity. *Biochimica et Biophysica Acta (BBA) - Biomembranes* **1788**, 234-244, doi:https://doi.org/10.1016/j.bbamem.2008.08.016 (2009).

121 Burns, A. R., Frankel, D. J. & Buranda, T. Local mobility in lipid domains of supported bilayers characterized by atomic force microscopy and fluorescence correlation spectroscopy. *Biophys J* **89**, 1081-1093, doi:10.1529/biophysj.105.060327 (2005).

122 Sachl, R. *et al.* On multivalent receptor activity of GM1 in cholesterol containing membranes. *Biochimica et biophysica acta* **1853**, 850-857, doi:10.1016/j.bbamcr.2014.07.016 (2015).

123 Wang, F., Curry, D. E. & Liu, J. Driving adsorbed gold nanoparticle assembly by merging lipid gel/fluid interfaces. *Langmuir : the ACS journal of surfaces and colloids* **31**, 13271-13274, doi:10.1021/acs.langmuir.5b03606 (2015).

124 Forstner, M. B., Yee, C. K., Parikh, A. N. & Groves, J. T. Lipid lateral mobility and membrane phase structure modulation by protein binding. *Journal of the American Chemical Society* **128**, 15221-15227, doi:10.1021/ja064093h (2006).

125 Scomparin, C., Lecuyer, S., Ferreira, M., Charitat, T. & Tinland, B. Diffusion in supported lipid bilayers: influence of substrate and preparation technique on the internal dynamics. *The European physical journal. E, Soft matter* **28**, 211-220, doi:10.1140/epje/i2008-10407-3 (2009).

126 Goins, B. M., M,; Barisas, B.; Freire, E. Lateral diffusion of ganglioside GM1 in phospholipid bilayer membranes. *Biophys J* **49**, 849-856, doi:10.1016/S0006-3495(86)83714-6 (1986).

127 Alouf, J. E. & Popoff, M. R. *The comprehensive sourcebook of bacterial protein toxins (Third Edition)*. (Academic Press, 2006).

128 Goluszko, P. & Nowicki, B. Membrane cholesterol: a crucial molecule affecting interactions of microbial pathogens with mammalian cells. *Infect Immun* **73**, 7791-7796, doi:10.1128/IAI.73.12.7791-7796.2005 (2005).

129 Bricarello, D. A., Mills, E. J., Petrlova, J., Voss, J. C. & Parikh, A. N. Ganglioside embedded in reconstituted lipoprotein binds cholera toxin with elevated affinity. *Journal of lipid research* **51**, 2731-2738, doi:10.1194/jlr.M007401 (2010).

130 Merritt, E. A. *et al.* Crystal structure of cholera toxin B-pentamer bound to receptor GM1 pentasaccharide. *Protein Science* **3**, 166-175, doi:10.1002/pro.5560030202 (1994).

131 Li, J. *et al.* Screening glycolipids against proteins in vitro using picodiscs and catch-and-release electrospray ionization-mass spectrometry. *Anal Chem* **88**, 4742-4750, doi:10.1021/acs.analchem.6b00043 (2016).

132 Han, L., Kitova, E. N. & Klassen, J. S. Detecting protein-glycolipid interactions using glycomicelles and CaR-ESI-MS. *J Am Soc Mass Spectrom* **27**, 1878-1886, doi:10.1007/s13361-016-1461-6 (2016).

133 Frances M. Platt, G. R., Raymond A. Dwek, and Terry D. Butters. Extensive glycosphingolipid depletion in the liver and lymphoid organs of mice treated with N-Butyldeoxynojirimycin. *The Journal of Biological Chemistry* **272**, 19365-19372 (1997).

134 Stryjewski, M. E. & Sexton, D. J. in *Severe Infections Caused by Pseudomonas Aeruginosa* (eds Alan R. Hauser & Jordi Rello) 1-15 (Springer US, 2003).

135 Gellatly, S. L. & Hancock, R. E. W. *Pseudomonas aeruginosa*: new insights into pathogenesis and host defenses. *Pathog. Dis.* **67**, 159-173, doi:10.1111/2049-632x.12033 (2013).

136 Chemani, C. *et al.* Role of LecA and LecB lectins in *Pseudomonas aeruginosa*-induced lung injury and effect of carbohydrate ligands. *Infection and immunity* **77**, 2065-2075 (2009).

137 Fong, J. N. & Yildiz, F. H. Biofilm matrix proteins. *Microbiology spectrum* **3** (2015).

138 Diggle, S. P. *et al.* The galactophilic lectin, LecA, contributes to biofilm development in *Pseudomonas aeruginosa*. *Environmental microbiology* **8**, 1095-1104 (2006).

139 Saiman, L. & Prince, A. *Pseudomonas aeruginosa* pili bind to asialoGM1 which is increased on the surface of cystic fibrosis epithelial cells. *Journal of Clinical Investigation* **92**, 1875 (1993).

140 Zheng, S. *et al.* The *Pseudomonas aeruginosa* lectin LecA triggers host cell signalling by glycosphingolipid-dependent phosphorylation of the adaptor protein CrkII. *Biochimica et Biophysica Acta (BBA) - Molecular Cell Research*, doi:http://doi.org/10.1016/j.bbamcr.2017.04.005.

141 Funken, H. *et al.* Specific association of lectin LecB with the surface of *Pseudomonas aeruginosa*: role of outer membrane protein OprF. *PloS one* **7**, e46857 (2012).

142 Cott, C. *et al. Pseudomonas aeruginosa* lectin LecB inhibits tissue repair processes by triggering β-catenin degradation. *Biochimica et Biophysica Acta (BBA)-Molecular Cell Research* **1863**, 1106-1118 (2016).

143 Kühn, K. *et al.* The interplay of autophagy and β-Catenin signaling regulates differentiation in acute myeloid leukemia. *Cell Death Discovery* **1**, 15031, doi:10.1038/cddiscovery.2015.31 https://www.nature.com/articles/cddiscovery201531#supplementary-information (2015).

144 Schneider, D. *et al.* Lectins from opportunistic bacteria interact with acquired variable-region glycans of surface immunoglobulin in follicular lymphoma. *Blood* **125**, 3287-3296, doi:10.1182/blood-2014-11-609404 (2015).

145 Eierhoff, T. *et al.* A lipid zipper triggers bacterial invasion. *Proceedings of the National Academy of Sciences* **111**, 12895-12900, doi:10.1073/pnas.1402637111 (2014).

146 Grishin, A. V., Krivozubov, M. S., Karyagina, A. S. & Gintsburg, A. L. *Pseudomonas Aeruginosa* Lectins As Targets for Novel Antibacterials. *Acta naturae* **7**, 29-41 (2015).

147 Cioci, G. *et al.* Structural basis of calcium and galactose recognition by the lectin PA-IL of *Pseudomonas aeruginosa*. *FEBS letters* **555**, 297-301 (2003).

148 Gilboa-Garber, N., Mizrahi, L. & Garber, N. Purification of the galactose-binding hemagglutinin of *Pseudomonas aeruginosa* by affinity column chromatography using sepharose. *FEBS Letters* **28**, 93-95, doi:http://dx.doi.org/10.1016/0014-5793(72)80685-9 (1972).

149 Lanne, B., Cîopraga, J., Bergström, J., Motas, C. & Karlsson, K.-A. Binding of the galactose-specificPseudomonas aeruginosa lectin, PA-I, to glycosphingolipids and other glycoconjugates. *Glycoconjugate journal* **11**, 292-298, doi:10.1007/bf00731201 (1994).

150 Blanchard, B. *et al.* Structural basis of the preferential binding for globo-series glycosphingolipids displayed by *Pseudomonas aeruginosa* lectin I. *J Mol Biol* **383**, 837-853, doi:10.1016/j.jmb.2008.08.028 (2008).

151 Chen, C.-P., Song, S.-C., Gilboa-Garber, N., Chang, K. S. S. & Wu, A. M. Studies on the binding site of the galactose-specific agglutinin PA-IL from *Pseudomonas aeruginosa*. *Glycobiology* **8**, 7-16, doi:10.1093/glycob/8.1.7 (1998).

152 Mahal, L. K. (Consortium for Functional Glycomics, 2011).

153 Momoeda, K. *et al.* Developmental Changes of Neutral Glycosphingolipids as Receptors for Pulmonary Surfactant Protein SP-A in the Alveolar Epithelium of Murine Lung. *The Journal of Biochemistry* **119**, 1189-1195 (1996).

154 Gomez, E. W., Clack, N. G., Wu, H. J. & Groves, J. T. Like-charge interactions between colloidal particles are asymmetric with respect to sign. *Soft Matter* **5**, 1931-1936 (2009).

155 Duncan, G. A. & Bevan, M. A. Tunable Aggregation by Competing Biomolecular Interactions. *Langmuir : the ACS journal of surfaces and colloids* **30**, 15253-15260, doi:10.1021/la503772g (2014).

156 Wu, H.-J. & Bevan, M. A. Direct measurement of single and ensemble average particle-surface potential energy profiles. *Langmuir : the ACS journal of surfaces and colloids* **21**, 1244-1254 (2005).

157 Wu, H.-J., Pangburn, T. O., Beckham, R. E. & Bevan, M. A. Measurement and interpretation of particle-particle and particle-wall interactions in levitated colloidal ensembles. *Langmuir : the ACS journal of surfaces and colloids* **21**, 9879-9888 (2005).

158 Agarwal, P., Smith, D., Eng, W., Cummings, R. D. & Mahal, L. K. Large Scale Glycan Array Analysis of Commercial Lectins and Antibodies: 86 lectins and 15 antibodies. *Glycobiology* **22**, 1646 (2012).

159 Redhead, H. M., Davis, S. S. & Illum, L. Drug delivery in poly(lactide-co-glycolide) nanoparticles surface modified with poloxamer 407 and poloxamine 908: in vitro characterisation and in vivo evaluation. *Journal of Controlled Release* **70**, 353-363, doi:http://doi.org/10.1016/S0168-3659(00)00367-9 (2001).

160 Cummings, R. D. E., J.D.;. in *Essentials of Glycobiology* (ed A.; Cummings Varki, R.D.; Esko, J.D.; et al.) Ch. 27, (Cold Spring Harbor Laboratory Press, 2009).

161 Simons, K. & Toomre, D. Lipid rafts and signal transduction. *Nature reviews. Molecular cell biology* **1**, 31 (2000).

162 van Meer, G., Stelzer, E. H., Wijnaendts-van-Resandt, R. W. & Simons, K. Sorting of sphingolipids in epithelial (Madin-Darby canine kidney) cells. *The Journal of Cell Biology* **105**, 1623 (1987).

163 Danielsen, E. M. & Hansen, G. H. Lipid raft organization and function in the small intestinal brush border. *Journal of Physiology and Biochemistry* **64**, 377-382, doi:10.1007/BF03174093 (2008).

164 Michael Danielsen, E. & Hansen, G. H. Lipid raft organization and function in brush borders of epithelial cells (Review). *Molecular Membrane Biology* **23**, 71-79, doi:10.1080/09687860500445604 (2006).

165 Parkin, E. T., Turner, A. J. & Hooper, N. M. Differential effects of glycosphingolipids on the detergent-insolubility of the glycosylphosphatidylinositol-anchored membrane dipeptidase. *Biochemical Journal* **358**, 209 (2001).

166 Mahfoud, R., Manis, A., Binnington, B., Ackerley, C. & Lingwood, C. A. A Major Fraction of Glycosphingolipids in Model and Cellular Cholesterol-containing Membranes Is Undetectable by Their Binding Proteins. *Journal of Biological Chemistry* **285**, 36049-36059, doi:10.1074/jbc.M110.110189 (2010).

167 Sonnino, S. *et al.* Role of very long fatty acid-containing glycosphingolipids in membrane organization and cell signaling: the model of lactosylceramide in neutrophils. *Glycoconjugate Journal* **26**, 615-621, doi:10.1007/s10719-008-9215-8 (2009).

168 Sheikhpour, M., Barani, L. & Kasaeian, A. Biomimetics in drug delivery systems: A critical review. *Journal of Controlled Release* **253**, 97-109, doi:http://doi.org/10.1016/j.jconrel.2017.03.026 (2017).

169 Allen, T. M. & Cullis, P. R. Liposomal drug delivery systems: From concept to clinical applications. *Advanced Drug Delivery Reviews* **65**, 36-48, doi:http://doi.org/10.1016/j.addr.2012.09.037 (2013).

170 Duncan, G. A. & Bevan, M. A. Computational design of nanoparticle drug delivery systems for selective targeting. *Nanoscale* **7**, 15332-15340, doi:10.1039/C5NR03691G (2015).

171 Worstell, N. C. *et al.* Hetero-Multivalency of *Pseudomonas aeruginosa* Lectin LecA Binding to Model Membranes. (2017).

172 Lis, H. & Sharon, N. Lectins: Carbohydrate-Specific Proteins That Mediate Cellular Recognition. *Chemical reviews* **98**, 637-674, doi:10.1021/cr940413g (1998).

173 Chabre, Y. M. & Roy, R. in *Advances in Carbohydrate Chemistry and Biochemistry* Vol. 63 (ed Derek Horton) 165-393 (Academic Press, 2010).

174 Mammen, M., Choi, S.-K. & Whitesides, G. M. Polyvalent Interactions in Biological Systems: Implications for Design and Use of Multivalent Ligands and Inhibitors. *Angewandte Chemie International Edition* **37**, 2754-2794, doi:10.1002/(SICI)1521-3773(19981102)37:20<2754::AID-ANIE2754>3.0.CO;2-3 (1998).

175 Wolfenden, M. L. & Cloninger, M. J. Carbohydrate-Functionalized Dendrimers To Investigate the Predictable Tunability of Multivalent Interactions. *Bioconjugate Chemistry* **17**, 958-966, doi:10.1021/bc060107x (2006).

176 Ponader, D., Wojcik, F., Beceren-Braun, F., Dernedde, J. & Hartmann, L. Sequence-Defined Glycopolymer Segments Presenting Mannose: Synthesis and Lectin Binding Affinity. *Biomacromolecules* **13**, 1845-1852, doi:10.1021/bm300331z (2012).

177 Jimenez Blanco, J. L., Ortiz Mellet, C. & Garcia Fernandez, J. M. Multivalency in heterogeneous glycoenvironments: hetero-glycoclusters, -glycopolymers and -glycoassemblies. *Chemical Society Reviews* **42**, 4518-4531, doi:10.1039/C2CS35219B (2013).

178 Sigal, G. B., Mammen, M., Dahmann, G. & Whitesides, G. M. Polyacrylamides Bearing Pendant α-Sialoside Groups Strongly Inhibit Agglutination of Erythrocytes by Influenza Virus: The Strong Inhibition Reflects Enhanced Binding through Cooperative Polyvalent Interactions. *Journal of the American Chemical Society* **118**, 3789-3800, doi:10.1021/ja953729u (1996).

179 Vico, R. V., Voskuhl, J. & Ravoo, B. J. Multivalent Interaction of Cyclodextrin Vesicles, Carbohydrate Guests, and Lectins: A Kinetic Investigation. *Langmuir : the ACS journal of surfaces and colloids* **27**, 1391-1397, doi:10.1021/la1038975 (2011).

180 Kemp, B. E. *et al.* Autologous red cell agglutination assay for HIV-1 antibodies: simplified test with whole blood. *Science* **241**, 1352 (1988).

181 Huet, M., Cubizolles, M. & Buhot, A. Real time observation and automated measurement of red blood cells agglutination inside a passive microfluidic biochip containing embedded reagents. *Biosensors and Bioelectronics* **93**, 110-117, doi:https://doi.org/10.1016/j.bios.2016.09.068 (2017).

182 Pan, D. *et al.* The Effect of Polymeric Nanoparticles on Biocompatibility of Carrier Red Blood Cells. *PLOS ONE* **11**, e0152074, doi:10.1371/journal.pone.0152074 (2016).

183 Sharon, N. & Lis, H. Lectins: Cell-Agglutinating and Sugar-Specific Proteins. *Science* **177**, 949-959 (1972).

184 Assenhaimer, C., Domingos, A. S., Glasse, B., Fritsching, U. & Guardani, R. Long-term monitoring of metalworking fluid emulsion aging using a spectroscopic sensor. *The Canadian Journal of Chemical Engineering* **95**, 2341-2349, doi:10.1002/cjce.22931 (2017).

185 Deluhery, J. & Rajagopalan, N. A turbidimetric method for the rapid evaluation of MWF emulsion stability. *Colloids and Surfaces A: Physicochemical and Engineering Aspects* **256**, 145-149, doi:https://doi.org/10.1016/j.colsurfa.2004.12.001 (2005).

186 Glasse, B., Assenhaimer, C., Guardani, R. & Fritsching, U. Analysis of the Stability of Metal Working Fluid Emulsions by Turbidity Spectra. *Chemical Engineering & Technology* **36**, 1202-1208, doi:10.1002/ceat.201200590 (2013).

187 O'Neill, M. L. *et al.* Emulsion Stabilization and Flocculation in CO2. 1. Turbidimetry and Tensiometry. *Macromolecules* **30**, 5050-5059, doi:10.1021/ma9616930 (1997).

188 Rahn-Chique, K., Puertas, A. M., Romero-Cano, M. S., Rojas, C. & Urbina-Villalba, G. Nanoemulsion stability: Experimental evaluation of the flocculation rate from turbidity measurements. *Advances in Colloid and Interface Science* **178**, 1-20, doi:https://doi.org/10.1016/j.cis.2012.05.001 (2012).

189 Mashaghi, S., Jadidi, T., Koenderink, G. & Mashaghi, A. Lipid Nanotechnology. *International Journal of Molecular Sciences* **14**, doi:10.3390/ijms14024242 (2013).

190 Lothian, G. F. & Chappel, F. P. The transmission of light through suspensions. *Journal of Applied Chemistry* **1**, 475-482, doi:10.1002/jctb.5010011102 (1951).

191 Salvia-Trujillo, L., Soliva-Fortuny, R., Rojas-Graü, M. A., McClements, D. J. & Martín-Belloso, O. Edible Nanoemulsions as Carriers of Active Ingredients: A Review. *Annual Review of Food Science and Technology* **8**, 439-466, doi:10.1146/annurev-food-030216-025908 (2017).

192 Shah, P., Bhalodia, D. & Shelat, P. Nanoemulsion: a pharmaceutical review. *Systematic Reviews in Pharmacy* **1**, 24 (2010).

193 Gupta, A., Eral, H. B., Hatton, T. A. & Doyle, P. S. Nanoemulsions: formation, properties and applications. *Soft Matter* **12**, 2826-2841, doi:10.1039/C5SM02958A (2016).

194 Sivakumar, M., Tang, S. Y. & Tan, K. W. Cavitation technology – A greener processing technique for the generation of pharmaceutical nanoemulsions. *Ultrasonics Sonochemistry* **21**, 2069-2083, doi:https://doi.org/10.1016/j.ultsonch.2014.03.025 (2014).

195 Kulmyrzaev, A., Chanamai, R. & McClements, D. J. Influence of pH and CaCl2 on the stability of dilute whey protein stabilized emulsions. *Food Research International* **33**, 15-20, doi:http://dx.doi.org/10.1016/S0963-9969(00)00018-1 (2000).

196 Oster, G. Light scattering from polymerizing and coagulating systems. *Journal of Colloid Science* **2**, 291-299, doi:https://doi.org/10.1016/0095-8522(47)90031-7 (1947).

197 Reddy, S. R. & Fogler, H. S. Emulsion stability: Determination from turbidity. *Journal of colloid and interface science* **79**, 101-104, doi:http://dx.doi.org/10.1016/0021-9797(81)90052-7 (1981).

198 Timasheff, S. N. Turbidity as a criterion of coagulation. *Journal of colloid and interface science* **21**, 489-497, doi:https://doi.org/10.1016/0095-8522(66)90047-X (1966).

199 Kerker, M. *The scattering of light and other electromagnetic radiation*. (Academic Press, Inc, 1969).

200 Kerker, M., Farone, W. A. & Matijevic, E. Applicability of Rayleigh–Gans Scattering to Spherical Particles*. *J. Opt. Soc. Am.* **53**, 758-759, doi:10.1364/JOSA.53.000758 (1963).

201 Dieguez, L. *et al. Effect of the Refractive Index of Buffer Solutions in Evanescent Optical Biosensors*. Vol. 7 (2009).

202 Heller, W., Bhatnagar, H. L. & Nakagaki, M. Theoretical Investigations on the Light Scattering of Spheres. XIII. The``Wavelength Exponent"of Differential Turbidity Spectra. *The Journal of Chemical Physics* **36**, 1163-1170 (1962).

203 Heller, W., Klevens, H. B. & Oppenheimer, H. The determination of particle sizes from tyndall spectra. *The Journal of Chemical Physics* **14**, 566-567 (1946).

204 Heller, W. & Vassy, E. Tyndall spectra, their significance and application. *The Journal of Chemical Physics* **14**, 565-566 (1946).

205 Zappacosta, R. *et al.* Liposome-induced exfoliation of graphite to few-layer graphene dispersion with antibacterial activity. *Journal of Materials Chemistry B* **3**, 6520-6527, doi:10.1039/C5TB00798D (2015).

206 Chen, X., Yin, Y. & Lu, J. *Influences of Branched Vinyl Silicone Oil on the Physical and Ultraviolet Transparent Properties of Silicone Rubber*. Vol. 17 (2014).

207 Good, N. E. *et al.* Hydrogen ion buffers for biological research. *Biochemistry* **5**, 467-477 (1966).

208 Parish, C. *UV atlas of organic compounds. : [UV Atlas] organischer Verbindungen*. (New York : Plenum Press, [1966-], 1966).

209 Matsuzaki, K. *et al.* Optical characterization of liposomes by right angle light scattering and turbidity measurement. *Biochimica et Biophysica Acta (BBA) - Biomembranes* **1467**, 219-226, doi:https://doi.org/10.1016/S0005-2736(00)00223-6 (2000).

210 Green, J. M. Peer reviewed: a practical guide to analytical method validation. *Analytical chemistry* **68**, 305A-309A (1996).

211 Worstell, N. C. & Wu, H. J. Semi-Quantitative Evaluation of Heterogeneous Glycolipid Mixture Binding Avidity Using a Turbidity Assay. (In Preparation).

212 Hsia, C.-Y., Chen, L., Singh, R. R., DeLisa, M. P. & Daniel, S. A Molecularly Complete Planar Bacterial Outer Membrane Platform. *Scientific Reports* **6**, 32715, doi:10.1038/srep32715 (2016).

213 Angeli, A. *et al.* Design and synthesis of galactosylated bifurcated ligands with nanomolar affinity for lectin LecA from *Pseudomonas aeruginosa*. *ChemBioChem* (2017).

214 Costello, D. A., Hsia, C.-Y., Millet, J. K., Porri, T. & Daniel, S. Membrane Fusion-Competent Virus-Like Proteoliposomes and Proteinaceous Supported Bilayers Made Directly from Cell Plasma Membranes. *Langmuir : the ACS journal of surfaces and colloids* **29**, 6409-6419, doi:10.1021/la400861u (2013).

215 Richards, M. J. *et al.* Membrane Protein Mobility and Orientation Preserved in Supported Bilayers Created Directly from Cell Plasma Membrane Blebs. *Langmuir : the ACS journal of surfaces and colloids* **32**, 2963-2974, doi:10.1021/acs.langmuir.5b03415 (2016).

216 Watty, A., Methfessel, C. & Hucho, F. Fixation of allosteric states of the nicotinic acetylcholine receptor by chemical cross-linking. *Proceedings of the National Academy of Sciences* **94**, 8202-8207 (1997).

217 Hughson, A. G. & Hazelbauer, G. L. Detecting the conformational change of transmembrane signaling in a bacterial chemoreceptor by measuring effects on disulfide cross-linking in vivo. *Proceedings of the National Academy of Sciences* **93**, 11546-11551 (1996).

218 Everett, W. N., Beltran-Villegas, D. J. & Bevan, M. A. Concentrated Diffusing Colloidal Probes of Ca2+-Dependent Cadherin Interactions. *Langmuir : the ACS journal of surfaces and colloids* **26**, 18976-18984, doi:10.1021/la1038443 (2010).

219 Bevan, M. A. & Prieve, D. C. Direct Measurement of Retarded van der Waals Attraction. *Langmuir : the ACS journal of surfaces and colloids* **15**, 7925-7936, doi:10.1021/la9813811 (1999).

220 Pailthorpe, B. A. & Russel, W. B. The retarded van der Waals interaction between spheres. *Journal of colloid and interface science* **89**, 563-566, doi:http://dx.doi.org/10.1016/0021-9797(82)90208-9 (1982).

221 Lewis, B. A. & Engelman, D. M. Lipid bilayer thickness varies linearly with acyl chain length in fluid phosphatidylcholine vesicles. *Journal of Molecular Biology* **166**, 211-217, doi:http://dx.doi.org/10.1016/S0022-2836(83)80007-2 (1983).

222 Wu, H.-J., Everett, W. N., Anekal, S. G. & Bevan, M. A. Mapping Patterned Potential Energy Landscapes with Diffusing Colloidal Probes. *Langmuir : the ACS journal of surfaces and colloids* **22**, 6826-6836, doi:10.1021/la060501j (2006).

223 Anekal, S. G., Bevan, M. A., F., B. J. & G., B. Self-diffusion in submonolayer colloidal fluids near a wall. *The Journal of Chemical Physics* **125**, 034906, doi:10.1063/1.2211616 (2006).

224 Honig, E. P., Roebersen, G. J. & Wiersema, P. H. Effect of hydrodynamic interaction on the coagulation rate of hydrophobic colloids. *Journal of colloid and interface science* **36**, 97-109, doi:http://dx.doi.org/10.1016/0021-9797(71)90245-1 (1971).

APPENDIX A*

Theoretical Model

A model for the binding of GM_1 to CTB was proposed by Klassen and his coworkers.[64] (**Figure 24**). We adapted and analyzed their stepwise binding model with minor changes. All equations are summarized below. Writing the material balance for a pentameric protein P,

Equation 23

$$P_T = [P] + [PL] + [PL_2'] + [PL_2''] + [PL_3'] + [PL_3''] + [PL_4] + [PL_5]$$

where P_T is the total concentration of protein, [P] is the concentration of free protein, and [PL]/[PL_2]/[PL_3]/[PL_4]/[PL_5] are the protein-ligand binding complexes with 1, 2, 3, 4, and 5 ligands/receptors respectively. [PL_2] and [PL_3] contain two bound states ([PL_2']/ [PL_2''] and [PL_3']/ [PL_3'']) that were defined by Klassen's model. [64]

Writing material balance for the ganglioside L,

Equation 24

$$L_T = [L] + [PL] + 2([PL_2'] + [PL_2'']) + 3([PL_3'] + [PL_3'']) + 4[PL_4] + 5[PL_5]$$

where L_T is the total concentration of ganglioside and L is concentration of unbound gangliosides. At equilibrium, the material balances for each reaction species were written as follows:

Equation 25

$$[PL] = 5K_1[P][L]$$

Equation 26

$$[PL_2'] = K_2[PL][L] = 5K_1K_2[P][L]^2$$

*Reprinted with permission from "Binding cooperativity matters: A GM1-like ganglioside-cholera toxin B subunit binding study using a nanocube-based lipid bilayer array" by Worstell, Nolan C., Krishnan, Pratik, Weatherston, Joshua D., Wu, H. J., 2016, *PLoS ONE*, 11, Copyright 2016 by Public Library of Science

Equation 27

$$[PL_3'] = K_2[PL_2'][L] = 5K_1K_2^2[P][L]^3$$

Equation 28

$$[PL_4] = K_2[PL_3'][L] = 5K_1K_2^3[P][L]^4$$

Equation 29

$$[PL_5] = \frac{K_3}{5}\,[PL_4][L] = K_1K_2^3K_3[P][L]^5$$

Equation 30

$$[PL_2''] = K_1[PL][L] = 5K_1^2[P][L]^2$$

Equation 31

$$[PL_3''] = K_2[PL_2''][L] = 5K_1^2K_2[P][L]^3$$

Equation 23 and **Equation 24** then become:

Equation 32

$$P_T = [P] + 5K_1[P][L] + 5K_1K_2[P][L]^2 + 5K_1^2[P][L]^2 + 5K_1K_2^2[P][L]^3 + 5K_1^2K_2[P][L]^3 + 5K_1K_2^3[P][L]^4 + K_1K_2^3K_3[P][L]^5$$

Equation 33

$$L_T = L + 5K_1[P][L] + 2(5K_1K_2[P][L]^2 + 5K_2^2[P][L]^2) + 3(5K_1K_2^2[P][L]^3 + 5K_1^2K_2[P][L]^3) + 4(5K_1K_2^3[P][L]^4) + 5K_1K_2^3K_3[P][L]^5$$

Klassen and his coworkers [64] determined the values for K_1, K_2, and K_3 for CTB binding with GM_1 to be 3.2×10^6 M^{-1}, 5.5×10^6 M^{-1}, and 9.5×10^6 M^{-1}, respectively. To account for cooperativity, we multiplied K_2 and K_3 with a factor 'α'

Equation 34

$$K_2 = \alpha \times K_1\,, K_3 = \alpha^2 \times K_1$$

α is approximately 2 when GM_1 is the binding receptor and α <1 represents negatively cooperative binding. From the fitting results of the Hill-Waud equation, we found the binding cooperativity of CTB to fucosyl-GM $_1$ was significantly reduced from CTB to GM_1 binding; hence, we considered the value of α to be less than 2. Although we selected an arbitrary α = 1/2

to demonstrate the enhanced binding capacity in **Figure 4a**, the increase of binding capacity was observed for all tested values of α smaller than the 2, representative of GM_1 binding to CTB. For all theoretical modeling, we set the total ganglioside concentration initially to 10^{-6} M (a similar order of magnitude as the experiments performed), and changed the concentration of unbound CTB from 10^{-10} to 10^{-6} M , and then we solved **Equation 33** to obtain [L]. Therefore, we could determine the concentration of the bound CTB by adding **Equation 25** to **Equation 31**.

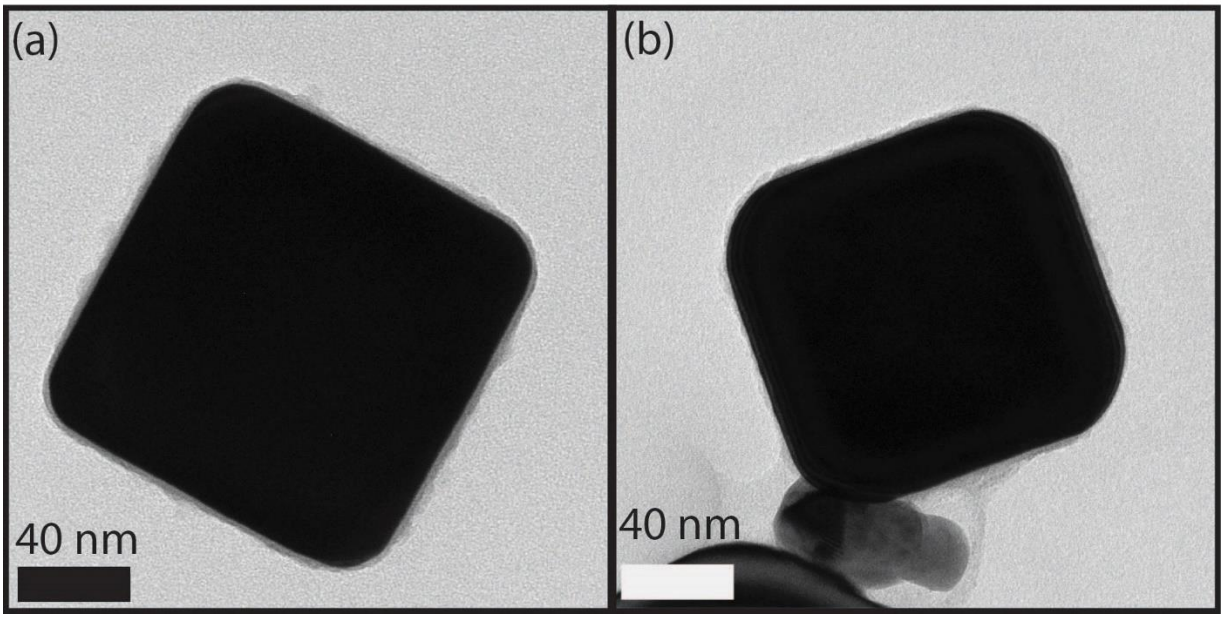

Figure 21: TEM image comparison of silica coating procedures. (a) A TEM image of the silica shell coated onto Ag nanocubes in 2-propanol. (b) A TEM image of the silica shell coated onto Ag nanocubes in ethanol. Reprinted with permission from Worstell *et al.*[75]

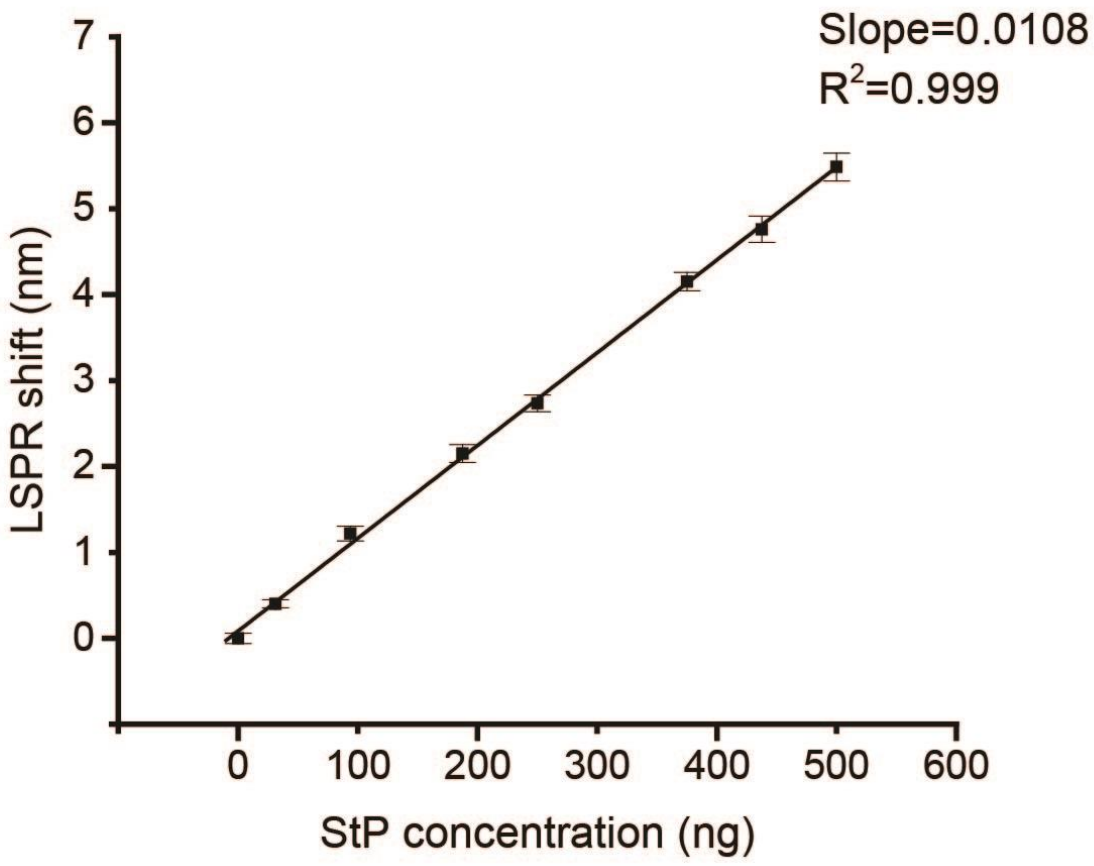

Figure 22: Equilibrium StP- Biotin binding for sensor calibration. Streptavidin (StP)-biotin-DPPE binding data assuming that all StP is bound to a biotin group resulting in the observed LSPR shift. Data are reported as mean ± S.D. (n=8). Reprinted with permission from Worstell *et al.*[75]

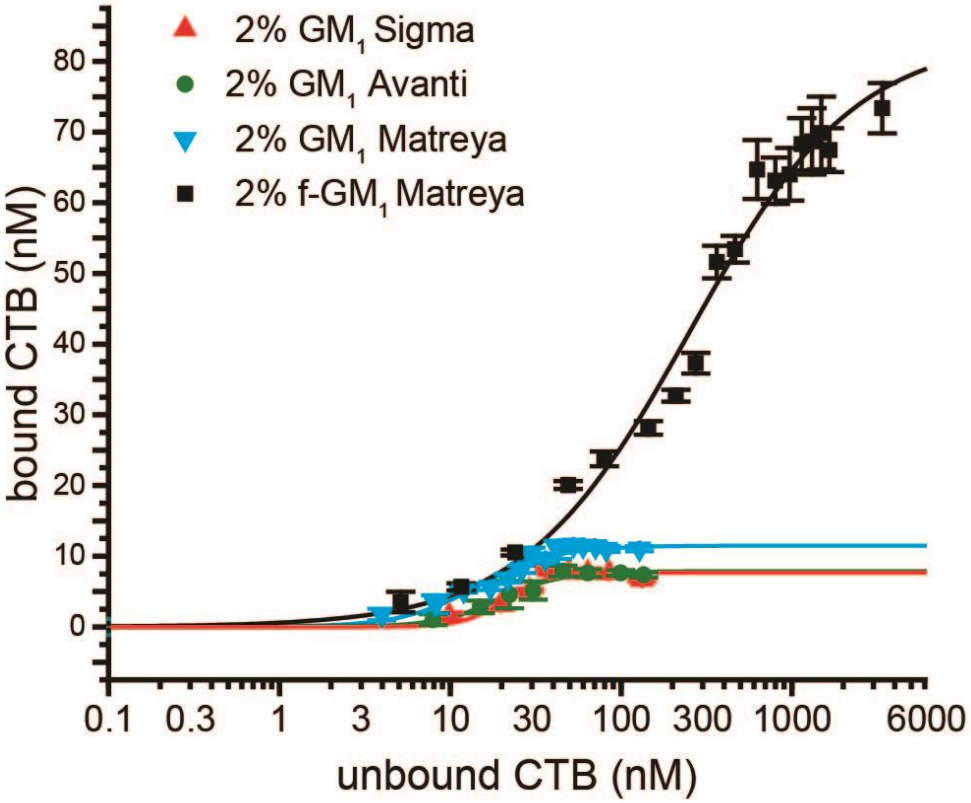

Figure 23: GM_1 quality comparison across vendors. Comparison of GM_1 gangliosides obtained from various companies with fucosyl-GM_1 plotted for reference. Data are reported as mean ± S.D. (n=8). Reprinted with permission from Worstell *et al.*[75]

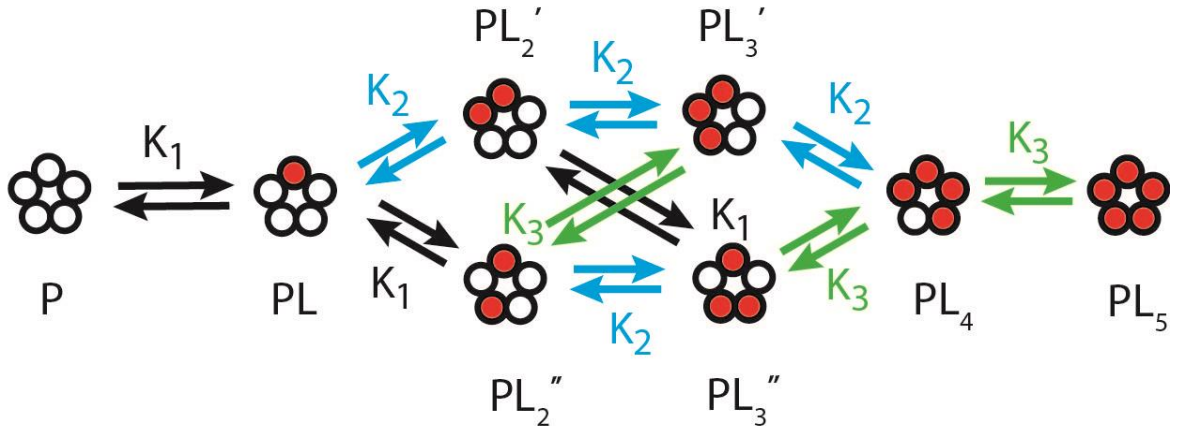

Figure 24: Stepwise CTB binding model with a single type of ganglioside. The stepwise model is adapted from.[64] Reprinted with permission from Worstell *et al.*[75]

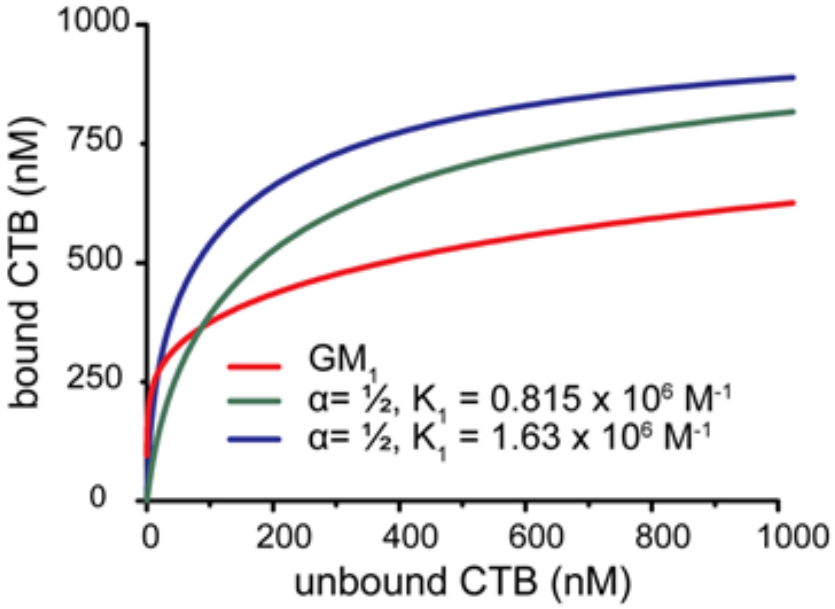

Figure 25: Effect of varying cooperativity and binding affinity (with a reduced K_1 to half its original value). Reprinted with permission from Worstell *et al.*[75]

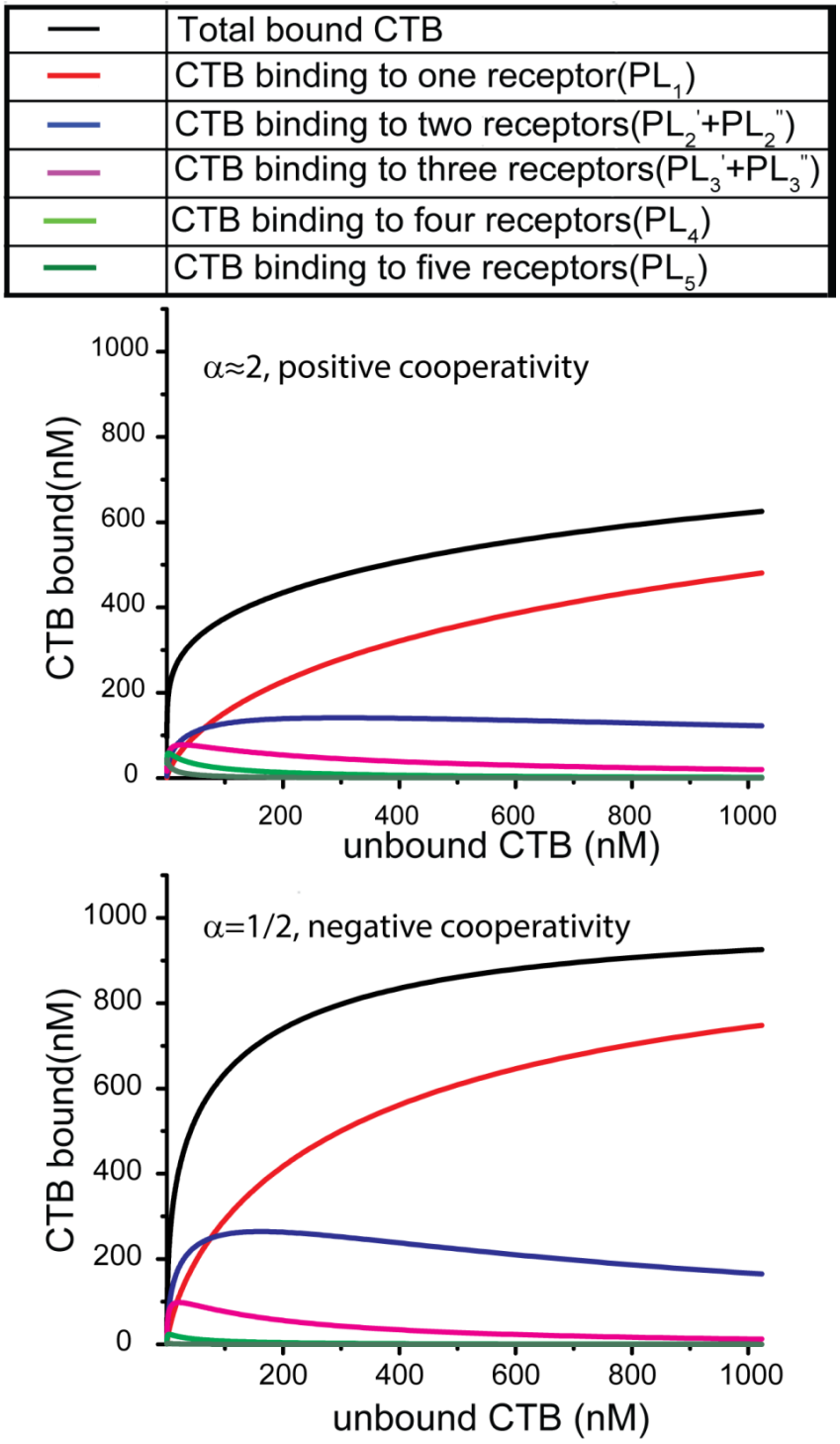

Figure 26: CTB bound as a function of unbound CTB concentration for each of the possible binding states. Reprinted with permission from Worstell *et al.*[75]

APPENDIX B*

Calculation of Reduction of Dimensionality

As described in the main text, the reaction rate, ϕ, can be written as[114]:

Equation 35

$$\phi = k_{obs} C_A C_B$$

where C_A and C_B are the number densities of the two reactants, and k_{obs} is the empirical rate constant. The reactant concentrations are measured in either units of mol/m^3 for bulk reactions or mol/m^2 for surface reactions. Thus, the three-dimensional reaction rates (ϕ_{3D}) are in units of $mol/(m^3 \cdot \text{sec})$; on the two-dimensional membrane surface, the unit of reaction rate (ϕ_{2D}) is $mol/(m^2 \cdot \text{sec})$. To evaluate the difference between three-dimensional and two-dimensional reactions, the two-dimensional reaction rate was multiplied by a constant S/V in order to covert the surface concentration to volume concentration. S is the total surface area of the outer leaflet of liposome confined in volume V. Using the DOPC lipid footprint in bilayer of 0.72nm^2,[120] the total surface area of outer leaflet of liposome containing 1 mol% of glycolipid can be estimated:

Equation 36

$$\frac{S}{V} = \left(\frac{C_{B,3D}}{1\%}\right) \cdot N_A \cdot 0.72nm^2/2 = 6.5 \times 10^3 m^{-1}$$

Thus, the reaction events per volume per time occurring on two-dimensional membrane surfaces is: $\phi_{2D} \cdot (S/V)$

*Reprinted with permission from "Hetero-multivalent Binding of Cholera Toxin Subunit B with Glycolipid Mixtures" by Krishnan, Pratik, Singla, Akshi, Lee, Chin-An, Weatherston, Joshua D., Worstell, Nolan C., Wu, Hung-Jen, 2017, *Colloids and Surfaces B: Biointerfaces*, 160,281-288, Copyright 2017 by Elsevier B.V.

In order to consider the influence of diffusion processes, we estimated the reaction rate in diffusion controlled reactions. For three-dimensional reactions, Smoluchowski equation gives[109,114]:

Equation 37

$$k_{obs,3D} = 4\pi N_A a\left(D_{A,3D} + D_{B,3D}\right)$$

where N_A is Avogadro's number, a is the encounter radius. Here, we assumed the encounter radius is equivalent to the head group size of DOPC in bilayer ($\sqrt{0.72nm^2/\pi} = 0.48nm$). three-dimensional diffusivities of CTB and glycolipid containing liposome were estimated using Stokes-Einstein equation. ($D_{A,3D} = 9.77\,\text{x}10^{-11}\ m^2/s$ and $D_{B,3D} = 4.88\,\text{x}10^{-12}\ m^2/s$)

For two-dimensional reactions, prior studies derived several analytical solutions using various approaches. We selected three classic models to evaluate the approximate reaction rate on two-dimensional membrane surfaces.[113-115] Hardt employed the approximate solution of mean diffusion time derived by Adam and Delbrück[109] and calculated the two-dimensional reaction rate[113]:

Equation 38

$$k_{obs,2D} = 2\pi N_A \left(\frac{D_{A,2D}}{ln\frac{1}{a\sqrt{\pi N_A C_{B,2D}}}} + \frac{D_{B,2D}}{ln\frac{1}{a\sqrt{\pi N_A C_{A,2D}}}} \right)$$

where $D_{A,2D}$ and $D_{B,2D}$ are the two-dimensional diffusivity of CTB and glycolipid obtained from the literature ($D_{A,2D} = 2.5 \times 10^{-13}\ m^2/s$ and $D_{B,2D} = 8.25 \times 10^{-12}\ m^2/s$).[118-120] $C_{A,2D}$ and $C_{B,2D}$ are the surface densities (unit:mol/m^2). Szabo et al. applied the first passage time approach to evaluate the surface reaction rate.[115] Keizer showed the solution for diffusion controlled reactions:[114]

Equation 39

$$k_{obs,2D} = 2\pi D'/(ln(b/a) - 3/4)$$

where $D' = D_{A,2D} + D_{B,2D}$, and b represents the diffusion distance. If CTB serves as the sink for the glycolipid, we can obtain $b = \sqrt{1/\pi N_A C_{A,2D}}$.[113] Keizer reported a similar formula for $k_{obs,2D}$ using a statistical thermodynamic theory:

Equation 40

$$k_{obs,2D} = 2\pi D'/(ln(b/a) - \gamma + ln\sqrt{2})$$

where γ is the Euler's constant = 0.5772…

In our experiments, the glycolipid concentration ($C_{B,3D}$) was controlled at 300 nM. Considering 300 nM of CTB, the two-dimensional reaction rate is around 10^4 higher than three-dimensional reaction rate. ($\phi_{2D} \cdot (S/V)/\phi_{3D}$ = ~8,000 for **Equation 38**, ~13,000 for **Equation 39**, and ~9,000 for **Equation 40**). Even if we consider the diffusivity value of GM_1 reported in literature [121,122], the two-dimensional reaction rate is still 5000-10000 times higher than the three-dimensional reaction rate. At higher CTB concentrations ($C_{A,3D} = 700nM$), the two-dimensional reaction rate could be up to 20,000 times higher than the three-dimensional reaction rate. In general, the reduction of dimensionality mechanism can enhance two-dimensional reaction rate by 3-4 orders of magnitude.

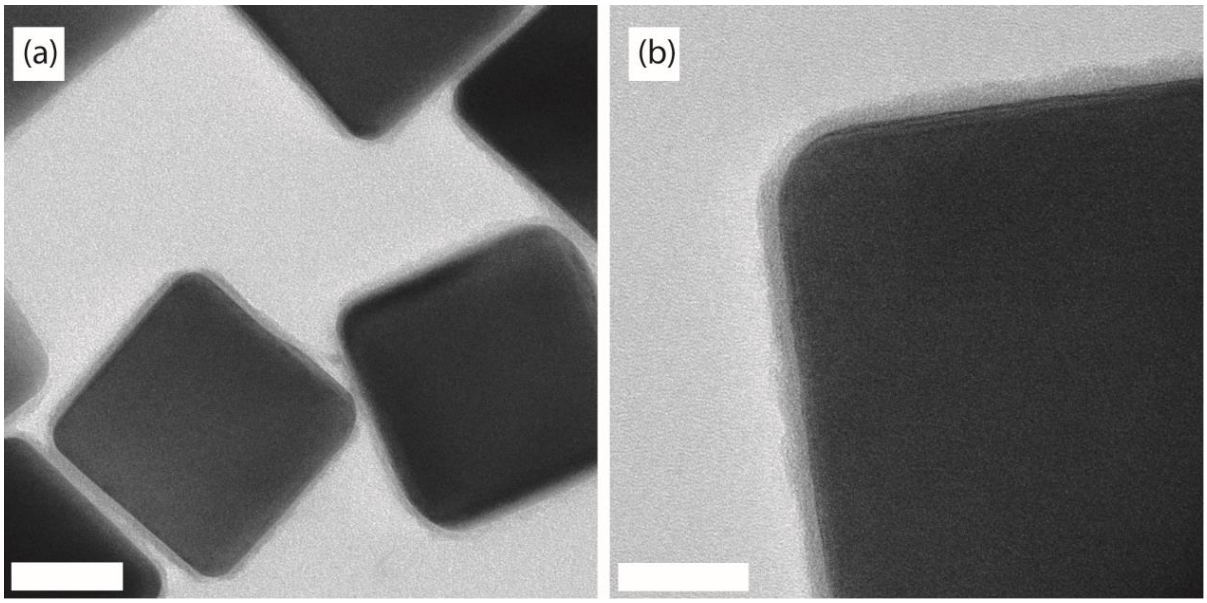

Figure 27: TEM images of the silica shell coated onto the Ag nanocubes. Scale bar = (a) 40nm and (b) 20nm. Reprinted with permission from Krishnan *et al*.[18]

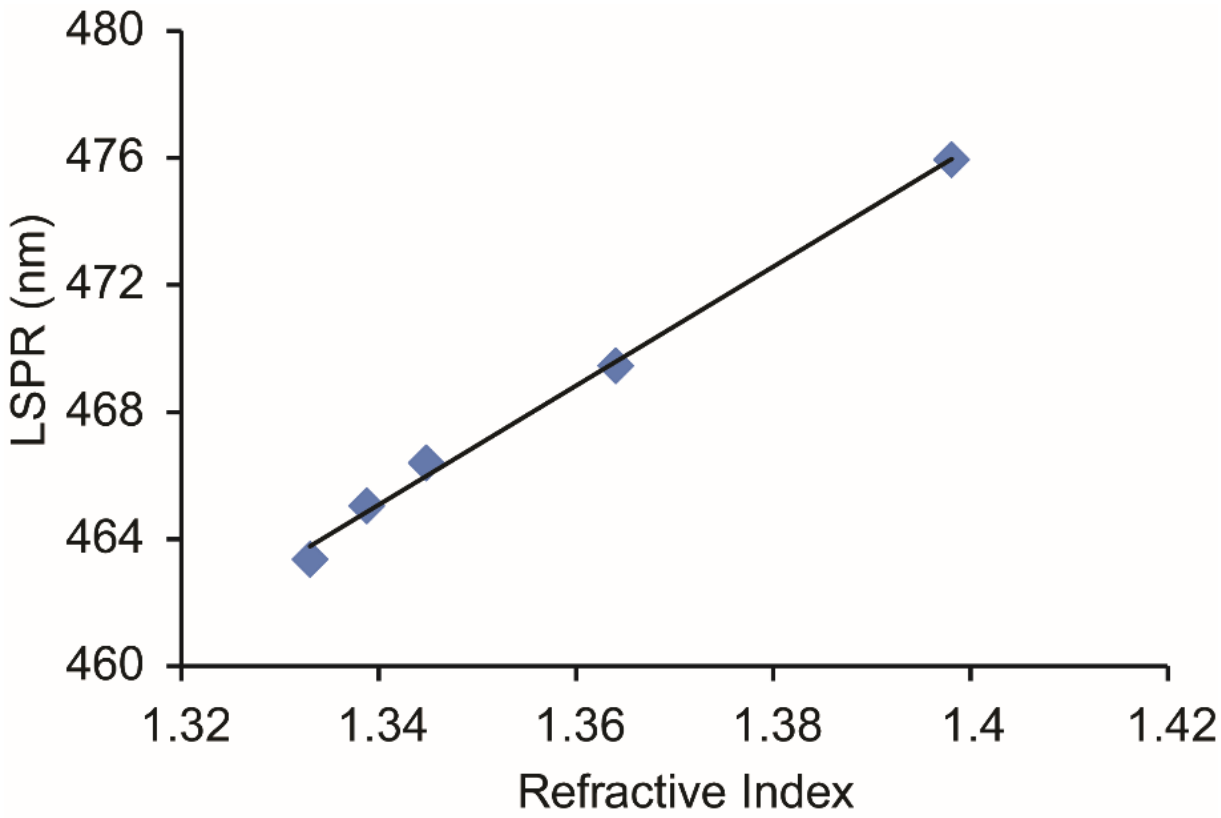

Figure 28: Sensor sensitivity characterization. Change in quadrupole LSPR peak location vs. Refractive Index (RI) using silica coated silver nanocubes in various glycerol-water mixtures measured with a spectrophotometer. The slope is 187.44 nm/RIU. Reprinted with permission from Krishnan *et al.*[18]

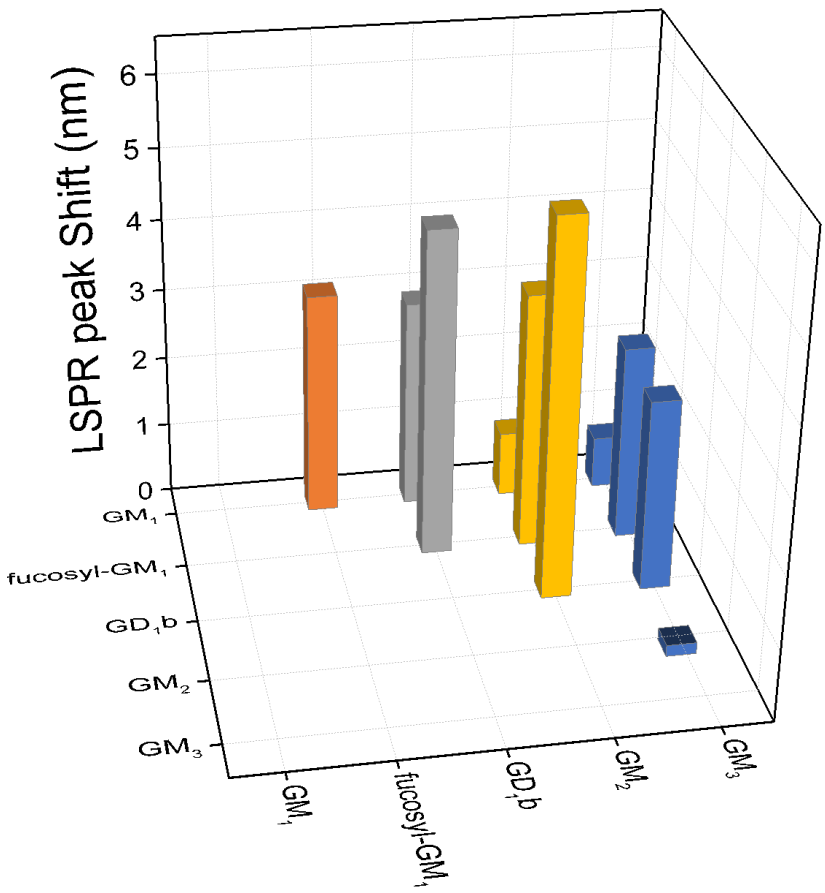

Figure 29: Equilibrium binding of CTB to membrane surfaces containing two glycolipids in a 1:1 mole ratio (1 mol% of each glycolipid). The CTB concentration used was 706 nM. Reprinted with permission from Krishnan *et al.*[18]

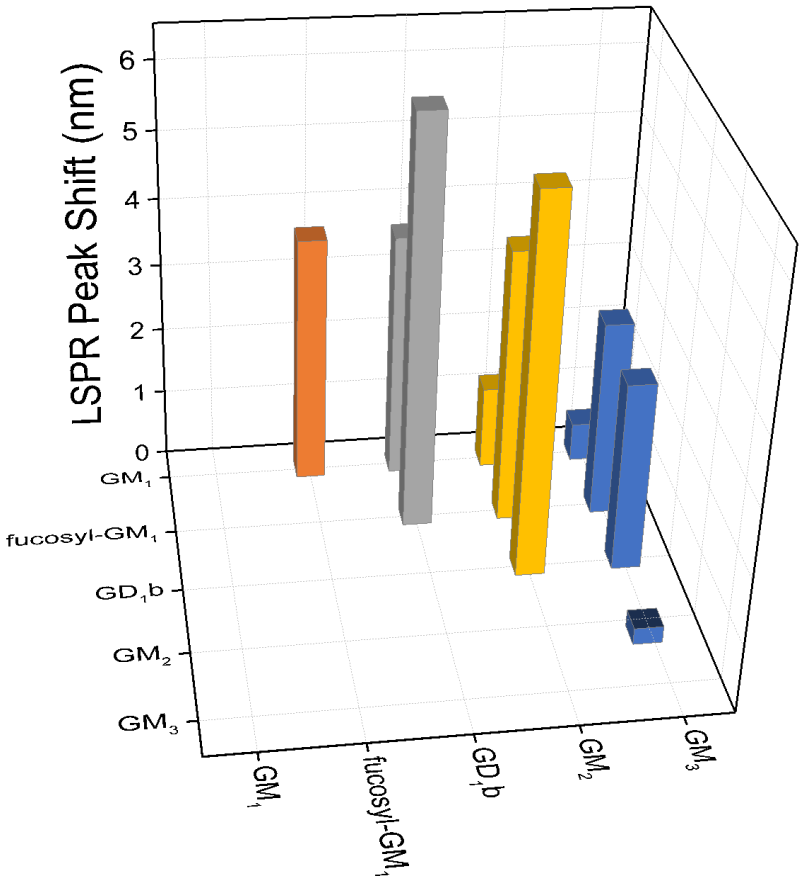

Figure 30: Equilibrium binding of CTB to membrane surfaces containing two glycolipids in a 1:1 mole ratio (1 mol% of each glycolipid). The CTB concentration used was 1726 nM. Reprinted with permission from Krishnan *et al*.[18]

APPENDIX C

Aggregation Kinetics Theory

To study the interaction between colloidal particles mediated by biomolecular interactions of LecA with glycolipids, we used the method as outlined by Duncan et al. for Concanavalin A binding to dextran.[155] The binding energy between LecA and glycolipid receptors was quantified using the single particle disappearance rate. However, we needed to identify the relevant time scales in which single particle-single particle interactions should dominate. This was done by calculating the mean diffusion time of first interaction for particles via the pair potential energy excluding biomolecular interactions in order to capture all relevant dynamics. The derivation of the theoretically predicted time scale based on the initial particle distribution is as follows.

Particle-Particle & Particle-Wall Interaction Potentials

For macromolecule-coated, micron-sized colloids, the interaction potential, u, that can be constructed as separate particle-wall and particle-particle interactions in which the u_{pw} is given by Duncan et al. as[155]:

Equation 41

$$u_{pw}(h) = u_G(h) + u_v(h) + u_s(h)$$

where h is the particle-wall hard surface separation, r is the particle center-particle center separation and the subscripts are G (for gravity), v (for van der Waals), and S (for steric). The potential energy due to gravity is:

Equation 42

$$u_G(h) = \frac{4}{3}\pi a^3(\rho_p - \rho_f)gh$$

where *a* is the particle radius (2520 nm), *g* is the acceleration due to gravity, and ρ_p and ρ_f are the particle and fluid densities, respectively. [218] The van der Waals potential between half spaces was calculated using Lifshitz theory with consideration of retarded and screened interactions in dielectric media as reported in our prior publication.[156] The values of water, polystyrene, and silica dielectric spectra are the same as those reported previously.[219] The particle-particle and particle-wall interactions were corrected by Derjaguin approximations.[220] For convenience, the van der Waals interactions calculated by Lifshitz theory and Derjaguin approximation are fitted to inverse power laws as:

Equation 43

$$u^{pw}{}_{vdW}(h) = -A_{pw} a h^{-p}$$

where A_{pp}, A_{pw} and p for **Equation 43** are effective Hamaker constants. The fitted parameters for **Equation 43** (silica particle-polystyrene well plate bottom) are A_{pw} = 0.3322 and p = 1.141. The steric potential represents the nonspecific osmotic repulsion due to macromolecules and is modeled as short range exponentials by Everett et al [218] as:

Equation 44

$$u_s^{pw}(h) = Be^{[-\kappa(h-\delta_{HW})]}$$

where κ is the inverse decay length and B is the intercept at separation. δ_{HW} is defined as the thickness of macromolecule layer (lipid bilayer is approximately 5 nm[218,221] and the thickness of F127 on polystyrene is 10 nm). [159] Thus, δ_{HW} = 16 nm in **Equation 44**.

Hydrodynamic Effects on Particle Diffusion

Particle diffusion in the bulk fluid is given by the Stokes-Einstein equation

Equation 45

$$D_o = \frac{k_B T}{6\pi\mu a}$$

when a particle stays near a planar surface, the particle-surface hydrodynamic interactions hinder the particle's diffusion parallel to the surface as given by:

Equation 46

$$D_{pw,\parallel}(h) = D_o f_{pw,\parallel}(h)$$

where the correction factor, $f_{pw,\parallel}$ is the function of particle-surface separation, reported by Wu et al. [222]:

Equation 47

$$f_{pw,\parallel}(h) = \frac{12420\alpha(h)^2 + 5654\alpha(h) + 100}{12420\alpha(h)^2 + 12233\alpha(h) + 431}$$

where $\alpha(h) = h/a$. Thus, the average lateral diffusion of particle depends on the interactions between a particle and a planar surface as given by[223]

Equation 48

$$\langle D_{pw,\parallel} \rangle = \frac{\int D_{pw,\parallel}(h) p(h) dh}{\int p(h) dh}$$

where $p(h)$ represent the distribution of particle elevation that is determined by Boltzmann equation:

Equation 49

$$p(h) = Ae^{\frac{-u_{pw}}{k_B T}}$$

Besides the wall hindering diffusion, particle-particle multibody hydrodynamics also play a role in further hindering the lateral diffusion in concentrated colloidal systems. This diffusion along the line of particle centers is given as[155]:

Equation 50

$$D_{pp,\perp}(r) = \langle D_{pw,\parallel} \rangle f_{pp,\perp}(r)$$

where $f_{pp,\perp}(r)$ is given by Honig et al.[224] as $\frac{1}{\beta(u)}$. β(u) is defined as:

Equation 51

$$\beta(u) \cong \frac{6u^2 + 13u + 2}{6u^2 + 4u}$$

where $u = (r - 2a)/a$.

Finally, τ is the two dimensional diffusion time required for the particles to come into contact and defined as [113]:

Equation 52

$$\tau = \left(2\pi\phi_{1,0}D_{pp,\perp}(r)\right)^{-1} \ln\left[\frac{\left(\pi\phi_{1,0}\right)^{-\frac{1}{2}}}{r_c}\right]$$

where r_c is the collision radius taken as $r_c = a + 0.5 * \delta_{HW,pp}$ where $\delta_{HW,pp}$=12 nm and r is taken as $r = \left(\phi_{1,0}\right)^{-\frac{1}{2}}$ corresponding to the average separation between particles. τ is the value that we used as a cut off time for measuring single particle aggregation rates.

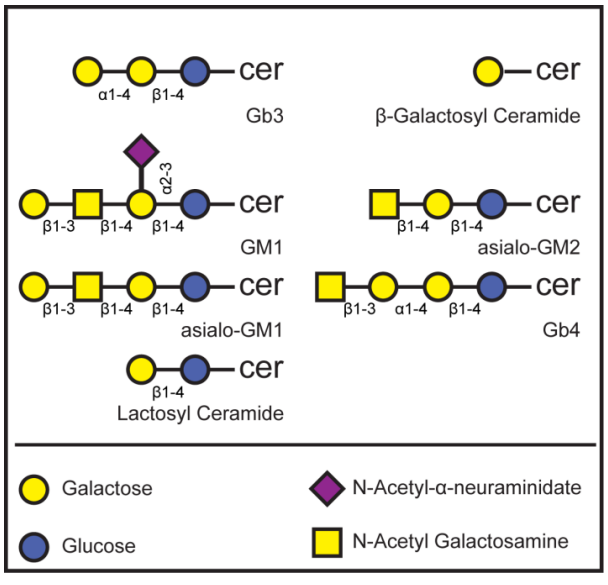

Figure 31: Cartoon representations of glycolipids used in Chapter IV.

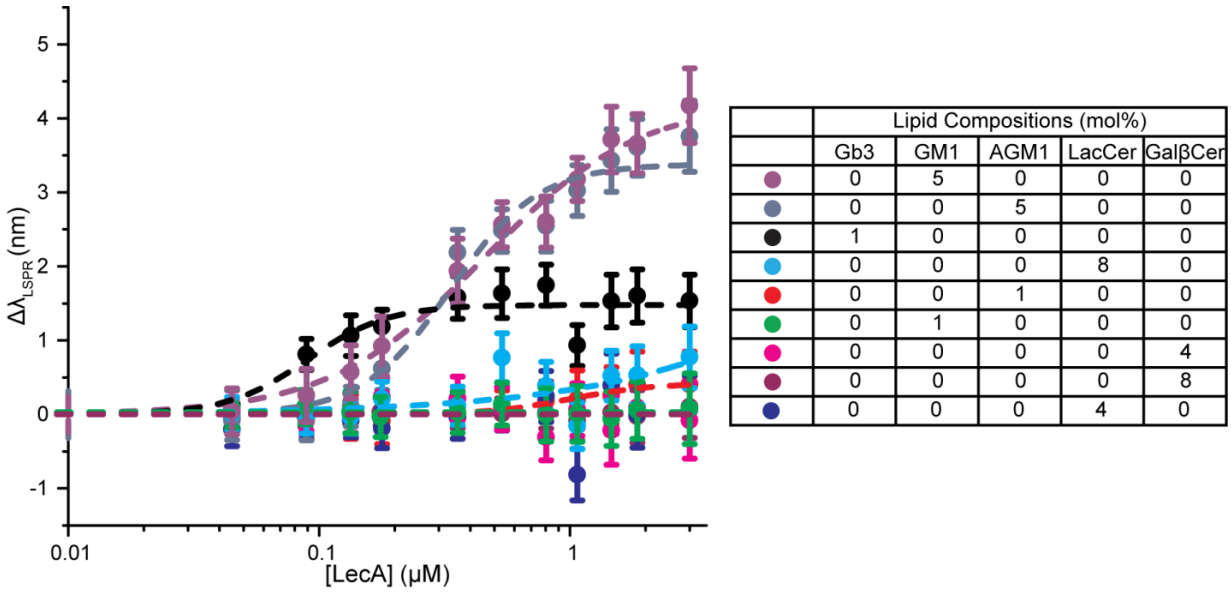

	Lipid Compositions (mol%)				
	Gb3	GM1	AGM1	LacCer	GalβCer
	0	5	0	0	0
	0	0	5	0	0
	1	0	0	0	0
	0	0	0	8	0
	0	0	1	0	0
	0	1	0	0	0
	0	0	0	0	4
	0	0	0	0	8
	0	0	0	4	0

Figure 32: Saturation curves for LecA binding to pure galactose terminated glycolipids given in semi-log form. The data are represented as mean±S.D. (n=8). The dashed lines are the Hill equation fits to the data.

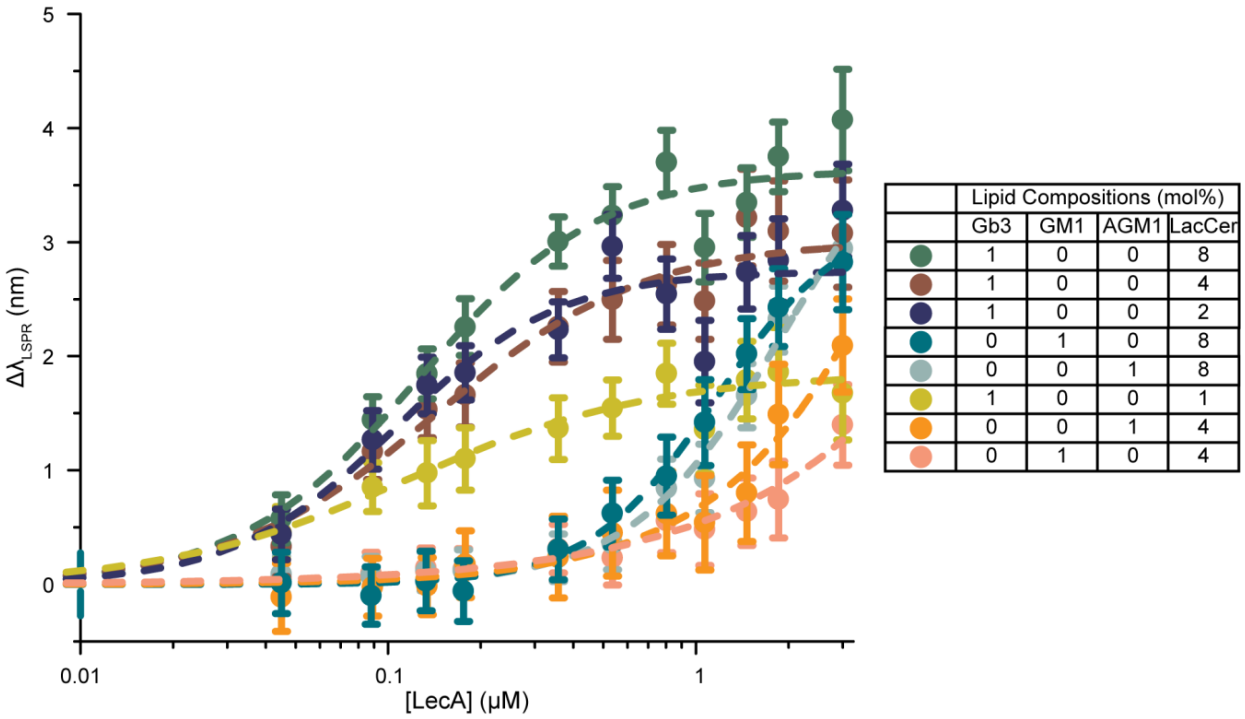

Figure 33: Saturation curves for LecA binding to Gb3, GM1, or AGM1 with LacCer bilayers as given in semi-log form. The data are represented as mean±S.D. (n=8). The dashed lines are the Hill equation fits to the data.

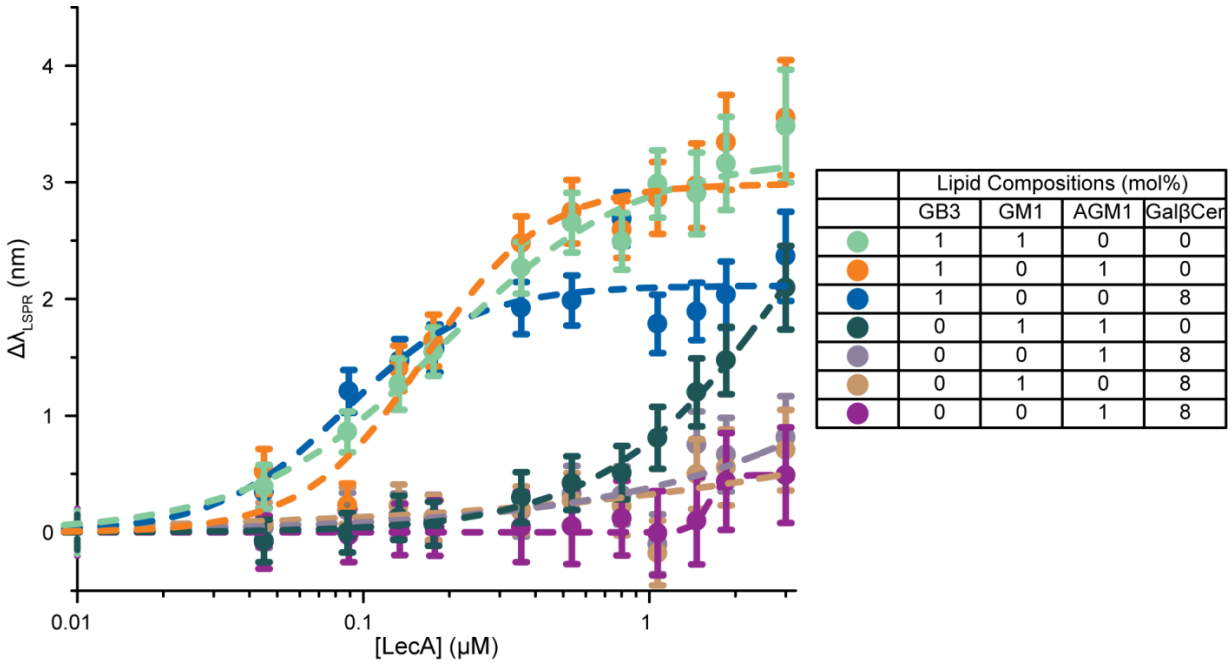

Figure 34: Saturation curves for LecA binding Gb3, GM1, AGM1, or GalβCer mixed together given in semilog form. The data are represented as mean±S.D. (n=8). The dashed lines are the Hill equation fits to the data.

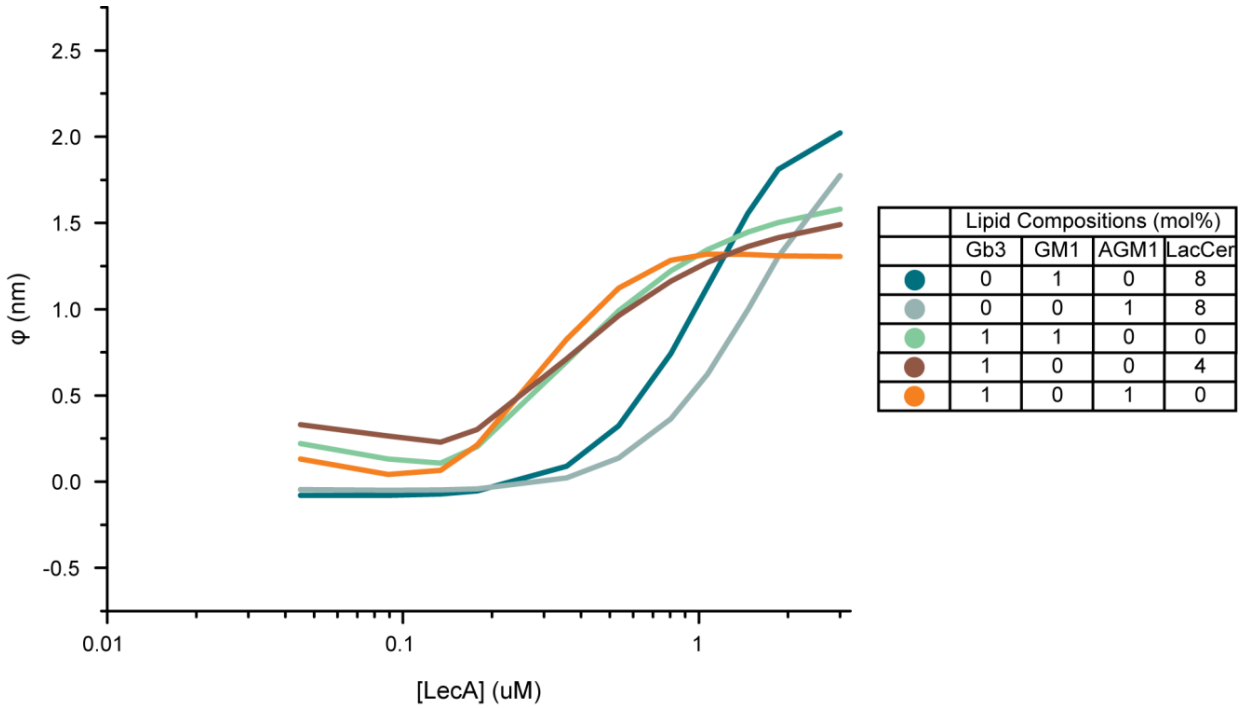

Figure 35: Predicted ϕ values (represented as a linear interpolated lines between the calculated mean values at various [LecA] for a variety of bilayer mixtures).

Table 5: Hill's equation parameters obtained by fitting in OriginLab. A * indicates that fitting was highly uncertain due to the data not reaching a plateau and – indicates fitting did not converge. The values are represented as a mean±SE (where the standard error of the fit is based on fitting 96 points for each curve).

Lipid Compositions (mol%)							Fitted Parameters			
Gb_3	GM_1	AGM_1	LC	Gal	POPS	POPC	V_m (μM)	K_h (μM)	n	
1	0	0	0	0	10	89	1.53±0.02	0.09± 0.00	2.68±0.24	
0	1	0	0	0	10	89	0.10±0.03	0.13± 0.00	0.00±0.40	*
0	5	0	0	0	10	85	4.37±0.08	0.48± 0.02	1.36±0.05	
0	0	1	0	0	10	89	0.44±0.06	1.10± 0.17	2.64±0.77	
0	0	5	0	0	10	85	3.58±0.04	0.37± 0.01	2.11±0.08	
0	0	0	4	0	10	86	-	-	-	*
0	0	0	8	0	10	82	$6.41*10^3$±$3.48*10^7$	$3.76*10^6$±$3.15*10^{10}$	0.65±0.22	*
0	0	0	0	4	10	86	0.12±0.04	0.18±0.00	0.00±0.42	*
0	0	0	0	8	10	82	-	-	-	*
1	1	0	0	0	10	88	3.24±0.04	0.19±0.01	1.26±0.04	
1	0	1	0	0	10	88	3.30±0.04	0.20±0.01	1.50±0.07	
1	0	0	1	0	10	88	1.83±0.04	0.12±0.01	1.08±0.07	
1	0	0	2	0	10	87	2.81±0.04	0.11±0.01	1.39±0.11	
1	0	0	4	0	10	85	3.18±0.04	0.17±0.01	1.16±0.05	
1	0	0	8	0	10	81	3.75±0.04	0.13±0.00	1.35±0.05	
1	0	0	0	8	10	81	2.11±0.02	0.09±0.00	1.92±0.14	
0	1	1	0	0	10	88	4.24±0.51	3.02±0.51	1.34±0.07	*
0	1	0	4	0	10	85	$9.30*10^3$±$1.96*10^7$	$3.81*10^5$±$1.05*10^9$	0.8±0.1	*
0	1	0	8	0	10	81	3.26±0.08	1.17±0.03	2.08±0.08	
0	1	0	0	8	10	81	$3.21*10^2$±$8.42*10^4$	$1.84*10^4$+$6.86*10^6$	0.71±0.22	*
0	0	1	4	0	10	85	14.32±16.95	13.67±18.53	1.15±0.13	*
0	0	1	8	0	10	81	3.91±0.13	1.66±0.07	2.00±0.08	
0	0	1	0	4	10	85	0.49±0.03	1.61±0.05	14.62±4.13	
0	0	1	0	8	10	81	$5.95*10^3$±$1.85*10^7$	$6.12*10^5$±$2.62*10^9$	0.73±0.18	*